THE UNIVERSITY OF CHICAGO

ASPECTS OF MSSM ASSOCIATED WITH ELECTROWEAK BARYOGENESIS

A DISSERTATION SUBMITTED TO
THE FACULTY OF THE DIVISION OF THE PHYSICAL SCIENCES
IN CANDIDACY FOR THE DEGREE OF
DOCTOR OF PHILOSOPHY

DEPARTMENT OF PHYSICS

BY
BING LI

CHICAGO, ILLINOIS
MARCH 2017

TABLE OF CONTENTS

LIST OF FIGURES

LIST OF TABLES

ACKNOWLEDGMENTS

I would like to express the deepest appreciation to Professor Carlos E.M. Wagner, from whom I learned the most important attitudes and skills in physics research. Without his guidance and persistent help this dissertation would not have been possible. The six and a half years I have spent at the University of Chicago were tough but exciting, and of course unforgettable. This precious experience of research would definitely become the treasure for my whole life.

I also want to thank my Committee members, Professor LianTao Wang, Professor Kathy Levin, and Professor Yau W. Wah. And I want to thank my first Professor at Chicago, David I. Schuster, a kind teacher and a talented researcher, with whom I spent my first two years. And I would like to thank my fellow doctoral student Aniket Joglekar and post-doc researcher Peisi Huang for their cooperation and friendship. At last, I want to thank my wife Ning and my parents who gave me the strongest support in those most difficult days.

I would like to thank the Aspen Center for Physics, which is supported by the National Science Foundation under Grant No. PHYS-1066293. Work at ANL is supported in part by the U.S. Department of Energy under Contract No. DE-AC02-06CH11357. Work at EFI is supported by the U.S. Department of Energy under Contract No. DE-FG02-13ER41958.

ABSTRACT

Electroweak Baryogenesis(EWBG) aims to explain the matter anti-matter asymmetry at the Electroweak energy level. However the Standard Model alone is not enough to provide all the three Sakharov Criteria, so we turned to the MSSM. First, we discussed the maximum CP Violation(CPV) that could exist in the neutral Higgs sector of MSSM, especially in the lightest neutral Higgs. We found that there is a constraint from the lightest Higgs mass and that the observed mass 126 GeV has already put a rather strong upper bound on CPV. Because the existence of CP-violating phases also modifies hVV and $hb\bar{b}$ coupling, the CPV also receives constraints from Higgs precision measurements. After taking EDM and flavor physics constraints into account, we showed that the maximal CPV we can get from the lightest neutral Higgs is no higher than 3%. In the second part of this thesis, we looked into another necessary condition of EWBG, a strong first-order Electroweak phase transition(EWPT). We discussed the order of EWPT in the most general effective Higgs potential and especially the interesting correlation between this order and the triple Higgs self-coupling. We showed that a strong first-order EWPT could lead to a large modification of the Higgs self-coupling and could even change its sign. And this possible deviation could be detected through the channel $H \to HH \to b\bar{b}\gamma\gamma$. We reported a significance of 7.5 σ for $\lambda_3 = -\lambda_3^{SM}$ at the LHC(14 TeV and 3000 fb^{-1}).

CHAPTER 1

INTRODUCTION: THE STORY OF ELECTROWEAK BARYOGENESIS

1.1 Baryogenesis

The first proposal of baryogenesis came out as an explanation for the matter anti-matter asymmetry problem, which started with the observation that the material we have seen is mostly made of protons and neutrons etc, which astrophysists called baryon content, instead of their anti-particles. Matter anti-matter asymmetry, more concisely, the phenomenon that matter and anti-matter are not uniform in scales of at least the Hubble scale, has been supported by evidences at different scales and from both the experimental and theoretical sides. At smaller scale, within our galaxy, the density of antiprotons in the cosmic ray is consistent with the secondary production $p + p \to 3p + \bar{p}$. Zooming out a little bit, at the scale of cluster of galaxies, a background of Gamma-radiation from the annihilation between matter and anti-matter is not observed. And the absence of diffuse Gamma ray and a distortion of CMB also strongly supports the existence of an asymmetry at an even larger scale. On the theoretical side, the premordial nucleosynthesis theory has displayed glorious success in predicting the cosmological abundances of light elements, H, He, D, B, Li and it needs an input parameter $\eta = \frac{n_B - n_{\bar{B}}}{s}$ to lie within the range $1.5 \times 10^{-10} < \eta < 7 \times 10^{-10}$, which is exactly the baryon asymmetry at the early stage of the universe evolution. Some theorists think that this asymmetry could be taken simply as an initial condition, however this explanation ended up with many unnatural parameter problems; while on the other hand, baryogenesis theories try to explain the generation of this asymmetry on the basis of quantum field theories and to tell the whole story from the very beginning.

In the widely cited paper published in 1967, Sakharov proposed the famous three necessary conditions for baryogenesis, the so-called Sakharov Criteria. Firstly, we need a baryon-number-violating process (otherwise asymmetry cannot be generated from symmetric initial

conditions); Secondly, both C and CP violations are needed (its easy to prove that any process which produces an excess of baryons will be accompanied by some complimentary process which produces an excess of antibaryons at the same rate); And the last condition is a departure from the thermal equilibrium state (one can prove that the equilibrium average of B is zero).

1.2 Electroweak Baryogenesis

There are many different theoretical attempts trying to explain the mechanism of baryogenesis, for example, Planck scale baryogenesis, GUT baryogenesis, Electroweak baryogenesis, Leptogenesis and the Affleck-Dine mechanism. Among these candidates, Electroweak Baryogenesis is especially attractive due to many reasons. Firstly, it's associated with Electroweak phase transition at 100 GeV, predicts new physics around 1 TeV and thus provides an important connection between cosmology and collider physics, having rich testable phenomenology at the LHC era. The second reason is that, naively speaking, within the mechanism of Electroweak Baryogenesis, the Standard Model(SM) alone can provide all the three Sakharov conditions. The Baryon number violation was realized by the sphaleron process, which is intrinsic to the SM gauge theory; The SM also has multiple sources of CP-Violation, such as the phase in the CKM matrix, that has been shown responsible for the CP-Violation in Meson decays; And at last the Electroweak phase transition itself is a non-thermal equilibrium process. However the Electroweak Baryogenesis also has its difficulties and as we'll show in a second, the Standard Model itself is not sufficient for generating such a large baryon asymmetry from many perspectives.

EWBG happens during the EWPT. This little cartoon below(Fig 1.1) demonstrates the process of EWPT[1]. The right side is the symmetric phase, and the left side is the phase after symmetry breaking and the Higgs field has obtained a finite vacuum expectation value. This transition is first-order, so it will start with nucleation of bubbles and bubbles expand

1. copyright of Fig 1 belongs to David E. Morrissey and Michael J. Ramsey-Musolf

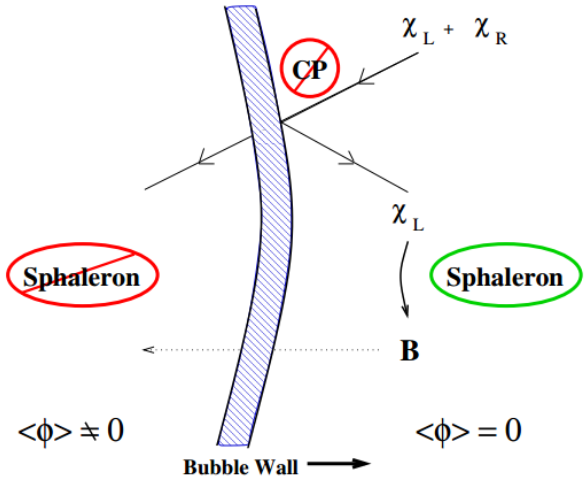

Figure 1.1: Electroweak Baryogenesis

until filling the whole space. To have baryogenesis, we need CP-violating interactions within the wall, so that when material hit the wall, the transmission and reflection coefficient is asymmetric for opposite charges. A charge asymmetry will develop in front of the wall and then this charge asymmetry would be converted into Baryon asymmetry through sphaleron process. This sphaleron process is intrinsic to SM Gauge vacuum structure. In the symmetric phase, its active but in the broken phase, its strongly suppressed by a Boltzmann factor. So when the wall passes and absorbs these newly generated baryons, this asymmetry could be preserved in the broken phase. The sphaleron rate in the symmetric phase is,

$$\Gamma(T) = \kappa(\alpha_W T)^4$$

But in the broken phase, the sphaleron process is suppressed by a Boltzmann factor,

$$\Gamma(T) = \mu(\frac{M_W}{\alpha_W T})^3 M_W^4 exp(-\frac{E_{sph}(T)}{T})$$

As we mentioned in the last paragraph, a more careful calculation shows that the SM alone is not enough to generate such a large baryon asymmetry. Firstly, even though the

CKM phase in the SM has been proved to have direct connection with the CPV observed in meson decay, it's not large enough to generate the currently observed baryon asymmetry. Second, it's confirmed that in SM, the EWPT cannot be strong first-order. In other words, a strong first-order phase transition needs the Higgs mass to be as low as 40 GeV, which is apparently inconsistent with the measurement of 125.5 GeV. Therefore both discrepancies point to the fact that we need new physics. New physics can not only provide new sources of CP violation, but also modify the Higgs effective potential through couplings between new particles and Higgs. And MSSM is a good candidate to achieve these two goals.

1.3 Thesis Outline

In this thesis, we'll focus on Electroweak Baryogenesis and especially its connection to the low-energy supersymmetric theories, such as MSSM and NMSSM. Here is the structure of this thesis work. In the first two parts, I talked about two necessary components of EWBG, the CP Violation and the strong first-order phase transition. More specifically, in the CP-Violation part, I discussed the possibility of obtaining a large enough CP-Violation within the MSSM neutral Higgs sector, how the existence of a large CP-Violation would affect the Higgs phenomenology and what's its implication for EDM experiments. In the second part, I introduced in detail our research on the most general effective Higgs potential that gives a strong first-order EW phase transition and assessed the possibility of telling the order of the EWPT by measuring the Higgs self-coupling in the future LHC experiments and thus making a bridge between cosmology and collider physics. The third part of the thesis is kind of independent from the other parts. I included here our recent work on the reversed sign of bottom Yukawa couplings and its phenomenology.

CHAPTER 2

CP VIOLATION IN THE NEUTRAL HIGGS OF MSSM

2.1 A little background of CP violaltion

From the introduction, we know that the CP violation is a necessary ingredient for the Electroweak Baryogenesis, and since SM (CKM) alone is not enough to explain the large baryon asymmetry, it then becomes a portal to new physics. Besides that, CP violation (CPV) is is also important in its own right. Throughout the history of particle physics, discoveries related to CPV have led to many spectacular progresses, e.g. CKM theory predicted the existence of three generations. What's more, the special CP-violation characteristics (also special flavor structures) confirmed in nature has put very strong constraints on new models, e.g. the smallness of EDMs in electron, neutron and Mercury has to be satisfied when constructing any new model beyond SM. At last, the CPV in the Higgs sector is an important subject. In 2012, a Higgs-like boson with mass 125.5 GeV has been discovered. But its CP nature and coupling constants are still waiting to be measured accurately. We would like to know the possible CP mixing within the Higgs sector and its relations with the Higgs couplings to fermions and W/Z gauge bosons.

CP transformation is such a transformation that in addition to taking the mirror image of the world, one also replaces each particle of matter with its anti-matter correspondent. CP invariance says that all physical processes look the same after taking the CP transformation of all participants. In 1957, parity violation was already proposed and discovered in the Co-60 β-decay experiments. Since then the charge conjugation and parity symmetries were believed to be maximally broken in the weak interactions. But the CP together might still be a good symmetry in the frame of SM. However in 1964, Christenson, Cronin, Fitch and Turlay discovered that the long-lived K meson also decays to two charged pions with a braching ratio of 2×10^{-3}, which shows that the physical eigenstates of neutral K meson are not the CP eigenstates, in other words provided indirect evidence of existence of CP

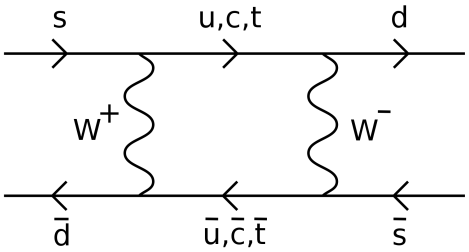

Figure 2.1: Box Diagram

violation.

Ususally people talk about 2 types of CP violation, the direct CPV and the indirect CPV. The indirect CP-violation, like the discovery in 1964, happens when the small admixture of opposite CP decays in a CP-conserving way, while in the direct CP-violation, the interference is not between two opposite CP eigenstates, but between two decay amplitudes. The K meson decay is a good example of indirect CPV. K_0 and $\overline{K}_0$ states are the strong eigenstates generated in the collider/reactor experiments and they decay through EW interactions. What's more, they can turn into each other through box diagrams as shown in Fig 2.1. The transformation between K_0 and $\overline{K}_0$ relies on the flavor changing current associated with the charged W bosons and this coupling corresponds to the off-diagonal term in the CKM matrix for example $V_{d\bar{t}}$. As we'll show right away, a non-vanishing CP violation needs a nonzero phase in it. The decay and transformation of K_0 and $\overline{K}_0$ can be described by the following matrix.

$$H = M + \frac{i}{2}\Gamma = \begin{pmatrix} H_{11} & H_{12} \\ H_{21} & H_{22} \end{pmatrix}$$

where M and Γ are hermitian matrix. It can be proved that the eigenstates of this Hamiltonian are CP eigenstates

$$|K_{1,2}\rangle = \frac{1}{\sqrt{2}}(|K_0\rangle \pm |\overline{K}_0\rangle)$$

only if $M_{12} = M_{21}$ and $\Gamma_{12} = \Gamma_{21}$, i.e. M_{12} and Γ_{12} are both real numbers. Therefore a

small CP violation can be characterized by the quantity ϵ

$$\epsilon = \frac{1}{2}\frac{\frac{1}{2}Im\Gamma_{12} + iImM_{12}}{ReM_{12} - \frac{i}{2}Re\Gamma_{12}}$$

such that the new eigenstates can be written as: $|K_S\rangle = |K_1\rangle + \epsilon|K_2\rangle$ and $|K_L\rangle = |K_2\rangle + \epsilon|K_1\rangle$. this is what physicists call indirect CP violation, where CPV happens due to a small mixing of CP-even and CP-odd components in the physical states. Here in the Kaon example, $K_{S,L}$ (short-life and long-life states) are the physical states while $K_{1,2}$ are the CP eigenstates. ϵ is the variable used to quantify the strength of an indirect CP violation. CP is conserved if ϵ is zero.

2.2 CP violations in MSSM

The Minimal Supersymmetric Extension of the Standard Model (MSSM) is an attractive scenario that leads to a well defined spectrum of particles at low energies, with dimensionless couplings that are related to the Standard Model (SM) ones by symmetry relations. For third generation superpartners with masses of the order of the TeV scale, this scenario leads to radiative electroweak symmetry breaking, it is consistent with unification of couplings at high energies [1] and in the presence of R-Parity contains a Dark Matter particle identified with the lightest neutralino [2],[3]. The Higgs sector of the theory contains two doublets, and at tree-level supersymmetry demands it to be of type-II and CP-conserving, with an upper bound on the lightest CP-even Higgs mass equal to the gauge boson mass M_Z. These properties are modified at the quantum level [4]–[23]. On one hand, as it is well known, in the absence of CP-violation, the upper bound on the lightest CP-even Higgs mass is no longer M_Z but could be raised to values of order 130 GeV for stop masses of the order of a few TeV and sizable values of the trilinear stop mass parameter A_t. The observed values of the Higgs mass may be then well explained in this scenario [24]. On the other hand, radiative corrections also induce deviations from the type-II behavior that become more prominent

for large values of the ratio of vacuum expectation values $\tan\beta$ and small values of the non-standard Higgs boson masses. In order to talk about the CPV happening inside the MSSM Higgs sector, first let's take a look at the Higgs sector of MSSM. The most general CP-violating Higgs potential of the MSSM may conveniently be described by the effective Lagrangian

$$\begin{aligned}\mathcal{L}_V &= \mu_1^2(\Phi_1^\dagger\Phi_1) + \mu_2^2(\Phi_2^\dagger\Phi_2) + m_{12}^2(\Phi_1^\dagger\Phi_2) + m_{12}^{*2}(\Phi_2^\dagger\Phi_1) + \lambda_1(\Phi_1^\dagger\Phi_1)^2 + \lambda_2(\Phi_2^\dagger\Phi_2)^2 \\ &\quad + \lambda_3(\Phi_1^\dagger\Phi_1)(\Phi_2^\dagger\Phi_2) + \lambda_4(\Phi_1^\dagger\Phi_2)(\Phi_2^\dagger\Phi_1) + \lambda_5(\Phi_1^\dagger\Phi_2)^2 + \lambda_5^*(\Phi_2^\dagger\Phi_1)^2 \\ &\quad + \lambda_6(\Phi_1^\dagger\Phi_1)(\Phi_1^\dagger\Phi_2) + \lambda_6^*(\Phi_1^\dagger\Phi_1)(\Phi_2^\dagger\Phi_1) + \lambda_7(\Phi_2^\dagger\Phi_2)(\Phi_1^\dagger\Phi_2) + \lambda_7^*(\Phi_2^\dagger\Phi_2)(\Phi_2^\dagger\Phi_1)\,. \end{aligned} \tag{2.1}$$

CP violation in the Higgs potential of the MSSM leads to mixing mass terms between the CP-even and CP-odd Higgs fields. Thus, one has to consider a (4×4)-dimensional mass matrix for the neutral Higgs bosons. In the weak basis (G^0, a, ϕ_1, ϕ_2), the neutral Higgs-boson mass matrix $\mathcal{M}_0^2$ may be cast into the form

$$\mathcal{M}_0^2 = \begin{pmatrix} \widehat{\mathcal{M}}_P^2 & \mathcal{M}_{PS}^2 \\ \mathcal{M}_{SP}^2 & \mathcal{M}_S^2 \end{pmatrix}, \tag{2.2}$$

where $\widehat{\mathcal{M}}_P^2$ and $\mathcal{M}_S^2$ describe the CP-conserving transitions $(G^0, a) \to (G^0, a)$ and $(\phi_1, \phi_2) \to (\phi_1, \phi_2)$, respectively, and $\mathcal{M}_{PS}^2 = (\mathcal{M}_{SP}^2)^T$ contains the CP-violating mixings $(G^0, a) \leftrightarrow (\phi_1, \phi_2)$. The analytic form of the submatrices is given by

$$\widehat{\mathcal{M}}_P^2 = \begin{pmatrix} -\dfrac{c_\beta T_{\phi_1} + s_\beta T_{\phi_2}}{v} & \dfrac{s_\beta T_{\phi_1} - c_\beta T_{\phi_2}}{v} \\ \dfrac{s_\beta T_{\phi_1} - c_\beta T_{\phi_2}}{v} & M_a^2 - \dfrac{s_\beta \tan\beta\, T_{\phi_1} + c_\beta \cot\beta\, T_{\phi_2}}{v} \end{pmatrix}, \tag{2.3}$$

$$\mathcal{M}_{SP}^2 = v^2 \begin{pmatrix} 0 & \mathrm{Im}(\lambda_5 e^{2i\xi})s_\beta + \mathrm{Im}(\lambda_6 e^{i\xi})c_\beta \\ 0 & \mathrm{Im}(\lambda_5 e^{2i\xi})c_\beta + \mathrm{Im}(\lambda_7 e^{i\xi})s_\beta \end{pmatrix} - \frac{T_a}{v}\begin{pmatrix} s_\beta & c_\beta \\ -c_\beta & s_\beta \end{pmatrix}, \tag{2.4}$$

$$\mathcal{M}_S^2 = M_a^2 \begin{pmatrix} s_\beta^2 & -s_\beta c_\beta \\ -s_\beta c_\beta & c_\beta^2 \end{pmatrix} - \begin{pmatrix} \frac{T_{\phi_1}}{v\, c_\beta} & 0 \\ 0 & \frac{T_{\phi_2}}{v\, s_\beta} \end{pmatrix} \tag{2.5}$$

$$-v^2 \begin{pmatrix} 2\lambda_1 c_\beta^2 + 2\mathrm{Re}(\lambda_5 e^{2i\xi}) s_\beta^2 + 2\mathrm{Re}(\lambda_6 e^{i\xi}) s_\beta c_\beta & \lambda_{34} s_\beta c_\beta + \mathrm{Re}(\lambda_6 e^{i\xi}) c_\beta^2 + \mathrm{Re}(\lambda_7 e^{i\xi}) s_\beta^2 \\ \lambda_{34} s_\beta c_\beta + \mathrm{Re}(\lambda_6 e^{i\xi}) c_\beta^2 + \mathrm{Re}(\lambda_7 e^{i\xi}) s_\beta^2 & 2\lambda_2 s_\beta^2 + 2\mathrm{Re}(\lambda_5 e^{2i\xi}) c_\beta^2 + 2\mathrm{Re}(\lambda_7 e^{i\xi}) s_\beta c_\beta \end{pmatrix}.$$

CP violation in the effective two Higgs Doublet Model (2HDM) can be induced by phases of the soft SUSY-breaking parameters at the loop level [25]–[33]. In this model, the lightest neutral Higgs is no longer a CP-eigenstate, but a mixture of CP-even and CP-odd states. The presence of CP-violation in the mass parameters of the theory is natural within the MSSM, and may be related to the mechanism that explains the baryon asymmetry in the universe [34]. The presence of CP-violation in the Higgs sector may lead to a modification of the neutral Higgs properties that may be tested at the LHC in the near future. In particular, the recently discovered Higgs boson at the LHC [35] may be the lightest of the three neutral states, with a non-vanishing CP-odd component.

Due to the current lack of observation of CP-violation observables beyond those present in the Standard Model, in particular the electron and the neutron electric dipole moments [36]–[39], large phases in the gaugino mass and the μ parameters tend to be in conflict with a light supersymmetric spectrum [40]–[47]. These restrictions may be alleviated by assuming large values of the first and second generation slepton and squark masses. Even in this case, two-loop CP-violating effects may be large enough to lead to observable CP-violating effects which may be in conflict with present experimental bounds.

In a recent article [49], the authors analyzed the CP-odd mixing of the heavy neutral states, allowed by the current flavor physics, Higgs and electric dipole moment constraints. In this article, we shall concentrate on an analysis of the CP-odd component of the lightest neutral Higgs in the MSSM, given all available constraints from both the experimental and the theoretical side (for a previous study, see Ref. [48]). We provide an analytical under-

standing of the parameters that control this CP-odd component and analyze the impact of these parameters on the Higgs observables. We shall compare these analytical results with the ones provided by CPsuperH2.3, which is used to calculate the masses of neutral Higgs, their production rates, decay widths and couplings with other particles [29, 32, 33]. Based on this analysis, we found that if the stop particles are assumed to be lighter than a few TeV, the requirement of obtaining a 125.5 GeV Higgs mass already puts a strong constraint to the parameter space and already restricts the possibility of a CP-odd mixing higher than about 10%. Moreover, the current measurements of the lightest CP-even Higgs production rates puts further constraints on this possibility and so does the non-observation of the electron, neutron and Mercury electric dipole moments. Based on these facts, we study the capability of the LHC to detect the small CP-odd components of the lightest neutral Higgs within the MSSM.

This part is organized as follows. In subsection 2.3 we describe the relevant parameters controlling the CP-violating effects in the neutral Higgs sector. In subsection 2.4 we provide analytical formulae for the neutral Higgs mass matrix elements and describe the interrelation between the CP-odd component of the lightest Higgs and its mass. In section 2.5 we describe similar constraints affecting the decay branching ratios of the lightest neutral Higgs boson. In sections 2.6 and 2.7 we discuss the constraints coming from electric dipole moments and flavor physics. We discuss the possible measurement of the lightest neutral Higgs CP-odd component at the LHC in section 2.8. We reserve section 2.9 for our conclusions.

2.3 CP-odd Component of the Lightest Neutral Higgs Boson

The CP-violating phases in the low energy 2HDM may come in the MSSM soft breaking parameters. Since these CP-violating effects are induced at the loop-level, the only relevant phases are the ones associated with supersymmetric particles that couple strongly to the Higgs bosons, namely the stops, sbottoms and staus, and the gluinos that couple strongly to these particles [25]–[33]. The relevant complex phases are then the ones of the trilinear soft

couplings of the stops, sbottoms and staus to the Higgs field, Φ_{A_t}, Φ_{A_b}, Φ_{A_τ}, respectively, the phase of the gluino mass parameter $\Phi_{M_{\tilde{g}}}$, and the one of the Higgsino mass parameter μ, Φ_μ. Besides, one should also consider the variations of the magnitude of $\tan\beta$, $|A_{t,b,\tau}|$, $|M_{\tilde{g}}|$, $|\mu|$, m_{H^+}, and the mass parameter $M_{\rm SUSY}$, that controls the overall third generation mass scale. CP-violating effects are induced by non-decoupling threshold corrections and become relevant whenever the imaginary part of $\mu A_{t,b,\tau}$ and/or of $\mu M_{\tilde{g}}$ is non-zero and of the order or larger than the square of the third generation sfermion masses, which we shall assume to be of the order of a few TeV.

Our objective is to study regions of parameter space in which a large CP-odd component of the lightest neutral Higgs is present. Since this component may only be induced by mixing between the would-be CP-even and CP-odd Higgs states, it is clear that the heavier neutral Higgs bosons should be light, with masses not much larger than the weak scale. Such values of the non-standard Higgs boson masses lead naturally to large variations of the fermion couplings to the lightest neutral Higgs with respect to the Standard Model ones, and also leads to a reduction of the lightest neutral Higgs mass via the mixing with the other neutral states.

In the analysis of the parameters of the model, we shall require the mass of the lightest neutral state to be consistent with the measured value of about 125.5 GeV. Due to theoretical uncertainties in the calculation of the neutral Higgs masses, which is of the order of 3 GeV, we shall retain values of the parameters which lead to a Higgs mass between 122.5 and 128.5 GeV. Moreover, the bottom and tau couplings of the lightest Higgs boson cannot differ significantly from the ones of the SM without leading to significant variations of the Higgs decay branching ratios, in conflict with observations at the ATLAS and CMS experiments. In general, since the electroweak gauge boson couplings of the lightest Higgs tend to be close to the SM ones, variations of the effective bottom coupling $g_{H_1 b\bar{b}}$ of more than about 20% with respect to the SM (leading to variations of the branching ratio of the decay of the Higgs boson to pairs of gauge bosons of about 30%) are disfavored by data.

Although currently only one Higgs boson has been detected, there is information on the possible presence of additional Higgs bosons within the MSSM due to the non-observation of non-standard Higgs signatures. Currently, the strongest bounds on the presence of non-standard neutral Higgs bosons come from the searches of the gluon fusion or $bb\Phi$ production of heavy neutral Higgs bosons at the LHC, with subsequent decays into tau pairs [50],[51],[52]. These searches become particularly efficient for large values of $\tan\beta$ and low values of the charged Higgs mass m_{H^+}, for which the production rate is large. These searches, combined with previous LEP results, gave a strong constraint on the $\tan\beta - M_A$ two dimensional plane (CP-violation was not considered in the LHC analyses). A small window of $\tan\beta$ survives in lower-M_A region, where larger CP-violation is most likely to arise. In particular, for non-standard Higgs boson masses of the order of the weak scale, values of $\tan\beta > 10$ are strongly restricted by the searches performed by the CMS and ATLAS experiments.

2.4 Constraints on CP violation in the Higgs sector from the lightest neutral Higgs mass

Since the LHC has measured a Higgs boson with mass around 125.5 GeV, it is natural to identify it with the lightest neutral Higgs boson, which tends to have SM-like properties when masses of the heavier Higgs bosons are larger than 200 GeV. For stop masses of the order of a few TeV, this strongly restricts the plausible MSSM parameter space. As the charged Higgs mass goes up, the lightest CP-even Higgs mass depends mostly on $|X_t|$, with $X_t = A_t - \mu^*/\tan\beta$ [25]–[31]. For values of the stop masses of the order of a few TeV a maximum value of the order of 130 GeV is obtained for values of $|X_t|$ of about 2.4 $M_{\rm SUSY}$, for large values of the charged Higgs mass, and goes smoothly down for smaller values of m_{H^+}. Thus acceptable values of the Higgs mass are obtained for values of $|X_t|$ larger than $M_{\rm SUSY}$ but not larger than $3M_{\rm SUSY}$. For values of $|X_t|$ larger than 3 $M_{\rm SUSY}$ the lightest CP-even Higgs mass decreases sharply and, in addition, problems with vacuum stability may

be generated [53].

To explore the correlation between the CP-odd component and the mass of the lightest Higgs, we'll start from the 3×3 mass matrix, defining the mixing between the would-be CP-even components of the two Higgs doublets and the CP-odd Higgs boson in the absence of CP-violating effects, ϕ_1, ϕ_2 and a, respectively. Let's separate out the tree-level terms and investigate the contributions from the CP-violating phases, taken as small perturbations here, to see how those perturbations affect the mass eigenstates of the neutral Higgs sector. The full mass matrix can be written as,

$$M^2 = M^2_{Tree} + M^2_{Loop} \tag{2.6}$$

$$= \begin{pmatrix} M_a^2 s_\beta^2 + M_z^2 c_\beta^2 & -(M_a^2 + M_z^2) s_\beta c_\beta & 0 \\ -(M_a^2 + M_z^2) s_\beta c_\beta & M_a^2 c_\beta^2 + M_z^2 s_\beta^2 & 0 \\ 0 & 0 & M_a^2 \end{pmatrix} + \begin{pmatrix} \Delta_{11} & \Delta_{12} & \delta_1 \\ \Delta_{21} & \Delta_{22} & \delta_2 \\ \delta_1 & \delta_2 & 0 \end{pmatrix} \tag{2.7}$$

where δ_i,Δ_{ij} can be considered as perturbations and we'll investigate their effects on Higgs mass in the following. With the relative phase ξ between the two Higgs doublets set to be zero, δ_i, Δ_{ij} can be expanded as follows,

$$\begin{aligned} \delta_1 &= v^2(Im(\lambda_5) s_\beta + Im(\lambda_6) c_\beta) \\ \delta_2 &= v^2(Im(\lambda_5) c_\beta + Im(\lambda_7) s_\beta) \\ \Delta_{11} &= -v^2(2\lambda_1 c_\beta^2 + 2Re(\lambda_5) s_\beta^2 + 2Re(\lambda_6) s_\beta c_\beta) - M_Z^2 c_\beta^2 \\ \Delta_{12} = \Delta_{21} &= -v^2(\lambda_{34} s_\beta c_\beta + Re(\lambda_6) c_\beta^2 + Re(\lambda_7) s_\beta^2) + M_Z^2 s_\beta c_\beta \\ \Delta_{22} &= -v^2(2\lambda_2 s_\beta^2 + 2Re(\lambda_5) c_\beta^2 + 2Re(\lambda_7) s_\beta c_\beta) - M_Z^2 s_\beta^2 \end{aligned} \tag{2.8}$$

The values of the quartic couplings may be found in Ref. [27]. In order to understand the main effects, we should go to the Higgs basis ($\{\phi_1, \phi_2\} \to \{h_1, h_2\}$) by rotating by the angle β, which becomes the proper diagonalization angle in the decoupling limit. The transformation matrix O links the 3 neutral Higgs further with their mass eigenstates by $\{h_1, h_2, a\}^T =$

$O\{H_1, H_2, H_3\}^T$, thus H_1 can be expanded as $H_1 = O_{11}h_1 + O_{21}h_2 + O_{31}a$. In this case, we get,

$$
\begin{aligned}
& OM^2_{\text{diag}}O^T \\
&= \begin{pmatrix} M_Z^2\cos^2 2\beta & M_Z^2\cos 2\beta\sin 2\beta & 0 \\ M_Z^2\cos 2\beta\sin 2\beta & \left(m_a^2 + M_Z^2\sin^2 2\beta\right) & 0 \\ 0 & 0 & m_a^2 \end{pmatrix} \\
&+ \begin{pmatrix} c_\beta & s_\beta & 0 \\ -s_\beta & c_\beta & 0 \\ 0 & 0 & 1 \end{pmatrix} \begin{pmatrix} \Delta_{11} & \Delta_{12} & \delta_1 \\ \Delta_{12} & \Delta_{22} & \delta_2 \\ \delta_1 & \delta_2 & 0 \end{pmatrix} \begin{pmatrix} c_\beta & -s_\beta & 0 \\ s_\beta & c_\beta & 0 \\ 0 & 0 & 1 \end{pmatrix}
\end{aligned}
$$

$$
= \begin{pmatrix} M_Z^2\cos^2 2\beta + \eta & \theta & \xi_2 \\ \theta & m_a^2 + M_Z^2\sin^2 2\beta + \rho & \xi_1 \\ \xi_2 & \xi_1 & m_a^2 \end{pmatrix} \tag{2.9}
$$

where M^2_{diag} is the eigenvalue matrix and

$$
\begin{aligned}
\xi_1 &= -\delta_1 s_\beta + \delta_2 c_\beta \\
\xi_2 &= \delta_1 c_\beta + \delta_2 s_\beta \\
\theta &= (\Delta_{22} - \Delta_{11})\sin\beta\cos\beta + \Delta_{12}\cos 2\beta - M_Z^2\cos 2\beta\sin 2\beta \\
\eta &= \Delta_{11}c_\beta^2 + \Delta_{22}s_\beta^2 + \Delta_{12}\sin 2\beta
\end{aligned} \tag{2.10}
$$

In the result of equation(4), we can see that the final corrections to $m^2_{H_1}$ come from the three terms, ξ_2, θ, η. In this limit, ξ_2 defines the strength of the mixing between a and h, i.e. it fixes the CP-odd component of the lightest Higgs. Defining the parameter

$Y_t = A_t + \mu^* \tan\beta$, one can demonstrate that, at one loop

$$\eta = \frac{3h_t^4 v^2 \sin^4\beta}{8\pi^2}\left[\log\left(\frac{M_{\rm SUSY}^2}{m_t^2}\right) + \frac{|X_t|^2}{M_{\rm SUSY}^2}\left(1 - \frac{|X_t|^2}{12\ M_{\rm SUSY}^2}\right)\right] \tag{2.11}$$

$$\begin{aligned}\theta = -M_Z^2 \cos 2\beta \sin 2\beta + \frac{3h_t^4 v^2 \sin^2\beta \sin 2\beta}{16\pi^2}\left[\log\left(\frac{M_{\rm SUSY}^2}{m_t^2}\right)\right. \\ \left. + \frac{|X_t|^2}{2M_{\rm SUSY}^2} + {\rm Re}\left(\frac{X_t Y_t^*}{2M_{\rm SUSY}^2}\left(1 - \frac{|X_t|^2}{6M_{\rm SUSY}^2}\right)\right)\right]\end{aligned} \tag{2.12}$$

$$\xi_2 = {\rm Im}\left(\frac{3h_t^4 v^2 \sin^2\beta \sin 2\beta}{32\pi^2}\left[\frac{X_t Y_t^*}{M_{\rm SUSY}^2}\left(1 - \frac{|X_t|^2}{6M_{\rm SUSY}^2}\right)\right]\right) \tag{2.13}$$

where $v \simeq 246$ GeV is the Higgs vacuum expectation value. The above equations provide a generalization of the expressions for the Higgs mixing parameters in terms of X_t and Y_t in the CP-conserving case [54]. The parameter η displays the well known one-loop radiative corrections to the lightest (would be CP-even) Higgs mass, which are maximized for values of the stop mixing parameter $|X_t| = \sqrt{6}\ M_{\rm SUSY}$. Notoriously, for the same values of the stop mixing parameter the parameter ξ_2 vanishes. Hence, a sizable CP-odd component of the lightest neutral Higgs boson is always associated with departures from the maximal values of its mass.

The above property is clearly shown in Figures 2.2 and 2.3 where we display the value of the CP-odd component of the lightest neutral Higgs against its mass, obtained by the CPsuperH code [32],[33]. for two different values of $\tan\beta$ and the charged Higgs boson mass, consistent with the current experimental bounds coming from direct searches for non-standard Higgs bosons at the LEP and LHC experiments. During this procedure, $400,000$ points were randomly generated and uniformly scattered all over the space spanned by the relevant parameters. We choose the values of the supersymmetry breaking parameter $M_{\rm SUSY} = 2$ TeV and the rest of the parameters were varied in the following ranges : A_t from 2 TeV to 6 TeV, $|\mu|$ from 2 TeV to 6 TeV, Φ_{M_3}, Φ_A, Φ_μ, Φ_{M_2} from -180° to $+180^\circ$, $|M_3|$

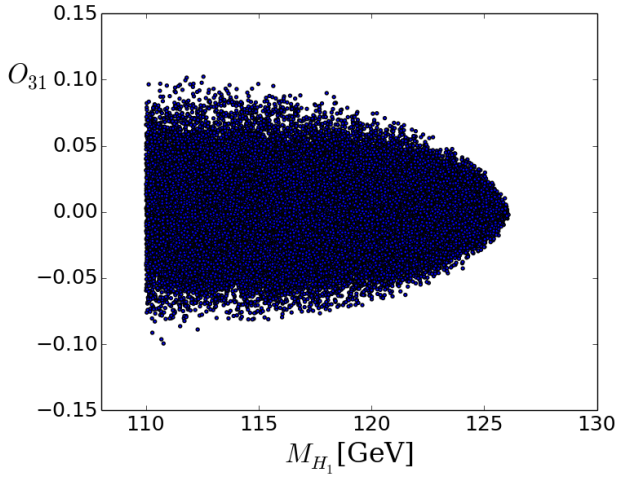

Figure 2.2: Correlation between the H_1 CP-odd component and its mass for $\tan\beta = 5.5$ and a charged Higgs mass $M_{H^+} = 260$ GeV. The moduli and phases of all relevant parameters A_f, $M_{\tilde{g}}$ and μ were varied in the range explained in the text and the overall stop mass scale $M_{\rm SUSY}$ was fixed at 2 TeV.

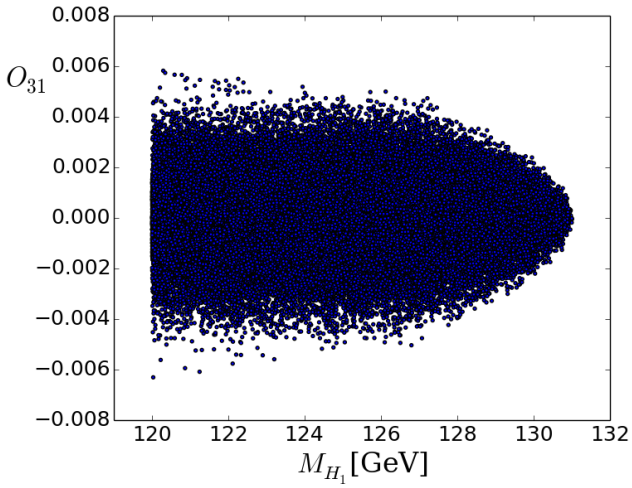

Figure 2.3: Correlation between the H_1 CP-odd component and its mass for $\tan\beta = 20$ and a charged Higgs mass $M_{H^+} = 800$ GeV. The moduli and phases of all relevant parameters A_f, $M_{\tilde{g}}$ and μ were varied in the range explained in the text and the overall stop mass scale $M_{\rm SUSY}$ was fixed at 2 TeV.

from 500 GeV to 3 TeV. The hierarchy factor ρ, denoting the difference between the masses of the first and second generation sfermions and the third generation ones plays only a small role in this analysis and was chosen to be equal to one. From this plot we see that there is an upper limit for the lightest neutral Higgs mass around 127 GeV for a charged Higgs mass, $M_{H^+} = 260$ GeV and $\tan\beta = 5.5$, which increases to 131 GeV for a larger $M_{H^+} = 800$ GeV and $\tan\beta = 20$. These maximal values arise with zero CP-odd component in Higgs sector, as expected from our discussion above.

For values of $|X_t|/M_{\rm SUSY} \neq \sqrt{6}$, the value of ξ_2 may increase and the CP-odd component of the lightest neutral Higgs may be sizable. However, the parameter η is pushed to lower values lowering the Higgs mass. Moreover, the existence of large ξ_2 or θ, no matter positive or negative, will drag $m^2_{H_1}$ further down due to mixing effects. That's the reason why we have a anti-correlation between CP-violation and Higgs mass in the MSSM.

In Figures 2.2 and 2.3 , as before, the CP-odd component was defined to be O_{31}. As the mass goes down, the CP-odd component may increase but is constrained by the requirement of obtaining agreement with the measured Higgs mass value. Although one obtains larger values of m_{H_1} for $M_{H^+} = 800$ GeV the parabola-like upper limit on the CP-odd component of the lightest Higgs is much sharper, which implies much smaller CP-odd components in the acceptable Higgs mass range. Such a behavior is not surprising, and reflects the decrease of the mixing angle O_{31} with the charged Higgs mass, namely

$$O_{31} \simeq -\xi_2/M^2_{H^+}. \tag{2.14}$$

Rewriting the above equation in terms of the mass parameters μ and A_t, from Eq. (2.13) one finds

$$O_{31} \propto -\frac{3h_t^4 v^2 \sin^4\beta}{16\pi^2 m^2_{H^+}} \frac{{\rm Im}(\mu A_t)}{M^2_{\rm SUSY}} \left(1 - \frac{|X_t|^2}{6M^2_{\rm SUSY}}\right), \tag{2.15}$$

where we have neglected subleading terms, suppressed by $1/\tan^2\beta$ factors.

Therefore, the largest CP-violating effects that can be generated at larger m_{H^+} is when

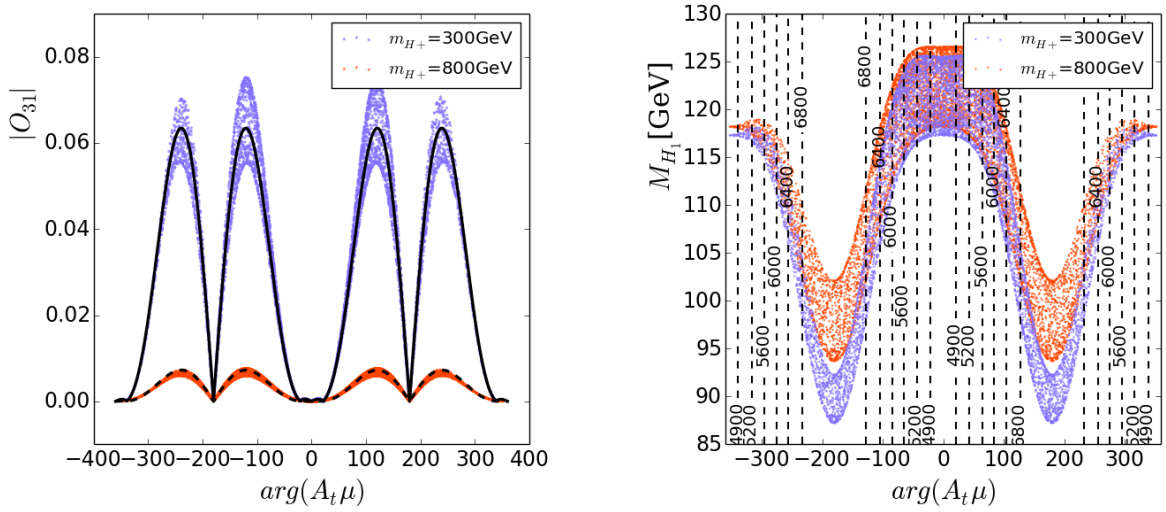

Figure 2.4: CP-odd component of H_1 and M_{H_1} as a function of the phase of $A_t\mu$, for $|A_t| = |\mu| = 3\ M_{\rm SUSY}$ and for values of other relevant parameters varied in the ranges given in the text. The blue and red points represent the values obtained for $M_{H^+} = 300$ GeV and 800 GeV, respectively. The solid and dashed black lines in the left panel are the estimated value of the H_1 CP-Odd component by using Eq. (2.15), with h_t evaluated at the M_{H^+} scale, for $M_{H^+} = 300$ GeV and 800 GeV, respectively. The dashed contour lines in the right panel represent the values of $|X_t|$/GeV. The overall supersymmetry breaking stop mass scale $M_{\rm SUSY}$ was fixed to 2 TeV.

$|A_t|$ and $|\mu|$ acquire large values, while the angle $\arg(\mu A_f)$ is fixed to give the largest possible value of the $\mathrm{im}(\mu A_t)$, but still rendering X_t at acceptable values to obtain the proper Higgs mass. For smaller values of the charged Higgs mass, the $\arg(\mu A_f)$ tends to be pushed to lower values, in order to reduce the mixing effects and keep the Higgs mass in an acceptable range.

To confirm this intuition, we swept the phases of μ and A_f from $-180°$ to $+180°$ but fixed the modulus of both μ and A_f to large values, $|\mu| = |A_f| = 3M_{\rm SUSY}$, with $M_{\rm SUSY} = 2$ TeV and $\tan\beta = 5$. The gaugino masses were fixed to $M_1 = 200$ GeV, $M_2 = 200$ GeV and $M_3 = 2.7$ TeV and the phases of three gaugino mass terms were fixed to zero. The left panel of Figure 2.4 shows the variation of the lightest neutral Higgs boson CP-odd component with the $\arg(\mu A_t)$. We see that, if the Higgs mass constraint is ignored, a maximum of the CP-odd component is obtained for phases larger than 90 degrees, actually near 120 degrees.

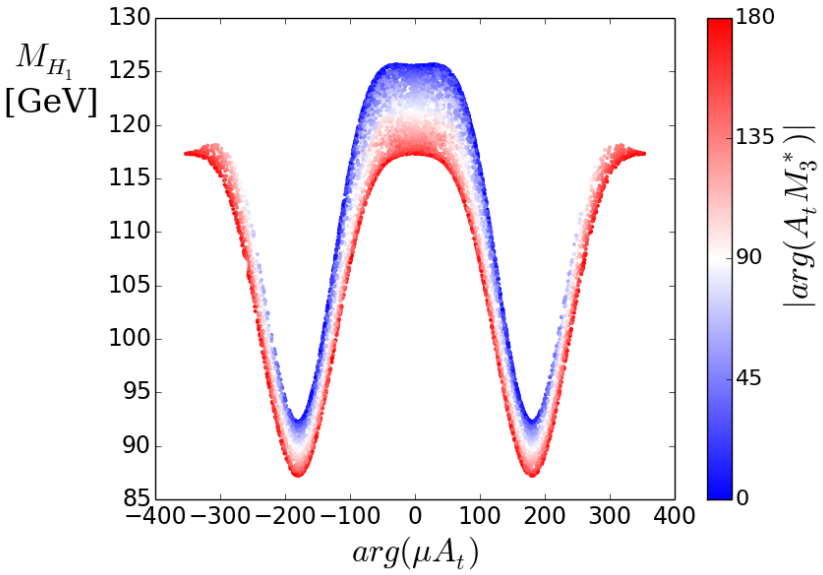

Figure 2.5: Values of the Higgs mass for $M_{H^+} = 300$ GeV, corresponding to the right panel of Fig. 2.4, but with the scattered points colored according to the value of $\arg(A_t M_3^*)$. The subdominant dependence of the Higgs mass on $\arg(A_t M_3^*)$ explains the spread of the Higgs mass values in Fig. 2.4. We can see an enhancement of Higgs mass when $\arg(A_t M_3^*) = 0$ and a minimum for values of $\arg(A_t M_3^*) = \pm 180°$.

The reason for that lies in Eq.(2.15). The dependence of O_{13} on this phase is parametrized by the multiplication of two terms, $\mathrm{Im}(\mu A_t)$ and $\left(1 - |X_t|^2/(6\ M^2_{\mathrm{SUSY}})\right)$. It is easy to show that for the parameters chosen the maximum moves away from a phase of 90 degrees, since larger values of the product of these terms may be obtained by decreasing $\mathrm{Im}(\mu A_t)$ but increasing the second term. The analytical extremes for $|\mu| = |A_t| = 3M_{\mathrm{SUSY}}$ and $\tan\beta = 5$ are located at values of $\phi_{A\mu} \equiv \arg(\mu A_t)$ such that $\cos\phi_{A\mu} \simeq -0.5$ and $\cos\phi_{A\mu} \simeq 0.94$. This correspond to $\arg(\mu A_t) \simeq 120°$ and $240°$ (maxima), and $20°$ and $340°$ (minima), respectively. To verify this effect, we plotted Eq. (2.15) as a function of $\arg(\mu A_t)$ on top of the left panel of Fig. (2.4) (the dashed line for $m_{H^+} = 800$ GeV and the solid line for $m_{H^+} = 300$ GeV). In each case, the top Yukawa coupling was chosen at the charged Higgs mass scale. We find that Eq. (2.15) describes within a good approximation the lightest neutral Higgs CP-odd component computed by CPsuperH.

Consistency with the observed Higgs mass puts additional constraints on $\arg(\mu A_t)$. The

right panel of Figure 2.4 shows the strong dependence of the Higgs mass on the amplitude of X_t for both $m_{H^+} = 300$ GeV and $m_{H^+} = 800$ GeV. Since $M_{\rm SUSY} = 2\ TeV$, the maximization of Higgs mass occurs close to $|X_t| = 4.8$ TeV, about 2.4 $M_{\rm SUSY}$, which is consistent with our analysis above and for $|\mu| = |A_t| = 3M_{\rm SUSY}$ and $\tan\beta = 5$ corresponds to a phase of μA_t close to zero. As the phase increase the CP-odd component increases, but the Higgs mass decreases. In order to keep the Higgs mass within the acceptable range, one needs $|X_t| < 6$ TeV, and should keep $|\arg(\mu A_t)|$ below 80 degrees, putting a bound on the possible CP-odd component of the lightest Higgs boson. This bound is about 5 percent in the particular case of $M_{H^+} = 300$ GeV.

Observe that the Higgs mass is not a single-valued function of $|X_t|$ but for each $|X_t|$ the Higgs mass values are within a broad band, which is due to the fact that there are small changes in the lightest Higgs mass induced by the variation in the phase of $A_t M_3^*$, and mostly coming from threshold corrections to the top Yukawa coupling. An example of this variation is shown in Figure 2.5, where we show that indeed, besides the overall dependence on X_t, which is fixed by the phase of μA_t, there is a dependence on the phase of $A_t M_3^*$ leading to larger Higgs mass values for these phases equal to zero. Observe that, since this effect does not depend on the sign of the $\arg(A_t M_3^*)$, in Figure 2.5 we present the results as a function of $|\arg(A_t M_3^*)|$.

2.5 Constraints from the Higgs H_1 branching ratios

As stressed above, a large CP-odd component of the lightest neutral Higgs may only be obtained for low values of the charged Higgs mass. Such values of the charged Higgs mass lead in general to large mixings not only with the would-be CP-odd Higgs but also between the two would-be CP-even Higgs bosons. Since the would-be CP-odd Higgs and the heavier would-be CP-even Higgs have $\tan\beta$ enhanced couplings to the down fermions, in general one expects significant deviations of the down couplings of the lightest neutral Higgs with respect to the SM one. This can be seen by writing the down-quark couplings [30], normalized to

the SM values, in the Higgs basis

$$\begin{aligned} g^S_{H_1dd} &= \frac{1}{h_d+\delta h_d+\Delta h_d\tan\beta}\left\{ Re(h_d+\delta h_d)\frac{-\sin\beta O_{21}+\cos\beta O_{11}}{\cos\beta}\right. \\ &\left. + Re(\Delta h_d)\frac{O_{21}\cos\beta+O_{11}\sin\beta}{\cos\beta} - [Im(h_d+\delta h_d)\tan\beta - Im(\Delta h_d)]\,O_{31}\right\} \quad (2.16) \end{aligned}$$

$$\begin{aligned} g^P_{H_1dd} &= \frac{1}{h_d+\delta h_d+\Delta h_d\tan\beta}\left\{ (Re(\Delta h_d) - Re(h_d+\delta h_d)\tan\beta)\,O_{31}\right. \\ &\left. - Im(h_d+\delta h_d)\frac{-\sin\beta O_{21}+\cos\beta O_{11}}{\cos\beta} - Im(\Delta h_d)\frac{O_{21}\cos\beta+O_{11}\sin\beta}{\cos\beta}\right\} \quad (2.17) \end{aligned}$$

where we have assumed that

$$h_d+\delta h_d+\Delta h_d\tan\beta = \frac{m_d\sqrt{2}}{v} \quad (2.18)$$

is real and positive. For moderate or small values of $\tan\beta$ one can in a first approximation ignore the small radiative correction effects and, hence

$$\begin{aligned} g^S_{H_1dd} &\simeq O_{11} - \tan\beta\; O_{21} \\ g^P_{H_1dd} &\simeq -O_{31}\tan\beta. \end{aligned} \quad (2.19)$$

Then, as anticipated, the corrections to the down-quark and charged lepton couplings are proportional to the non-standard components of the lightest neutral Higgs, O_{21} and O_{31}, but enhanced by a $\tan\beta$ factor. Morever, while O_{31} is approximately given by Eq. (2.14),

$$O_{21} \simeq -\frac{\theta}{m^2_{H^+}}. \quad (2.20)$$

As we can see from Fig.2.6, the scalar coupling of the lightest Higgs boson, $g^S_{H_1b\bar{b}}$, normalized to its SM value, can grow significantly when m_{H^+} is pulled down. Large deviations, however, are in tension with current experimental measurements [55],[56],[57] that show a

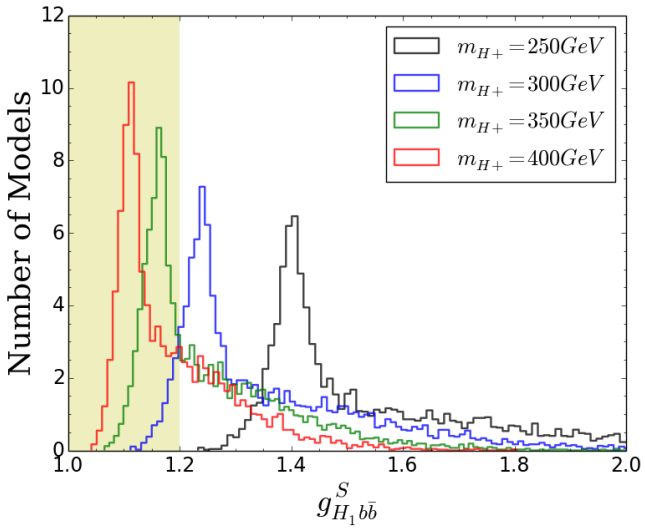

Figure 2.6: $g^S_{H_1 b\bar{b}}$ coupling for different values of m_{H^+}. We have fixed $|A_f| = 3M_{SUSY}$= 6 TeV; varying $|\mu|$ from 2 to 6TeV, and $\Phi_A, \Phi_{M2}, \Phi_{M3}, \Phi_\mu$ from $-180°$ to $180°$.

good agreement of the Higgs production rates with the SM predictions.

Since we are considering the possibility of sizable values of ξ_2 (the CP-odd component), the deviations from SM Higgs branching ratios may be minimized if θ, which controls the mixing between two CP-even components, is kept small. Small values of θ correspond to the condition of alignment in the case of CP-conservation [54],[58],[59] and can be achieved for moderate values of $\tan\beta \simeq \mathcal{O}(10)$ if $|\mu|/M_{\rm SUSY}$ and $|A_t|/M_{\rm SUSY}$ become sizable. However, as we shall see, for alignment to happen with $|A_t|$ and $|\mu|$ smaller than 3 $M_{\rm SUSY}$, $\mathrm{Re}(A_t\mu)$ must be maximized. Since maximal values of this quantity are obtained for small values of $\mathrm{Im}(A_t\mu)$ controlling the CP-odd component of the lightest Higgs, there must be some correlation between the CP-odd component of H_1 and the deviation of the H_1 down quark couplings with respect to the SM-ones. We can obtain an analytical understanding of this correlation by approximating the mass of the lightest Higgs by

$$m^2_{H_1} \simeq M^2_Z \cos^2 2\beta + \eta, \tag{2.21}$$

with η given in Eq. (2.11). This is what happens for small or moderate mixing in the neutral

Higgs sector. One can now rewrite Eqs. (2.12) and (2.13) as

$$\theta = \frac{1}{\tan\beta}\left[-M_Z^2\cos 2\beta + m_{H_1}^2 + \frac{3h_t^4 v^2 \sin^4\beta}{16\pi^2}\mathrm{Re}\left(\frac{X_t(Y_t^* - X_t^*)}{M_{\mathrm{SUSY}}^2}\left(1 - \frac{|X_t|^2}{6M_{\mathrm{SUSY}}^2}\right)\right)\right], \tag{2.22}$$

$$\xi_2 = \frac{1}{\tan\beta}\frac{3h_t^4 v^2 \sin^4\beta}{16\pi^2}\mathrm{Im}\left(\frac{X_t(Y_t^* - X_t^*)}{M_{\mathrm{SUSY}}^2}\left(1 - \frac{|X_t|^2}{6M_{\mathrm{SUSY}}^2}\right)\right). \tag{2.23}$$

Since for moderate or large values of $\tan\beta$, $X_t \simeq A_t$, $Y_t^* - X_t^* \simeq \mu\tan\beta$ and $\cos 2\beta \simeq -1$, one can see that the parameter θ can only be reduced if the real part of a loop suppressed quantity proportional to $\mathrm{Re}(A_t\mu)$ is of order of $m_{H_1}^2 + M_Z^2$. This loop suppressed quantity is the same one whose imaginary part controls the CP-odd component. Hence, when ξ_2 becomes sizable, quite generally θ cannot be suppressed and becomes also sizable. Therefore, from Eqs. (2.14), (2.20) and (2.19), we conclude that a significant CP-odd component in general leads to large deviations of the bottom coupling to H_1 with respect to the SM value.

The deviation of the H_1 couplings to the gauge bosons with respect to the SM ones depend on O_{21}^2 and O_{31}^2, which are in general small quantities, much smaller than the parameters controlling the deviation of the bottom and tau couplings. It is then expected that for moderate or large values of $\tan\beta$ the variation in the $\mathrm{BR}(H_1 \to VV)$, with $V = W, Z, \gamma$, is mainly governed by the variation of the bottom quark coupling to H_1. The deviation in H_1 down quark coupling with respect to the SM can then be inferred by the observed branching ratios of the lightest neutral Higgs to gauge bosons, namely $H \to WW^*$, $H \to ZZ^*$,$H \to \gamma\gamma$, which have been measured at the LHC up to rather high confidence level [55],[56],[57].

We calculated the $H \to ZZ^*$ branching ratio in the MSSM using CPSuperH2.3 and also its value predicted by the SM for the same Higgs mass. We plotted the correlation between the CP-odd component of H_1 and its decay branching ratio into Z gauge bosons. In the left panel of Fig. 2.7 we show the dependence of these quantities on the variables $\tan\beta$ and Φ_μ. $\tan\beta$ is varied from 4.0 to 10.0 and Φ_μ from -180° to 180°. Other parameters are chosen to maximize the Higgs mass i.e. $\arg(A_t M_{\tilde{g}}^*) \simeq 0$, (in this particular example the choice of $\Phi_A = -177.9^\circ$ and $\Phi_{M_{\tilde{g}}} = 173.9^\circ$ came from a scan of parameters to be presented

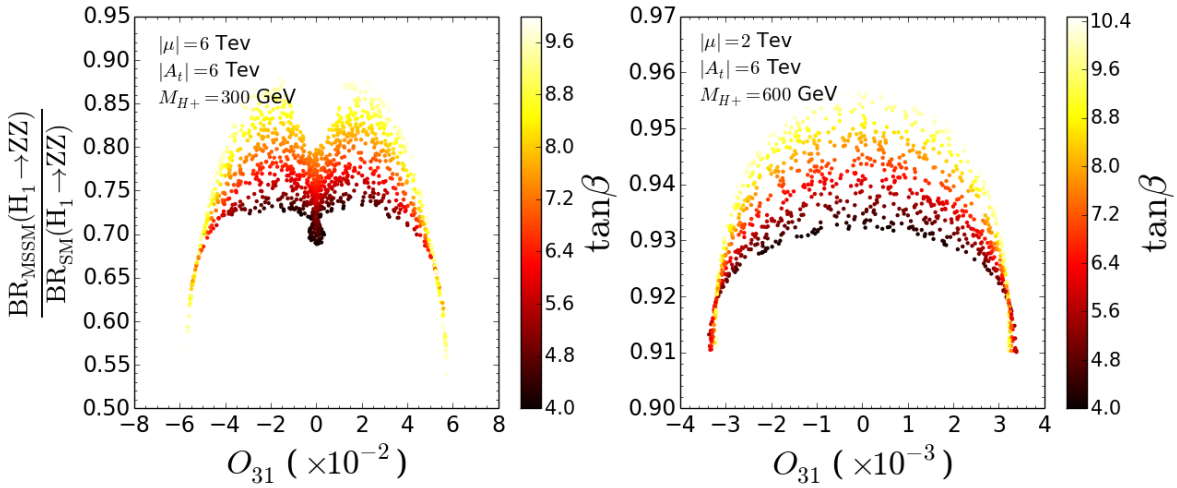

Figure 2.7: Correlation between the CP-odd component of H_1 and the H_1 decay branching ratio in the ZZ channel. The left panel shows the case when $m_{H^+} = 300$ GeV, $|\mu| = 3M_{\rm SUSY}$=6 TeV, while the right panel corresponds to $m_{H^+} = 600$ GeV and $|\mu| = M_{\rm SUSY}$=2 TeV. In both scans, we have varied the phase of μ and the value $\tan\beta$, while the rest of the relevant parameters were fixed to the values shown on the plot. All points shown here satisfy our M_{H_1} constraint(122.5-128.5 GeV). The different colors represent different values of $\tan\beta$.

below). Seen from this plot, the variation of $\tan\beta$ determines the shape of the arch, while Φ_μ explains the spreading along the axis of the CP-odd component. A correlation between the lightest Higgs boson CP-odd component and its branching ratio into gauge bosons is thus observed for each independent $\tan\beta$, more specifically, the larger CP-odd component is chosen, the lower becomes the branching ratios, i.e. the more deviated from the SM values. The requirement that these branching ratios do not deviate by more than 30% of the SM values sets a constraint for the CP-odd component of H_1, which according to Fig. 2.7 is tightly below 5% for $M_{H^+} = 300$ GeV.

For comparison, in the right panel of Fig. 2.7 we present the results for smaller values of $|\mu|$ and larger values of the charged Higgs mass, namely $|\mu| = M_{\rm SUSY} = 2$ TeV and $m_{H^+} = 600$ GeV. The value of the stop mixing parameter was kept at $|A_t| = 3\ M_{\rm SUSY}$. The values of the CP-odd component are reduced by an order of magnitude with respect to the case described in the left panel, as it is expected from the fact that O_{31} is proportional

to $|\mu|/m^2_{H^+}$. There is an additional small reduction, associated with the fact that for this value of $|\mu|$ the possible range of $\Phi_{A_t\mu}$ required to obtain values of $|X_t|$ consistent with the m_{H_1} constraints is smaller than in the previous case. On the other hand, the branching ratio $BR(H_1 \to ZZ)$ becomes closer to the SM value. Due to the correlation between O_{13} and the deviation of the H_1 decay branching ratios with respect to the SM ones discussed above, if in the future LHC constrains the H_1 decay branching ratios to be closer to the SM ones, this will lead to further constraints on the possible CP-odd component of H_1. In the following, we shall concentrate on finding the maximal value of the CP-violating phase consistent with present constraints.

Under the above considerations, a careful scan of the whole parameter space was conducted to find the maximum CP-odd component of H_1. In order to maximize it, we chose as low values of m_{H^+} as possible and for each fixed m_{H^+} we scan $\tan\beta$ within the area not excluded by heavy Higgs boson searches. Since all what matters are relative phases, and the CP-violating effects are maximized for large values of $|\mu A_t|$, we fixed $M_Q = M_U = M_D = M_{\rm SUSY} = 2$ TeV, $|\mu| = |A_t| = 3\, M_{\rm SUSY}$, $M_1 = 0.2$ TeV, $M_2 = 0.2$ TeV. All five varied parameters can be found in the table. The maximal CP-odd component for each scan is listed in Table 2.1 and 2.2.

In Table 2.1, we show the results without including the constraints from the H_1 branching ratios. For all values of m_{H^+}, the larger CP-odd component of H_1 is obtained when the lightest Higgs mass reached the lower bound we have set, i.e. 122.5 GeV, due to the tension between a large CP-odd component and a large enough H_1 mass we have proved before. As m_{H^+} goes up, we see that $\Phi_{\mu A_f}$ is moving closer to 120° (or 240°). That's because m_{H^+} is bringing up the mass of the lightest Higgs and allowing more fluctuation range in $\Phi_{\mu A_f}$. However the value of the H_1 CP-odd component gets lower because the suppression coming for a larger m_{H^+} greatly compensates the impact of a larger phase $\Phi_{\mu A_f}$.

In Table 2.2, we added the constraint on the H_1 decay branching ratios, which lead to somewhat smaller CP-odd components for each fixed m_{H^+}. For $m_{H^+} = 250$ GeV and

Table 2.1: Maximum CP-odd(only mass constraint)

m_{H^+}(fixed)	$\tan\beta$	Φ_{A_f}	Φ_μ	$\lvert M_{\tilde{g}}\rvert$	$\Phi_{M_{\tilde{g}}}$	$\Phi_{\mu A_f}$	CP-odd	Mass	$\frac{BR_{\rm MSSM}(H_1\to ZZ)}{BR_{\rm SM}(H_1\to ZZ)}$
250	8.0	158.2°	114.0°	3000.0	134.0°	272.2°	8.87%	122.6	0.469
300	9.2	98.8°	2.67°	3000.0	108.6°	101.5°	5.72%	122.6	0.555
350	9.0	138.2°	115.9°	3000.0	129.5°	254.1°	3.87%	122.5	0.656
400	8.7	66.6°	39.3°	3000.0	76.5°	106.0°	2.81%	122.6	0.739

Table 2.2: Maximum CP-odd (mass + Boson coupling constraints)

m_{H^+}(fixed)	$\tan\beta$	Φ_{A_f}	Φ_μ	$\lvert M_{\tilde{g}}\rvert$	$\Phi_{M_{\tilde{g}}}$	$\Phi_{\mu A_f}$	CP-odd	Mass	$\frac{BR_{\rm MSSM}(H_1\to ZZ)}{BR_{\rm SM}(H_1\to ZZ)}$
250	8.3	18.3°	-78.1°	3000.0	17.7°	300.2°	4.83%	126.6	0.703
300	9.5	-177.9°	-94.0°	3000.0	173.9°	88.1°	5.01%	124.4	0.701
350	7.8	-44.3°	-53.8°	3000.0	-52.1°	261.9°	3.80%	122.6	0.709
400	8.7	66.6°	39.3°	3000.0	76.5°	106.0°	2.81%	122.6	0.739

300 GeV, we see the branching ratio bound dominates the selection of the right Higgs mass and for the maximum H_1 CP-odd components, the Higgs mass tends to be pushed away from its theoretical lower bound. For $m_{H^+} = 350\ GeV$ and 400 GeV, instead, the Higgs mass is still the main constraint for CP violation. The maximum value of the CP-odd component appears for charged Higgs masses of about 300 GeV given both constraints. The trend in $\Phi_{\mu A_f}$ is the same as that in table 2.1.

2.6 EDM Experiments and CP violation

In addition to the collider results on the high-energy end, low-energy experiments, especially the Electric Dipole Moment (EDM) measurement with extremely high precision, impose strong constraints on the CP violation. The relation between EDM and CP violation can be understood this way. For elementary particles with spin, the electric and magnetic dipole moments must be in parallel with spin $\vec{s}$. Thus the potential energy of an electric or magnetic dipole in an external field is given by

$$-d_e\vec{s}\cdot\vec{E} - d_m\vec{s}\cdot\vec{B} \tag{2.24}$$

Here d_e and d_m are the electric and magnetic dipole moments. Now let's consider the transformation properties of $\vec{s}$, $\vec{E}$ and $\vec{B}$ under T. $\vec{E}$ is invariant under T while $\vec{s}$ and $\vec{B}$ change sign under T. To keep the potential energy unchanged, we need $d_e \to -d_e$. Thus any observation of a non-vanishing electric dipole moment would violate the invariance under time-reversal transformation, and thus also violate CP.

Following the discussion, it's clear that current EDM experiments will also put constraints on the CP violating properties in the Higgs sector (see for instance Refs. [60],[61]). In this section we shall explore the constraints on the possible CP violation in the MSSM Higgs sector given the present bounds on the electron EDM (eEDM), the neutron EDM and the Mercury EDM, namely [36]–[39].

$$\begin{aligned} \left|\frac{d_n}{e}\right| &< 2.9 \times 10^{-26}\text{cm (95\% confidence level)} \\ \left|\frac{d_{Hg}}{e}\right| &< 3.1 \times 10^{-29}\text{cm (95\% confidence level)} \\ \left|\frac{d_e}{e}\right| &< 8.7 \times 10^{-29}\text{cm (90\% confidence level)} \end{aligned} \tag{2.25}$$

Theoretical calculations show that the primary contributions to EDM come from both one-loop and two-loop diagrams [42]. The dominant two-loop contributions come from the so-called Barr-Zee type diagrams [43],[44](there are other two-loop contributions [45], not included in CPsuperH, which become subdominant in the regime we are working on). The contribution of the neutral Higgs sector also comes in through the so-called Barr-Zee type diagrams as following: The approximate amplitude of this diagram can be calculated as:

$$iM^{\nu}_{BZ} \sim i\frac{4}{3}\frac{m_e}{v^2}\frac{\alpha_{em}e}{(4\pi)^3}\kappa_e\tilde{\kappa_t}\{f(\frac{m_t^2}{m_h^2}) - g(\frac{m_t^2}{m_h^2})\} \tag{2.26}$$

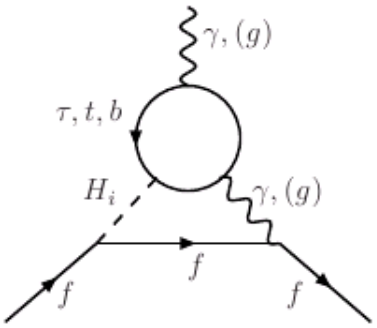

where,

$$f(z) = \frac{z}{2}\int_0^1 dx \frac{1-2x(1-x)}{x(1-x)-z}\ln\left(\frac{x(1-x)}{z}\right)$$
$$g(z) = \frac{z}{2}\int_0^1 dx \frac{1}{x(1-x)-z}\ln\left(\frac{x(1-x)}{z}\right) \tag{2.27}$$

The largest of this kind of diagram are associated with the $t/\tilde{t}/chargino$ loop, and have amplitude comparable to the one-loop contribution due to the large Yukawa coupling with the 3rd generation of fermions, this diagram can be written as

$$-d_e \frac{i}{2}\bar{e}\sigma^{\mu\nu}\gamma_5 e F_{\mu\nu} \tag{2.28}$$

where d_e is just the electric dipole moment. Again we will need a γ_5 term which comes from the mixing of scalar part(CP-even) and pseudoscalar part(CP-odd) in the Higgs, recall the pseudoscalar coupling between Higgs fermions has the shape of

$$-\frac{m_f}{v}h\bar{\Phi}_f i p_f \gamma_5 \Phi_f \tag{2.29}$$

The dominant two-loop electric dipole moment contributions are proportional to the same CP-violating phases which governs the CP violating strength in the Higgs sector, contrary to the one-loop contributions which are governed by CP-violating phases associated to particles that couple only weakly to the Higgs fields. In other words, large CP violation effects in the

Higgs sector are likely to be associated with large two-loop EDM contributions, beyond the experimentally observed limits and could be therefore constrained by EDM experiments.

Therefore, to allow for large CP-violation effects in the Higgs sector we may need to resort to cancellations between one-loop and two-loop EDM contributions. The main one-loop contributions are from those diagrams involving loops of charginos, neutralinos and gluinos with first and second generation sfermions [46],[47]. Therefore, the amplitudes of one-loop diagrams are in part determined by the mixing in the mass eigenstates of charginos and neutralinos, which is associated with the values of $\mu, M_1, M_2, tan\beta$, and in particular the phases $\arg(\mu M_i)$, which also affect the two loop chargino and neutralino contributions. The one-loop contributions decrease for heavier first and second generation squarks and sleptons. As we said before, we shall characterize the ratio of the first and second to the third generation sfermion masses by a hierarchy factor ρ, which is an input parameter in the CPsuperH code.

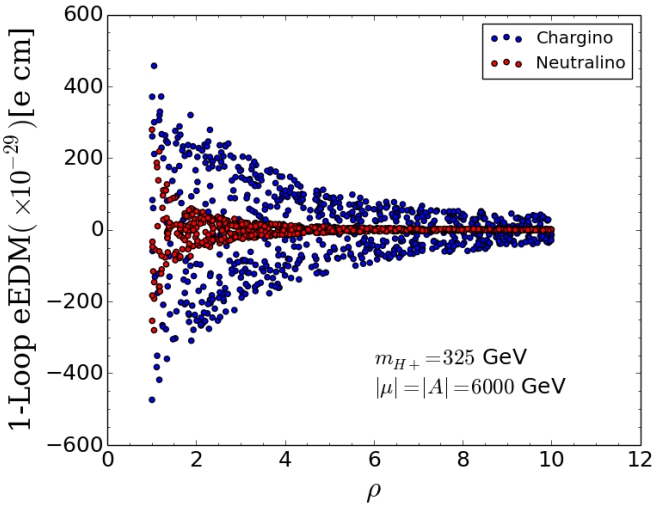

Figure 2.8: One-loop contribution to the electron EDM. All the points shown in this plot lead to a value of M_{H_1} compatible with the observed Higgs mass. The relevant parameters are fixed as follows : m_{H^+} is fixed at 325 GeV, $|\mu| = |A| = 3M_{\rm SUSY}$=6 TeV, $\tan\beta$ is varied from 4 to 9, $\Phi_\mu, \Phi_A, \Phi_{M_2}, \Phi_{M_3}$ are varied from -180 to 180 and $|M_3|$ from 1.5 TeV to 3 TeV.

In Figure 2.8 we display the one-loop contribution to the electron EDM. From Figure 2.8, we find that, as expected, both the one-loop chargino and neutralino contributions to the

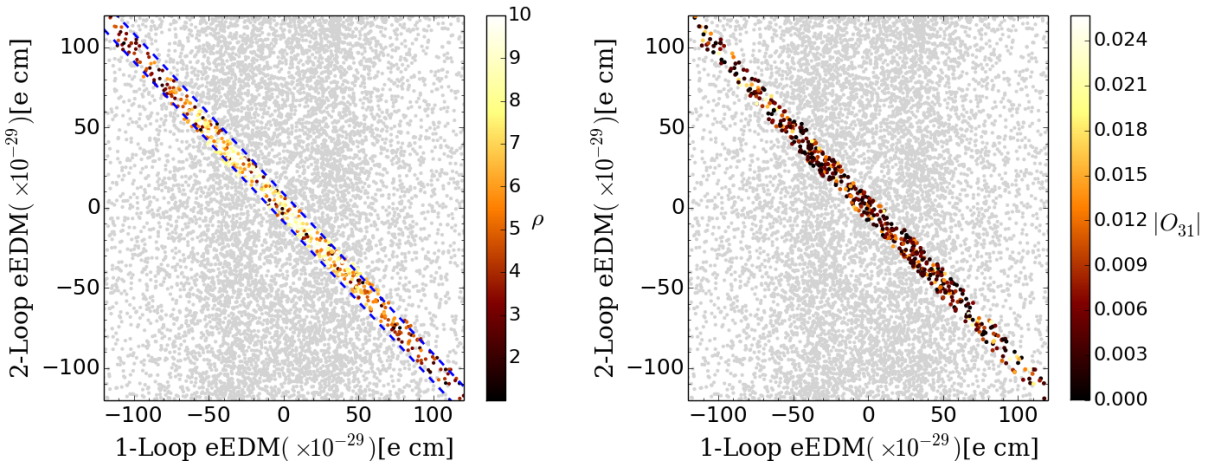

Figure 2.9: Correlation between 1-loop and 2-loop Contributions to the electron EDM('eEDM' in the axis labels stands for electron EDM). All the points shown give appropriate H_1 mass values, among which the colored ones satisfy the electron EDM bound of 8.7×10^{-29}e cm. This is the same scan as in Fig. 2.8. The colors in the left panel represent the values of ρ and in the right panel the H_1 CP-Odd component. This plot illustrates that the eEDM constraint can be avoided by cancellation between the 1-loop and 2-loop contributions.

electron EDM decrease as we raise ρ. Up to ρ. The maximum chargino contribution remains higher than the acceptable eEDM limit (8.7×10^{-29}cm) up to values of $\rho = \mathcal{O}(10)$. Another feature seen from this plot is that the amplitude of chargino-loop diagrams is pronouncedly larger than that of neutralino-mediated ones, differing by an order of magnitude. Thus, unless the phases are highly fine tuned, it is very difficult for EDM to cancel within one-loop level diagrams.

The left panel of Fig. 2.9 shows the correlation between the one and two-loop contributions to the electron EDM for parameters which survive the current bounds on this quantity(eEDM$< 8.7 \times 10^{-29}$e cm). Points in this figure are colored according to the value of the hierarchy factor ρ. In the right panel we show the same correlation but points are colored according to the size of the CP-odd component of the lightest neutral Higgs boson.

We find that most of the allowed points lie closely around a straight line across the origin point with slope -1 which indicates that an approximately exact cancellation occurs between one-loop and two-loop contributions to the electron EDM. Figure 2.10 shows the correlation

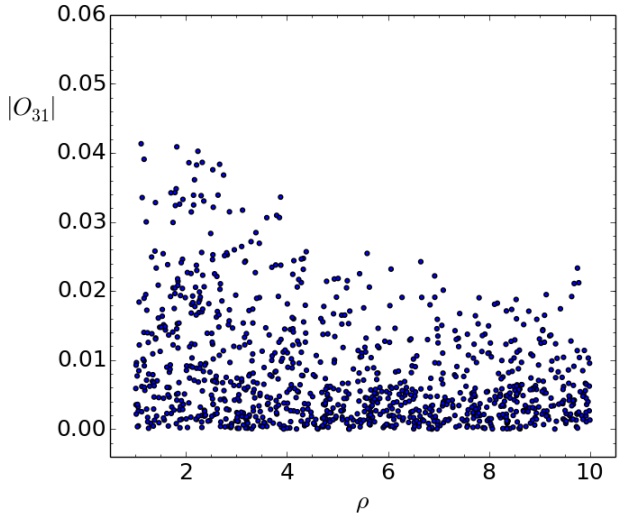

Figure 2.10: The H_1 CP-odd component vs the hierarchy factor ρ, using the same scan as in Fig. 2.8. All the points shown in this plot give appropriate H_1 mass values and satisfy the eEDM bound.

between the CP-odd component of H_1 and the hierarchy parameter ρ. As shown in the right panel of Fig. 2.9 and Fig. 2.10, larger CPV coexists with larger two-loop (or one-loop) EDM components and, for third generation squark masses of the order of one TeV, appears around a $\rho = 2$ peak, where the one-loop contributions are sizable and cancellations between one and two-loop contributions are significant. Therefore the possibility of a pronounced CP-violating effect in the Higgs sector relies on significant cancellations between one-loop and two-loop EDM contributions.

In order to explore the maximum allowed CP-odd component of H_1 given currently measured EDMs, we use CPSuperH2.3 to scan over all relevant variables, choosing low values of the charged Higgs mass and large values of the stop mixing. More specifically, we chose $M_{\rm SUSY} = 2$ TeV (including all squark and slepton masses) and $|\mu| = |A_f| = 3\ M_{\rm SUSY}$. The electroweak gaugino masses values were fix at $|M_1| = |M_2| = 200$ GeV, $\Phi_{M_1} = 0$ (since only the relative phases matter), and the charged Higgs mass was fixed at $m_{H^+} = 300$ GeV so that we can get sizable CP violation and also keep $BR(H \to VV)$ within an acceptable range at the same time. The value of $\tan\beta$ was varied from 5.5 to 9.5 (consistent with the current

Table 2.3: Maximum CP odd component points after taking EDM constraints into account.The values of the stop and Higgsino mass parameter were fixed to $|A_t| = |\mu| = 3M_{\rm SUSY} = 6\ TeV$. The other relevant parameters were varied in the range explained in the text.

No.	$\tan\beta$	Φ_μ	Φ_A	$\lvert M_{\tilde{g}}\rvert$	$\Phi_{M_{\tilde{g}}}$	ρ	Φ_{M2}	m_h	$\frac{BR_{\rm MSSM}(H_1\to ZZ)}{BR_{\rm SM}(H_1\to ZZ)}$	CP-odd component
1	9.5	-45.7°	-18.5°	2300	54.2°	9.17	11.3°	122.7	0.782	3.00%
2	9.0	-34.1°	-31.6°	3000	39.0°	3.86	10.2°	122.7	0.776	3.07%
3	8.9	-2.8°	-62.7°	3000	9.9°	5.26	-18.9°	122.5	0.774	3.04%
4	8.5	23.3°	-88.0°	3000	-17.0°	3.44	-39.9°	122.6	0.772	2.96%
5	8.6	177.4°	-121.3°	2750	172.7°	8.53	-149.4°	123.8	0.796	2.41%

experimental bounds), the hierarchy factor ρ was varied between 1 and 10, while $|M_3|$ was varied from 1.5 TeV to 3 TeV. The phases of the mass parameters Φ_{A_f}, Φ_μ, Φ_{M_3}, Φ_{M_2} were varied from -180° to $+180^\circ$. To fight against the high elimination rate associated with the experimental constraints and the huge complexity in computing EDMs, we implemented a gradient descent method in the 3D subspace spanned by parameters Φ_{M_2}, Φ_μ, and ρ to bring the three EDM values into acceptable ranges. The descending process was fast with proper steps and iteration algorithm. Finally we found 4200 points passing all constraints, with a maximum CP-odd component of H_1 to be 3.07%, which is consistent with our observations above.

To exemplify the values of the parameters leading to relevant O_{31}, in Table 2.3 we show some of the points with maximal H_1 CP-odd component, the parameters for which they are obtained, as well as the relevant parameters in the Higgs sector.

Observe that these five different examples have similar characteristics : The values of $\arg(\mu M_{\tilde{g}}) \lesssim 10^\circ$, as expected in order to cancel the large one-loop contribution to the neutron EDM, induced by the gluino loops. Moreover, the value of $\arg(\mu M_2)$ is within 30° of 0 or 180°. The value of $\arg(\mu A_t) \simeq 65^\circ$, being sizable and of similar order in all examples, is necessary to obtain a sizable CP-odd component of H_1 without inducing a large negative correction to its mass or to the branching ratio of its decay into vector bosons. As is shown in the table 2.3 the maximal CP-odd component is now again associated with the minimal allowed values of the Higgs mass. This may be understood from the fact that, as shown in Fig. 2.5, the largest values of m_{H_1} are associated with values of $\arg(A_t M_3^*) = 0$. However,

since the electric dipole moment constraints lead to $\arg(A_t M_3^*) \simeq \arg(A_t \mu)$, a large CP-odd component of H_1 leads to values of the Higgs mass away from its maximal value. Hence, the Higgs mass combined with the constraints on electric dipole moments puts an additional bound on the possible values of the H_1 CP-odd component.

We want to stress that $|M_1|$ and $|M_2|$ are not determinant factors in the determination of the maximal H_1 CP-odd components. We changed $|M_1| = |M_2|$ to be 1 TeV but kept $|\mu| = |A_f| = 3\ M_{\rm SUSY}$, and got the maximum CP-odd to be 2.91%, not much different from the previous 3.07%. We also checked the maximal CP-violation in the CPX scenario in which $|\mu| = 4\ M_{\rm SUSY}$, $|A_f| = 2\ M_{\rm SUSY}$, $|M_1| = |M_2| = 1$ TeV, $M_3 = 3$ TeV, while the three trilinear coupling phases $\Phi_{A_{t,b,\tau}}$ are independent. We did the scan for this scenario and found that it gave a smaller CP-odd component of about 2%. This effect comes mostly from the change of $|\mu|$ and $|A_f|$, which can be easily seen from Eq. 2.15. This agrees with the numerical results of a recent paper [49] focusing on the CP Violation in the heavy Higgs sector of the MSSM.

In general, we observe that the cancellation of the three EDMs needs some fine tuning at level of order 10 in relevant phases. In order to illustrate the general pattern of cancellations we investigate the behavior of the three EDMs around the points of maximal H_1 CP-odd component found above. For instance, Fig. 2.11 shows the values of the three EDMs considered here, for points around point 1 in Table III, and varying ρ and Φ_{M_2} only. The mass and the lightest neutral Higgs boson CP-odd component contour lines are not shown on these plots since they are almost constant over the whole region displayed (122.7 GeV and 3.0% respectively). The dashed contour line indicates the ratio of the $BR(H \to ZZ)$ to the SM values, showing acceptable values over this whole region of parameter space. The parameters ρ and Φ_{M_2} are chosen because they have nearly nothing to do with the neutral Higgs masses and affect only weakly the CP-violation in the Higgs sector (i.e. O_{31}) but they affect strongly the EDMs through one-loop diagrams. As illustrated in these plots, there seems to be no difficulty in finding some combinations of ρ and Φ_{M2} to circumvent the strong EDM

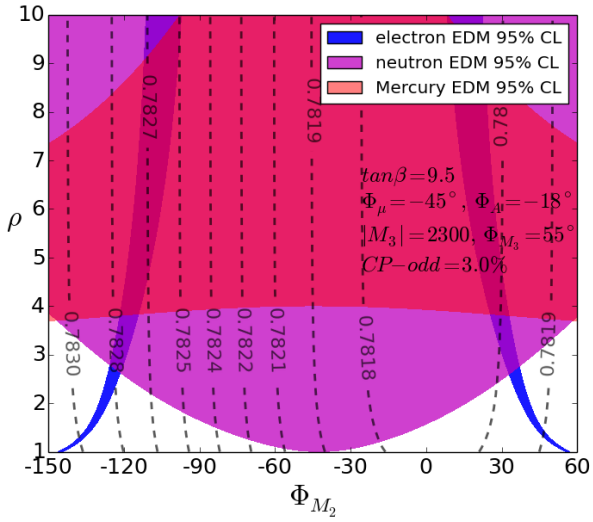

Figure 2.11: EDM constraints in the Φ_{M_2}–ρ plane. The allowed regions for the three kinds of EDMs are drawn in different colours on this patch of the 2D parameter plane. The other relevant parameters were chosen to be the same as in parameter set 1 in Table 2.3, i.e. $\tan\beta = 9.5$,$\Phi_\mu = -45°$, $\Phi_A = -18°$, $M_3 = 2300$ GeV, $\Phi_{M_3} = 55°$. The dashed lines show countors of the ratio $BR_{\rm MSSM}\left(H_1 \to ZZ\right)/BR_{\rm SM}\left(H_1 \to ZZ\right)$, which displays a tiny fluctuation of about 0.1% over the whole range.

constraints, at least for the current bounds. All points allowed in these examples, however, have values of $\rho \gtrsim 4$, implying that in this example one cannot achieve the maximum H_1 CP-odd component, as we showed before, which are obtained for values of $\rho \simeq 2$.

Figure 2.12 shows the correlation between the phases of μ and M_2 for the points which are consistent with the electron, neutron and mercury EDM's. As Fig. 2.12 shows, no matter what value the hierarchy factor ρ takes, there is always some point where the three constraint regions overlap with each other. As ρ goes up, one-loop contribution fades away and two-loop diagrams dominate since propagators of first 2 generations of squarks and sleptons only come into play in one-loop diagrams. The blue stripe allowed by eEDM measurement rotates towards constant Φ_μ. This phenomenon can be easily understood since Φ_{M_2} affects the mass structure of charginos and neutralinos, which control the main one-loop contributions to the eEDM. The red stripe stands for Mercury EDM, which depends only weakly on Φ_{M_2}, and it grows wider as ρ increases, which may be understood due to the smaller degree of cancellation

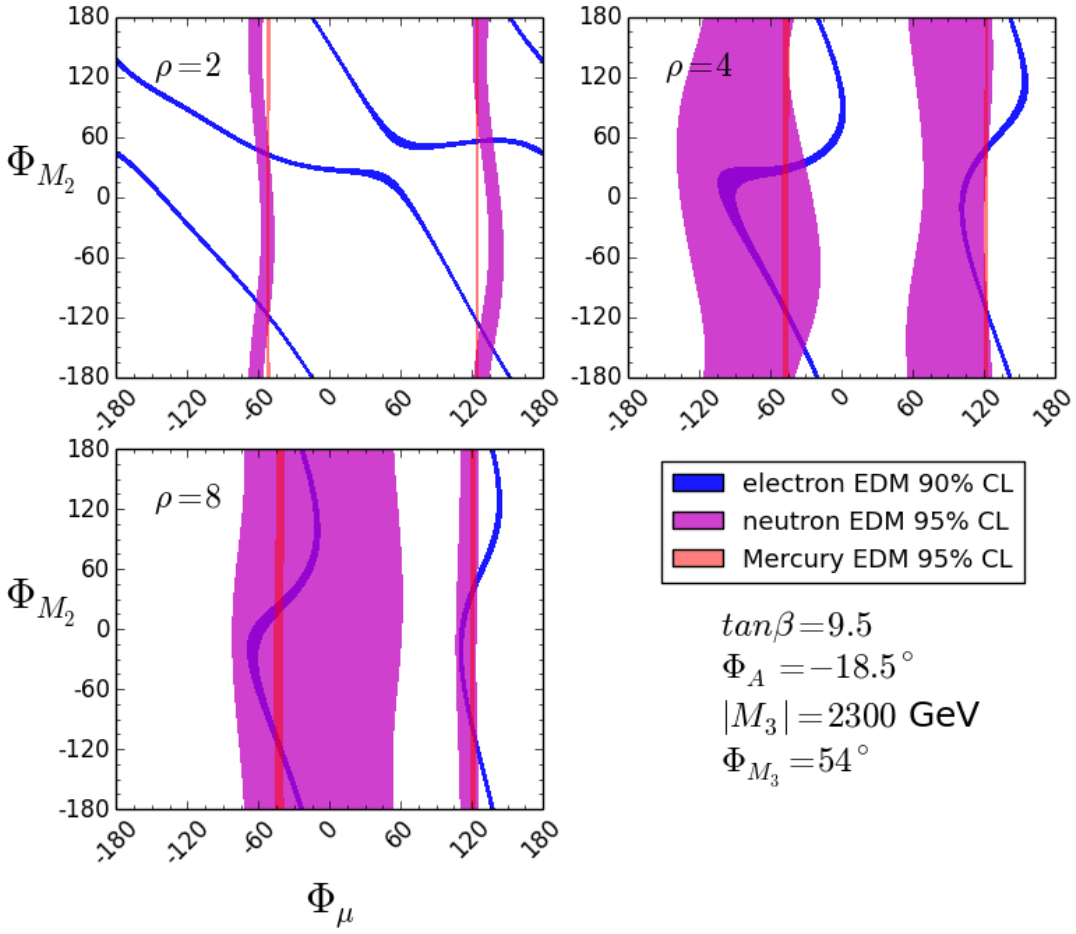

Figure 2.12: EDM constraints in the Φ_μ – Φ_{M_2} plane for different values of ρ. All other relevant parameters are consistent with the ones in parameter set 1 in Table 2.3 (the same as in Fig. 2.11).

between Φ_μ and the gluino phase necessary to be consistent with the current experimental bounds on this quantity.

2.7 Flavor Physics Constraints

The flavor physics implications of the MSSM depend very strongly on the exact flavor structure of the soft supersymmetry breaking parameters. Small missalignments between the squark and the quark mass matrices can induce large flavor violating effects, without having an impact on any other observables. Since in our work we are considering the MSSM as a low energy effective theory, without any assumption of the supersymmetry breaking mechanism at high energies, it is not possible to obtain precise predictions on the flavor observables. In order to obtain an estimate of the flavor violating effects, we used the results of CPsuperH, which are based on the assumption of minimal flavor violation, with additional flavor misallignments induced by up-Yukawa effects [62]–[68], which lead to non-vanishing contributions from flavor violating couplings of the gluino with the left-handed down-quarks and scalar down-quarks.

In general, since in the models under consideration the squarks are heavier than about 2 TeV, $\tan\beta$ is moderate and the charged Higgs mass is about 300 GeV, one does not expect large flavor violating effects. These effects, however, may be enhanced by the presence of large trilinear couplings between the Higgs and the third generation squarks. In Figure 2.13 we show the predictions for two relevant observables, namely the branching ratios of the decays of $B_s \to \mu^+\mu^-$ and $B \to X_s\gamma$. The current experimental values of these observables,

$$BR(B \to X_s + \gamma) = (3.55 \pm 0.24^{+0.09}_{-0.10} \pm 0.03) \times 10^{-4}$$

as estimated by the Heavy Flavor Averaging Group for $E_\gamma > 1.6$ GeV [69], and

$$BR(B_s \to \mu^+ + \mu^-) = (2.9 \pm 0.7) \times 10^{-9}$$

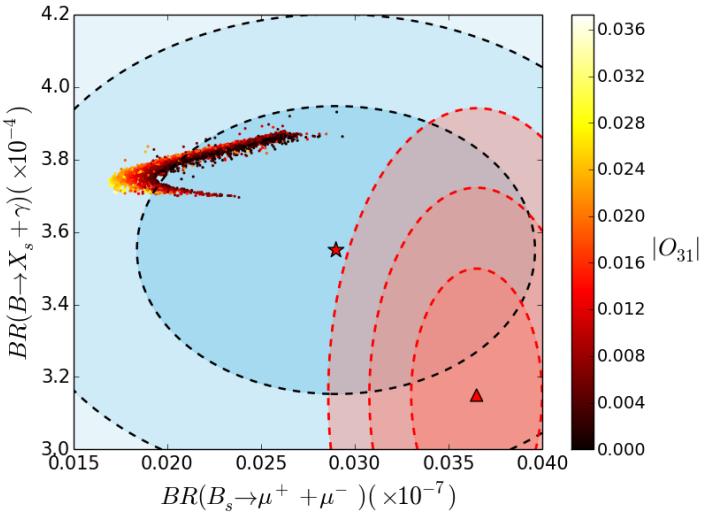

Figure 2.13: The branching ratio values of the decay channels $B_s \to \mu^+ + \mu^-$ and channel $B \to X_s + \gamma$, computed in CPsuperH, are displayed for points allowed by all experimental constraints considered in this article. The points are colored by the CP-odd component of H_1. The red pentagram marks the current experimental values. The red triangle in the plot displays the prediction by Standard Model. The regions allowed at the 68% and 96% C.L. are displayed by dashed lines.

as recorded by LHCb and CMS analyses [70] are in somewhat good agreement with the SM predictions [71],[72],[74] given by

$$BR(B \to X_s\gamma) = (3.15 \pm 0.23) \times 10^{-4}$$

(see Ref. [73] for an alternative calculation of this rate) and

$$BR(B_s \to \mu^+\mu^-) = (3.65 \pm 0.23) \times 10^{-9}.$$

In our analysis, we performed a small rescaling of the values of $B \to X_s\gamma$ given by CPsuperH in order to obtain the proper SM results [72] for large squark and charged Higgs masses.

In Figure 2.13 we show with dashed lines the regions allowed at the 68% and 96% confidence level (C.L.). We see that under the above assumptions, for the maximal CP-violating effects in the Higgs sector, the predicted values of these two observables are in good agreement

with the experimental values and actually this model leads to a similarly good description of these observables to the one obtained in the SM. Therefore, these flavor observables do not put additional constraints on the allowed values of the CP-odd component of the lightest neutral Higgs boson.

2.8 Probes of the H_1 CP-odd Component at the LHC.

The small CP-odd components of the lightest CP-even Higgs boson make its detection difficult. A variety of observables that may lead to the determination of the H_1 CP-odd component have been constructed and different experiments are proposed to measure a CP mixing directly, for example, the azimuthal angle correlations between two jets in Higgs plus two jets channel via gluon fusion [75], the polarization correlation in the $H \to \gamma Z$ and $H \to \gamma\gamma$ channels [76], the angular distribution of the products in the $t\bar{t}H$ channel [77],[78], as well as the distribution over the angle between the planes of e^-e^+ pairs arising from conversion in diphoton decays [79],[80].

A promising channel, $h \to \tau^-\tau^+$, has been proposed to investigate the CP nature of the Higgs boson at the LHC [81],[82],[83], and becomes suitable to test CP-violation in the Higgs sector of the MSSM. In the recent proposal, Ref. [82], the mixing angle, ϕ_τ, defined as:

$$\tan\phi_\tau = \frac{g^P_{h\tau\tau}}{g^S_{h\tau\tau}} \tag{2.30}$$

can be determined by measuring the spin correlation of the tau lepton pairs, which lead to particular differential distributions of the tau pairs in the Higgs decays. These correlations are characterized by an angle ϕ^*_{CP}, defined from the impact parameters and momenta of the charged prongs a^- and a^+ in the decays $\tau^- \to a^- + X$ and $\tau^+ \to a'^+ + X$ in the $a^-a'^+$ zero-momentum frame. The measured differential distribution of the Higgs boson decaying into tau-pairs with respect to ϕ^*_{CP} can be described by:

$$\frac{d\sigma(pp \to H_1 \to \tau\tau)}{d\phi^*_{CP}} \simeq u\cos(\phi^*_{CP} - 2\phi_\tau) + v \tag{2.31}$$

The major background comes from the Drell-Yan production of τ pairs whose effects can be minimized by cuts. It is claimed that the Higgs mixing angle ϕ_τ can be measured to a precision of $\Delta\phi_\tau \approx 14.3^\circ(5.1^\circ)$ at the high luminosity LHC (14 TeV) with an integrated luminosity of 500 fb^{-1}(3 ab^{-1}) (Ref. [81], instead, claims a sensitivity of about 11° at 3 ab^{-1}).

In the Higgs basis, considering only the dominating terms, $\tan\phi_\tau$ can be approximated by

$$\tan\phi_\tau \simeq \frac{O_{31}\tan\beta}{O_{11} - O_{21}\tan\beta}, \tag{2.32}$$

which leads to values of ϕ_τ of order of 10° for values of O_{31} and O_{21} of a few percent and $\tan\beta \simeq 10$, and grows for larger values of $\tan\beta$.. For instance, for point 1 in Table 2.3, a value of $\tan\phi_\tau = 0.236$ is obtained, corresponding to $\phi_\tau = 13^\circ$, within the reach of LHC. This is well within the claim reach of the high luminosity LHC.

To get a better perception of the power of the $h \to \tau^-\tau^+$ measurement, in Fig.2.14 we plot, for the points we found satisfying all current experimental constraints considered in this paper, the maximum value of ϕ_τ in the $\tan\beta - \rho$ plane. In other words, these values represent the experimental sensitivity needed in order to start probing the CP-odd component of H_1 in the MSSM for that particular parameter region.

It is then clear that if the value of O_{31} is close to the maximal values consistent with current experimental constraints, the LHC may probe this CP-violating effects in the high luminosity run. It is also clear that in order for the LHC to probe the CP-odd component of H_1 in the MSSM, the charged Higgs mass should be of order of the weak scale and $\tan\beta > 5$. This region of parameters will be efficiently probed by the LHC in the search for Higgs bosons decaying into τ-pairs in the near future. Moreover, as stressed before a large CP-odd component of H_1 is in general associated with a modification of the branching ratios

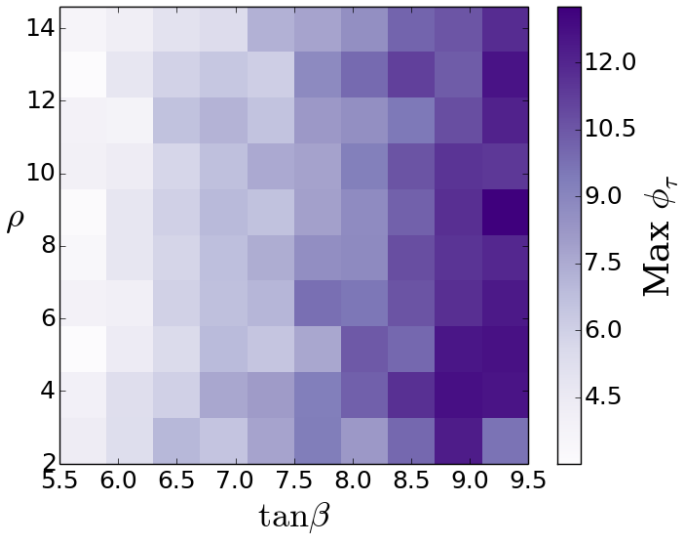

Figure 2.14: Maximum value of ϕ_τ, Eq. (2.30), in the $\tan\beta$ - ρ plane, obtained from a a scan of the phases of all relevant parameters, A_f, μ, M_3 and M_2, for $m_{H^+} = 300$ GeV, $|A_t| = |\mu| = 3M_{\rm SUSY} = 6$ TeV. The values of $\tan\beta$ and ρ are varied within a fairly large range, and points consistent with the present experimental constraints are selected.

of H_1 and hence precision measurements of the H_1 properties will further test the region of parameter space consistent with a significant CP-odd component of H_1.

2.9 Conclusion

In this article, we studied the values of the CP-odd component of the lightest neutral Higgs allowed by current experimental constraints. We derived new analytical expressions in the Higgs basis that allow a good understanding of the parametric dependence of this component on the supersymmetry breaking parameters. We showed that the values of the stop left-right mixing parameter that maximize the lightest CP-even Higgs mass lead to a suppression of the dominant loop contribution to the CP-odd component of the lightest Higgs boson. Since for stop masses of order of the TeV scale, stop mixings close to the ones that maximize m_{H_1} are necessary in order to obtain SM-like Higgs masses of order of the one observed experimentally, the measured Higgs mass puts a significant constraint on the possible values of the H_1 CP-odd component.

Moreover, we showed that large H_1 CP-odd components lead necessarily to a significant increase of the width of the lightest neutral Higgs decay into bottom quarks. Since the width of $H_1 \to b\bar{b}$ is the dominant decay width of H_1, this increase leads also to a significant modification of the branching ratio of the decays of H_1 to gauge bosons, what leads to a further constraint into large H_1 CP-odd components.

Electric dipole moments put a further constraint on this possibility. Although cancellations between one-loop and two-loop contributions may lead to acceptable values of the electron EDM, which is the most precisely bounded one at this point, the strong alignment between the phases of μ and the gluino mass leads to further restrictions on the possible obtention of a large H_1 CP-odd component. At the end, we showed that the CP-odd component of H_1 is restricted to be smaller than about 3%. Furthermore, we analyzed relevant flavor physics observables and shoed that they do not set additional constraints on this H_1 property.

We also studied the possible experimental detection of the H_1 CP-odd component at the LHC. The $h \to \tau^- \tau^+$ channel presents a very efficient probe of this possibility. The CP-odd coupling of the τ lepton to H_1 is proportional to the H_1 CP-odd component but it is enhanced by a $\tan\beta$ factor. Due to this enhancement, we showed that, for values of the charged Higgs mass of the order of the weak scale and $\tan\beta > 5$, a determination of the H_1 CP-odd mixing is possible at a high luminosity LHC, but only for values close to the largest allowed values of this mixing. The observation of a non-vanishing CP-odd component of H_1 would then put strong constraints on the parameter space of the MSSM. Further constraints coming from precision measurement of the H_1 branching ratios and searches for heavy Higgs bosons may further probe the parameter space consistent with an observable CP-odd component of H_1 in the MSSM.

Let us emphasize in closing that the constraints on the CP-violating components of H_1 discussed in this paper are specific for the MSSM and could not be generalized to more general two Higgs doublet models, where larger CP-violating effects in the Higgs sector may

be present, as has been discussed in Refs. [75]–[83]. Some of these constraints are related to the specific properties of the radiative corrections leading to the Higgs mass generation in the MSSM and may be avoided in non-minimal supersymmetric extensions, like the NMSSM (see for instance Ref. [84]). Finally, while the LHC capabilities are limited, measurement of the CP-violating component of H_1 may be improved at lepton colliders, as was discussed in detail in Refs. [85]–[88]. We plan to come back to these subjects in the near future.

CHAPTER 3

STRONG FIRST-ORDER EW PHASE TRANSITION

3.1 Introduction

After the Higgs discovery at the LHC [89, 90], the Higgs properties, including the Higgs mass and the Higgs couplings to the Standard Model (SM) particles have been measured [91–93]. Those measurements show that the Higgs boson properties are close to the SM ones. Those properties are related to the gauge transformation properties of the Higgs field and with the mechanism of electroweak symmetry breaking, but provide little information about the properties of the Higgs potential. In the SM, a quadratic coupling and a quartic coupling completely specify this potential. In the theories beyond the SM, there can be contributions to the effective potential from the higher dimensional operators, with an effective cut-off given by the characteristic new physics scale of the theory. As a result, the self-interactions of the Higgs field, most notably the triple Higgs coupling (λ_3), are modified.

We know from the introduction that understanding the nature of the EPT will advance our knowledge of the possible realization of electroweak baryogenesis[102], which is an attractive explanation of the baryon anti-baryon asymmetry, that can only happen if the EPT is first order. And λ_3 is closely related to the strength of the electroweak phase transition (EPT) [94–101].

A first order electroweak phase transition (FOEPT) may lead to the production of gravitational waves, but the characteristic scales associated with it make their detection very difficult, albeit not impossible, to detect in the near future [108–112]. Alternatively, the models that lead to a FOEPT through a relevant modification of the zero temperature effective potential can be probed from the deviation of λ_3 from its SM value, as suggested in previous studies [96, 99, 100].

At the LHC, λ_3 can be probed by the process of double Higgs production. Mainly due to the destructive interference between the one-loop diagrams, the production cross section

reduces initially, as the λ_3 is enhanced from its SM value. At the next-to-leading order, the minimum occurs for $\lambda_3 \sim 2.45\,\lambda_3^{SM}$ [113]. Further enhancement of the λ_3 value increases the cross section again, which exceeds the SM value for $\lambda_3 > 5\lambda_3^{SM}$. The cross-section also increases if the correction to λ_3^{SM} is negative. The $b\bar{b}\gamma\gamma$, $b\bar{b}\tau^+\tau^-$, $b\bar{b}W^+W^-$ and $bb\bar{b}\bar{b}$ channels [114–122] have been studied. These studies showed that around 50% accuracy can be achieved from the $b\bar{b}\gamma\gamma$ channel alone assuming that λ_3 is not too far away from its SM value and the acceptance for different values of λ_3 stays the same. However, as pointed out in [118], the acceptance drops significantly for large values of λ_3. In this article we perform a detailed study of the impact of a large deviation from λ_3^{SM} on the double Higgs production process. We also present an analysis of the LHC searches for this process including relevant QCD background contributions that have been overlooked in the previous studies.

The organization of this article is as follows : In Sec. 3.2, we calculate the values of λ_3 if the EPT is first order in a simplified model, where we include higher order terms in the effective potential. In Sec. 3.4, we compare our results to those obtained in singlet extensions like the ones that may be obtained from the scalar Higgs sector in the Next to Minimal Supersymmetric Standard Model (NMSSM). In Sec. 3.5, we discuss the measurement of λ_3 at the LHC, for the SM-like values as well as for values of λ_3 that present a large positive or negative deviation with respect to the SM value. We reserve Sec. 3.6 for the conclusions and some technical details to the Appendices.

3.2 The Effective Potential and the Trilinear Higgs Coupling

A modification of the nature of the phase transition may be achieved by adding extra terms to the Higgs potential [123–125]. These may appear through relevant temperature dependent modifications of the Higgs potential, beyond those associated with the increase of the effective mass parameter, which lead to the symmetry restoration phenomenon (see, for example, Refs. [126–139]).

Alternatively, these effects may be already present at zero temperature, through addi-

tional terms in the Higgs potential induced by integrating out new physics at the scales above the weak scale. In this section we concentrate on the second possibility and illustrate the impact of such additional terms on the enhancement of λ_3 in minimally extended models.

Several simple extensions of the SM are capable of generating the required extra terms in the potential and have been studied in the literature [94–101, 140–144]. In Sec. 3.4, we analyze one such example, where a gauge singlet is added to the SM. This can lead to a relevant modification of the trilinear Higgs coupling with respect to the SM value λ_3^{SM}, even for values of the singlet mass much larger than the weak scale. In such a case, the singlet decouples from physics processes at the LHC, allowing a comparison of these results with the ones obtained in the effective low energy field theory.

In this section, we take a general approach to the effective field theory (EFT), where non-renormalizable terms are added to the Higgs potential. We investigate whether these can potentially generate considerably larger cross-sections for $gg \to hh$ process compared to the standard model. We also explore the possibility of these being compatible with a strongly first order electroweak phase transition (SFOEPT). Such modifications to λ_3^{SM} would make for a viable probe to the new physics at the LHC and beyond.

3.3 Non-renormalizable terms in the low energy Higgs potential

The general formalism in this section is as follows. All the tree-level effective operators represented by powers of $\left(\phi^\dagger\phi\right)$ are added to the usual Higgs potential at the temperature $T = 0$ as follows

$$V(\phi, 0) = \frac{m^2}{2}(\phi^\dagger\phi) + \frac{\lambda}{4}(\phi^\dagger\phi)^4 + \sum_{n=1}^{\infty} \frac{c_{2n+4}}{2^{(n+2)}\Lambda^{2n}} \left(\phi^\dagger\phi\right)^{n+2}, \tag{3.1}$$

where $\phi = v + h$ and hence the VEV is given as $\langle\phi\rangle = 246$ GeV. This leads to a correction to the SM value of the triple Higgs coupling as shown in the Appendix A.1.

$$\lambda_3 = \frac{3m_h^2}{v}\left(1 + \frac{8v^2}{3m_h^2}\sum_{n=1}^{\infty}\frac{n(n+1)(n+2)c_{2n+4}v^{2n}}{2^{n+2}\Lambda^{2n}}\right). \tag{3.2}$$

The non-zero temperature effects are approximately accounted for by adding a thermal mass correction term to the Higgs potential. This term is generated in the high-T expansion of the one loop thermal potential. At temperature T, we get $m^2(T) = m^2 + a_0T^2$. We have ignored the small cubic term contributions as well as the logarithmic contributions as they are suppressed compared to the contributions from higher order terms. Here we have assumed that the heavy new physics is not present in the EFT at the weak scale and therefore its contribution is Boltzmann suppressed at the EPT scale. In such a case a_0 is a constant proportional to the square of SM gauge and Yukawa coupling constants. Assuming all $c_{2n} \simeq 1$, the minimum value that Λ can achieve is 174 GeV in this formulation, at which point the convergence of the series is lost for values of ϕ close to its VEV. However, in any consistent EFT, the cut-off scale Λ will be considerably higher than 174 GeV.

Using Eq. (3.2), we define another quantity δ which quantifies the deviations of the trilinear Higgs coupling with respect to the SM value as

$$\delta = \frac{\lambda_3}{\lambda_3^{SM}} - 1 = \frac{8v^2}{3m_h^2}\sum_{n=1}^{\infty}\frac{n(n+1)(n+2)c_{2n+4}v^{2n}}{2^{n+2}\Lambda^{2n}}, \tag{3.3}$$

where we restrict $|c_{2n+4}| < 1$.

The values of the enhancement of λ_3 for a given Λ for all potentials satisfying these conditions are shown in Fig. 3.1. This maximal possible value, shown in the the upper-most black (dashed) line in all the panels in Fig. 3.1, is obtained assuming all $c_{2n} = 1$ and leads to a large enhancement even at a relatively large value of Λ. However, the only condition that we have imposed on the potential so far is the existence of a local minimum with a second derivative consistent with the measured Higgs mass $m_h \simeq 125$ GeV. For this minimum

to represent the physical vacuum of the theory, however, it should be a global one. As we shall show, the global minimum requirement imposes strong constraints on the possible enhancement of the triple Higgs coupling.

In our further analysis, we choose not to consider the terms of the order higher than $\left(\phi^\dagger\phi\right)^5$ as they introduce negligible corrections for the cut-offs higher than v as shown in Fig. 3.1. We separately analyze the nature of the phase transition and the maximum positive and negative values for δ in each of the three cases corresponding to $\left(\phi^\dagger\phi\right)^3$, $\left(\phi^\dagger\phi\right)^4$ and $\left(\phi^\dagger\phi\right)^5$. Let us stress that these momentum independent operators preserve the custodial symmetry and evade the tight phenomenological constraints coming from the ρ parameter. The momentum dependent non-renormalizable operators [101, 145–147], instead, may contribute to the oblique corrections and are very tightly constrained by the electroweak precision measurements. A particularly relevant one for our analysis is

$$\frac{c_H}{8\Lambda^2}\partial_\mu(\phi^\dagger\phi)\partial^\mu(\phi^\dagger\phi), \tag{3.4}$$

This correction plays a relevant role in the singlet case that we shall discuss below, but is also restricted by Higgs precision measurements and tend to be small. Hence, in most of our analysis we shall ignore the momentum dependent corrections but we shall consider them in the comparison with the singlet case in section 3.4.2.

3.3.1 Higgs Potential of order $(\phi^\dagger\phi)^3$

From Eq. (3.1) and Eq. (3.2), the potential and the triple Higgs coupling are given by

$$V(\phi,T) = \frac{m^2+a_0T^2}{2}\left(\phi^\dagger\phi\right) + \frac{\lambda}{4}\left(\phi^\dagger\phi\right)^2 + \frac{c_6}{8\Lambda^2}\left(\phi^\dagger\phi\right)^3 \tag{3.5}$$

$$\lambda_3 = \frac{3m_h^2}{v}\left(1+\frac{2c_6v^4}{m_h^2\Lambda^2}\right) \tag{3.6}$$

This case has been studied in the literature in various contexts [94–101]. We point out a few key things pertaining to this case in the present context.

We require $c_6 > 0$ for the stability of the potential. The requirement that there should be a minimum of the potential at $\phi = \phi_c$ degenerate with the extreme at $\phi = 0$ for the temperature $T = T_c$ leads to

$$\lambda^2 = 4m^2(T_c)\frac{c_6}{\Lambda^2}. \tag{3.7}$$

This implies that $m^2(T)$, which is the curvature of the potential at $\phi = 0$, should be greater than zero at $T = T_c$ for the phase transition to be of the first order. The minimum of the potential at the critical temperature is at

$$\left(\phi_c^\dagger \phi_c\right) = v_c^2 = -\frac{\lambda\Lambda^2}{c_6}. \tag{3.8}$$

what implies that an additional condition to obtain a FOEPT is that the effective quartic coupling should be negative, namely $\lambda < 0$.

The value of the Higgs mass imposes a relation between λ and c_6, namely

$$\lambda + \frac{3c_6}{2\Lambda^2}v^2 = \frac{m_h^2}{2v^2} \tag{3.9}$$

Using Eq. (3.8) and Eq. (3.9) gives

$$\frac{c_6}{\Lambda^2} = \frac{m_h^2}{3v^2\left(v^2 - \frac{2}{3}v_c^2\right)} \tag{3.10}$$

From where all coefficients m^2, λ and c_6 may be written in terms of the m_h, v_c and v. Using these relations one obtains

$$T_c^2 = \frac{3c_6}{4\Lambda^2 a_0}\left(v^2 - v_c^2\right)\left(v^2 - \frac{v_c^2}{3}\right). \tag{3.11}$$

Demanding both c_6 and T_c^2 to be positive, we get $v_c < v$. This translates into an upper bound on c_6 using Eq. (3.10)

$$\frac{c_6}{\Lambda^2} < \frac{m_h^2}{v^4}\ . \tag{3.12}$$

Then from the Eq. (3.6), we conclude that the coupling can be enhanced by a factor of three at most. Moreover, demanding $v_c^2 > 0$, or equivalently $\lambda < 0$, puts an additional constraint on the obtention of a FOEPT, namely

$$\frac{c_6}{\Lambda^2} > \frac{m_h^2}{3v^4} \tag{3.13}$$

what implies a minimal enhancement of a factor two thirds.

This implies that a FOEPT may only be obtained if the following conditions are fulfilled.

$$\frac{2}{3} \leq \quad \delta \quad \leq 2. \tag{3.14}$$

Moreover, for $c_6 = 1$, Eq (3.12) and Eq (3.13) imply a bound on the effective cutoff Λ, namely

$$\frac{v^2}{m_h} < \quad \Lambda \quad < \frac{\sqrt{3}v^2}{m_h}, \tag{3.15}$$

which correspond to upper and lower bounds on Λ of approximately 484 GeV and 838 GeV respectively, and larger enhancement δ is obtained for the smaller values of the cutoff. The phase transition becomes stronger first order for smaller values of the cutoff and becomes a weakly first order one for values of Λ close to the upper bound in Eq. 3.15. Let us stress that

for values of Λ below the lower bound in Eq. 3.15, $\Lambda < 484$ GeV, the minimum at $T = 0$ is no longer a global minimum and hence electroweak symmetry breaking does not occur.

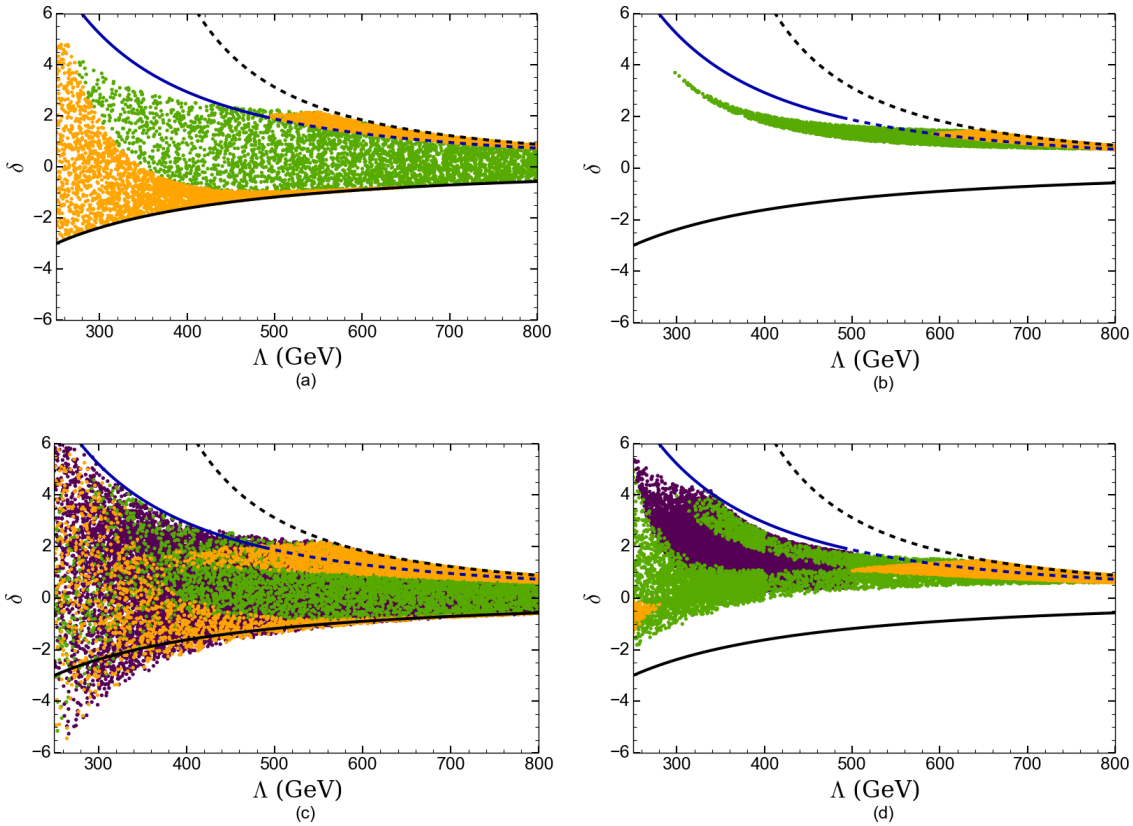

Figure 3.1: Triple Higgs coupling correction δ as a function of the cutoff Λ. The upper dashed black line shows the maximum value of δ for the infinite sum with all $|c_{2n}| = 1$. The dashed dark blue shows the values consistent with a FOEPT for the $\left(\phi^\dagger\phi\right)^3$ potential extension, for $c_6 = 1$, while for the same conditions solid light blue line is forbidden due to the absence of electroweak symmetry breakdown. Fig. 1(a) and 1(b) show the results for the $\left(\phi^\dagger\phi\right)^4$ potential. The different colors correspond to the different hierarchies of the effective potential coefficients as explained in the text. Fig.1(a) shows the general case while the Fig. 1(b) shows the result if a first order electroweak phase transition (FOEPT) is demanded. Fig. 1(c) and 1(d) show similar results but for the $\left(\phi^\dagger\phi\right)^5$ potential, with different colors again corresponding to different coefficient hierarchies defined in the text. The lower solid black line shows the maximal negative values of δ possible for the order $\left(\phi^\dagger\phi\right)^4$ potential.

In Fig 3.1, we show the possible triple Higgs coupling enhancement factor δ as a function of the cutoff Λ for different extensions of the SM effective potential. The particular case of

the potential of order $\left(\phi^\dagger\phi\right)^3$ is represented by the blue curve. The maximum enhancement $\lambda_3 = 3\lambda_3^{SM}$ is achieved at $\Lambda \sim 484$ GeV. For the cut-offs above $\Lambda \sim 838$ GeV, not shown in the figure, the phase transition is not first order anymore, but the Higgs potential is still a viable one. Note that the low value of the cut-off does not necessarily correspond to any physical mass scale, as will be discussed in the singlet case, in Sec. 3.4.

Let us note before closing that in Ref. [148] it is found that for a FOEPT to take place, the enhancement due to a six-dimensional operator to the Higgs potential cannot be larger than $\sim 20\%$. In order to understand the difference of their result with ours we notice that in their normalization, the coefficient of the $(\phi^\dagger\phi)^3$ term is written as $\frac{\bar{c}_6\lambda}{f^2}$, where λ is the coefficient of the $(\phi^\dagger\phi)^2$ term. The discrepancy is due to the assumption in Ref. [148] that $\bar{c}_6 > 0$ and $\bar{c}_6 v^2/f^2$ small. As we showed above, for a FOEPT to take place, the effective quartic coupling $\lambda < 0$, which means $\bar{c}_6 < 0$ is required for the stability of the potential. Also, for $\lambda < 0$, the required condition to obtain a positive Higgs mass is $\bar{c}_6 v^2/f^2 < -\frac{2}{3}$. Thus, in the notation of Ref. [148], $|\bar{c}_6| v^2/f^2$ cannot be used as a small expansion parameter in the region of parameters consistent with a FOEPT. Finally, the upper bound assumed on $\bar{c}_6/\Lambda^2$, coming from Ref. [95], is similar to the one we derived in Eq. (3.12) and is applicable to c_6/Λ^2 and not to $\bar{c}_6/\Lambda^2$.

3.3.2 Higgs Potential of order $(\phi^\dagger\phi)^4$

From Eq. (3.1) and Eq. (3.2), the potential and the triple Higgs coupling are

$$V(\phi, T) = \frac{m^2 + a_0 T^2}{2}\left(\phi^\dagger\phi\right) + \frac{\lambda}{4}\left(\phi^\dagger\phi\right)^2 + \frac{c_6}{8\Lambda^2}\left(\phi^\dagger\phi\right)^3 + \frac{c_8}{16\Lambda^4}\left(\phi^\dagger\phi\right)^4 \tag{3.16}$$

$$\lambda_3 = \frac{3m_h^2}{v}\left(1 + \frac{2c_6 v^4}{m_h^2\Lambda^2} + \frac{4c_8 v^6}{m_h^2\Lambda^4}\right) \tag{3.17}$$

This case is particularly interesting because contrary to the $(\phi^\dagger\phi)^3$ case, the trilinear Higgs couplings may be either enhanced or suppressed and one can even get an inversion of the sign of λ_3 with respect to λ_3^{SM}. As mentioned before, a suppression or change of sign

of λ_3 would be interesting from the collider perspective as it avoids the problem of a strong destructive interference between the box and the triangle diagrams for $gg \to hh$.

The orange and green regions in Fig. 3.1(a) and Fig. 3.1(b) correspond to the regions consistent with the experimental values of the Higgs mass and the Higgs VEV. Fig. 3.1(a) shows the possible modifications (δ) of the λ_3^{SM} possible in this case. Fig. 3.1(b) outlines the region in Fig. 3.1(a) which corresponds to the FOEPT. This shows that an inversion of sign or suppression of λ_3 with respect to λ_3^{SM} necessarily implies that the phase transition is not a first order one. In the construction of Fig. 3.1(b), we have not considered the region of the parameter space corresponding to potentials with barriers between the minima at $\phi = 0$ and $\phi = v$ at $T = 0$. This is due to the fact that a metastability analysis would be required to determine the part of this region in which a FOEPT takes place. Therefore, this rather small region is neglected in our analysis. As a result of this, a small part of the dashed blue curve is not surrounded by the shaded regions. The same is true for Fig. 3.1(d).

In Fig. 3.1(a) and Fig. 3.1(b), the different colors indicate different regions of the parameter space. The orange region corresponds to $|c_6| = 1$, $0 < c_8 < 1$, while the green region corresponds to $|c_6| < 1$, $c_8 = 1$. The regions can overlap, because a different combination of c_6 and c_8 can produce the same value of δ for the same cut-off. In fact, beneath all of the orange region above the blue curve, there exists a green region. We observe that it is possible to obtain λ_3 values ranging from $-2\lambda_3^{SM}$ to $6\lambda_3^{SM}$ for cut-offs higher than 250 GeV. Demanding a FOEPT reduces it to a smaller range from $\frac{5}{3}\lambda_3^{SM}$ to $5\lambda_3^{SM}$. We also note from Fig. 3.1(b) that the FOEPT has a lower bound on the cut-off ~ 300 GeV, which is somewhat lower than in the $(\phi^\dagger\phi)^3$ case. Note that, the contribution to λ_3 from the dim-8 operators is suppressed compared to that from the dim-6 operators. The fact that in a $(\phi^\dagger\phi)^4$ theory, λ_3 has a much larger range in the general case compared to a $(\phi^\dagger\phi)^3$ theory, and in the region consistent with the FOEPT is because with c_8 being a positive number, c_6 is allowed to take negative values in the range of $|c_6| < 1$ in a $(\phi^\dagger\phi)^4$ theory, while $0 < c_6 < 1$ has to be fulfilled in a $(\phi^\dagger\phi)^3$ theory.

Let us stress that negative values of δ imply that the curvature is decreasing at $\phi = v$. If this behavior is preserved at larger values of ϕ, one would expect a maximum of the potential for $\phi > v$. Then the stability of the potential means there has to be one more minimum for $\phi > v$. The deeper the extra minimum, the more negative is the value of λ_3. Thus, demanding the physical minimum to be a global one, a maximal negative value would occur at the point where both minima have the same potential value.

In order to retain the analytic control, we plot the analytical bound coming from the point marking the end of the absolute stability. For $(\phi^\dagger\phi)^4$ case, this bound is the black curve at the bottom of each panel of Fig. 3.1. As shown in appendix A.2, this maximally negative enhancement is given as

$$\delta > -\frac{x}{1+\sqrt{1+x}}, \quad \text{where} \quad x = \frac{4v^4}{m_h^2\Lambda^2}. \tag{3.18}$$

Observe, however, that for $\Lambda \simeq 250$ GeV the second minimum would occur at values of ϕ of order or larger than Λ, and hence this analytical result should be taken with care. The numerical results of Fig. 3.1 were obtained by only demanding the physical minimum to be the global one. The largest negative enhancements obtained numerically are consistent with the predictions of Eq. (3.18) up to values of $\Lambda \simeq v$. Let us stress again that although we show examples with very low cutoff values, those low cutoff values may be hard to realize in any realistic model.

3.3.3 Higgs Potential of order $(\phi^\dagger\phi)^5$

From Eq. (3.1) and Eq. (3.2), the potential and the triple Higgs coupling in this case are

$$V(\phi,T) = \frac{m^2+a_0T^2}{2}\left(\phi^\dagger\phi\right) + \frac{\lambda}{4}\left(\phi^\dagger\phi\right)^2 + \frac{c_6}{8\Lambda^2}\left(\phi^\dagger\phi\right)^3 + \frac{c_8}{16\Lambda^4}\left(\phi^\dagger\phi\right)^4 + \frac{c_{10}}{32\Lambda^6}\left(\phi^\dagger\phi\right)^5 \tag{3.19}$$

$$\lambda_3 = \frac{3m_h^2}{v}\left(1 + \frac{2\,c_6v^4}{m_h^2\Lambda^2} + \frac{4\,c_8v^6}{m_h^2\Lambda^4} + \frac{5\,c_{10}v^8}{m_h^2\Lambda^6}\right) \tag{3.20}$$

Most of the analysis is the same as that for the $\left(\phi^\dagger\phi\right)^4$ case, and the extra minimum develops for $\phi > v$, when the correction to λ_3^{SM} is negative. Barring the possibility of metastability, the bound on the maximal negative correction corresponds to the point in which the extra minimum is degenerate with the physical one.

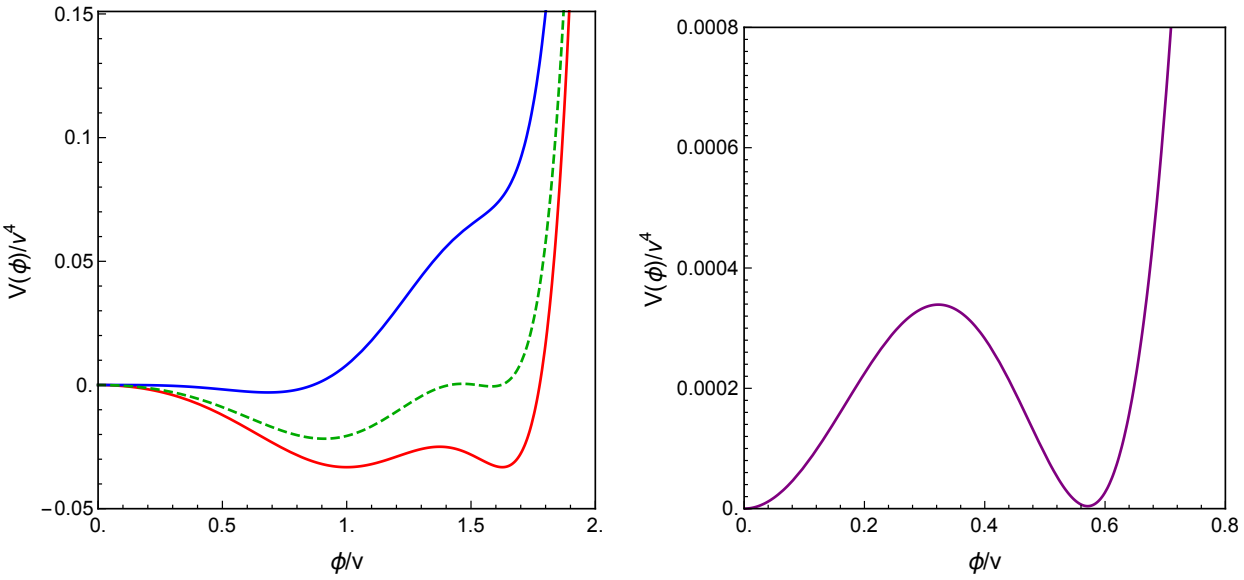

Figure 3.2: Example of order $(\phi^\dagger\phi)^5$ potentials that correspond to the negative correction and also produce SFOEPT. In the left panel, the red line indicate the potential at $T = 0$, the blue line correspond to the temperature where the curvature at $\phi = 0$ is 0. The green line correspond to the intermediate temperature of ~ 35 GeV. The purple curve on the right shows the potential at $T = T_c$. The coefficients $c_6 = 0.906$, $c_8 = -1$, $c_{10} = 0.346$, while $\Lambda \sim 263$ GeV, $T_c \sim 44$ GeV assuming $a_0 \sim 3$ as in the SM and $\delta = -1.23$.

Fig. 3.1.c shows the possible modifications to λ_3^{SM} by viable Higgs potentials that obey the experimental constraints on the Higgs mass and the VEV. We see that for the cut-offs near 250 GeV, one can obtain variation in the λ_3 from $-5\lambda_5^{SM}$ to $7\lambda_3^{SM}$. Such large deviations make the triple Higgs coupling measurements at the LHC an exciting probe to the new physics. Fig. 3.1(d) shows a subset of the region in the left panel, in which a SFOEPT can take place. The black and the blue lines are retained from the Fig. 3.1.a and Fig. 3.1.b and serve as a reference for the comparison between the top and the bottom rows.

In Fig. 3.1.c and Fig 3.1.d the orange regions correspond to $|c_6| = 1$, $|c_8| < 1$, $0 < c_{10} < 1$, green region corresponds to $|c_6| < 1$, $|c_8| = 1$, $0 < c_{10} < 1$ and the purple region corresponds

to $|c_6| < 1$, $|c_8| < 1$, $c_{10} = 1$. As expected, two clusters are observed in the orange and green regions corresponding to the sign flips of c_6 and c_8 respectively. As in the case of $(\phi^\dagger\phi)^4$, there is overlap between the regions. The green region being present beneath all the area occupied by the orange region, while the purple region is present beneath all the area occupied by the other two colors.

An interesting feature of this kind of potential is the presence of negative enhancements in Fig. 3.1.d for the orange and green regions. This means that in principle there are regions of parameters in which a negative enhancement of λ_3 may be obtained consistently with a FOEPT.

Fig. 3.2 shows an example of the Higgs potentials, which is of order $(\phi^\dagger\phi)^5$, and satisfies the Higgs mass and the VEV constraints and also undergo a SFOEPT with large negative enhancements of the triple Higgs coupling. In the left panel, the red line at the bottom corresponds to the potential at $T = 0$, while the blue line depicts the potential at $T = T_f$ that corresponds to the curvature at $\phi = 0$ being 0. The green (dashed) line represents an intermediate temperature. In the right panel, the purple curve shows the phase transition of the corresponding potential in the left panel at $T = T_c$. Let us stress that negative enhancements of the triple Higgs couplings are only consistent with a FOEPT for small values of the cutoff, $\Lambda \lesssim 350$ GeV. Hence, the correlation between the negative enhancements and the absence of a FOEPT remains generally valid.

3.4 Minimal extension with a singlet

Minimal extensions of the SM with just one singlet and their impact on electroweak baryogenesis have been studied in the literature [96, 97, 99, 148–154]. Well motivated UV complete scenarios such as the NMSSM also have an additional singlet, which can mix with the SM Higgs [94].

In subsection A we calculate the maximum enhancement of the triple Higgs coupling that can be allowed under the constraints of electroweak baryogenesis and the experimental

constraints coming from the LHC. In subsection B we assume that the singlet is heavy and integrate it out giving rise to an EFT. The resultant expressions for the triple Higgs enhancement and bounds on the FOEPT region can be shown to be the same as those generated from the full Lagrangian in the small mixing angle limit. At the same time, this approach represents an example of the potentials discussed in the previous section and therefore allows to discuss the validity and limitations of the effective theory approach.

3.4.1 Enhancement in the full scalar Lagrangian of the singlet extension

Consider a general scalar potential, with one-loop thermal correction only in the mass term, that can be written in a canonically normalized Lagrangian for the SM extended with one singlet field ϕ_s

$$V(\phi_h, \phi_s, T) = \frac{m_0^2 + a_0 T^2}{2}\phi_h^2 + \frac{\lambda_h}{4}\phi_h^4 + a_{hs}\phi_s\phi_h^2 + \frac{\lambda_{hs}}{2}\phi_s^2\phi_h^2 + t_s\phi_s + \frac{m_s^2}{2}\phi_s^2 + \frac{a_s}{3}\phi_s^3 + \frac{\lambda_s}{4}\phi_s^4 \tag{3.21}$$

Here, ϕ_h is the higgs field. The VEV for the Higgs field is $v = 246$ GeV. We assume that m_s is larger than the weak scale and we therefore ignore the very small temperature corrections affecting the singlet mass.

We stay in the limit, where a_s and λ_s are much smaller compared to a_{hs} and λ_{hs} and drop the a_s and λ_s terms. In this limit, we can retain analytical control over the expressions for the mixing and triple Higgs enhancement, which helps us clearly demonstrate the connection with the EFT. Within this approximation, the mass squared matrix in the basis $(\phi_h\ \phi_s)$ is

$$\mathcal{M}^2 = \begin{pmatrix} m_{11}^2 & m_{12}^2 \\ m_{21}^2 & m_{22}^2 \end{pmatrix} = \begin{pmatrix} 2\lambda_h v^2 & 2\left(a_{hs} + \lambda_{hs} v_s\right) v \\ 2\left(a_{hs} + \lambda_{hs} v_s\right) v & m_s^2 + \lambda_{hs} v^2 \end{pmatrix}, \tag{3.22}$$

where the VEV of the singlet field calculated at the Higgs vacuum is

$$v_s = -\frac{t_s + a_{hs}v^2}{m_s^2 + \lambda_{hs}v^2}. \tag{3.23}$$

The gauge eigenstate basis can be converted to the mass eigenstate basis as follows

$$\phi_h = \cos\theta\, h_1 - \sin\theta\, h_2 + v, \tag{3.24}$$

$$\phi_s = \sin\theta\, h_1 + \cos\theta\, h_2 + v_s. \tag{3.25}$$

The mixing is given as

$$\tan 2\theta = \frac{4v(a_{hs} + \lambda_{hs}v_s)}{2\lambda_h v^2 - m_s^2 - \lambda_{hs}v^2} = \frac{4v(a_{hs}m_s^2 - t_s\lambda_{hs})}{(2\lambda_h v^2 - m_s^2 - \lambda_{hs}v^2)(m_s^2 + \lambda_{hs}v^2)} \tag{3.26}$$

We use Equations (3.22) and (3.26), to convert the potential in Eq. (3.21) to the mass basis (h_2 h_1) at the temperature $T = 0$, where h_1 is the lighter of the two scalar fields. The third derivative of the potential in Eq. (3.21) with respect to h_1 gives the triple Higgs coupling for the lower mass excitation as

$$\lambda_3 = 6\lambda_h v_h \cos^3\theta \left[1 + \left(\frac{\lambda_{hs}v_s + a_{hs}}{\lambda_h v_h}\right)\tan\theta + \frac{\lambda_{hs}}{\lambda_h}\tan^2\theta\right]. \tag{3.27}$$

In the limit of $v^2 \ll m_s^2$, one can easily show that the h_1 mass is given by

$$m_h^2 = 2\lambda_h v^2 - 4v^2\frac{(a_{hs}m_s^2 - t_s\lambda_{hs})^2}{(m_s^2 + \lambda_{hs}v^2)^3} \tag{3.28}$$

Using Eq. (3.29), Eq. (3.28), and Eq. (3.26), we get

$$\lambda_3 = \frac{3m_h^2}{v}\left[\cos^3\theta + \left(\frac{2\lambda_{hs}v^2}{m_h^2}\right)\sin^2\theta\cos\theta\right]. \tag{3.29}$$

For $\theta = 0$, we recover the SM result of $\lambda_3 = \frac{3m_h^2}{v}$.

In the small θ limit, the above formula reduces to

$$\lambda_3 = \frac{3m_h^2}{v}\left[1 + \left(\frac{2\lambda_{hs}v^2}{m_h^2} - \frac{3}{2}\right)\tan^2\theta\right]. \tag{3.30}$$

The same result can be recovered in the EFT approach by integrating out the heavier state as shown in the next section 3.4.2. For the FOEPT in such a potential, we impose the following conditions.

$$V(0, T_c) = V(v_c, T_c), \quad V'(v_c, T_c) = 0. \tag{3.31}$$

This leads to [94]

$$v_c^2 = \frac{1}{\lambda_{hs}}\left(-m_s^2 + \sqrt{\frac{2}{\lambda_h}}\left|m_s\, a_{hs} - \frac{\lambda_{hs}\, t_s}{m_s}\right|\right). \tag{3.32}$$

Here v_c is the value of the doublet scalar field at the critical Temperature (T_c). The value of S is set to

$$v_{s,c} = -\frac{t_s + a_{hs}v_c^2}{m_s^2 + \lambda_{hs}v_c^2}, \tag{3.33}$$

which minimizes the potential at $\phi_h = v_c$. The constraints on the derivatives

$$V'(\phi_c, T_c) = 0, \quad V'(v, 0) = 0, \tag{3.34}$$

imply $a_0 T_c^2 = 8\left(F(v_c^2) - F(v^2)\right)$. Here $F(\phi^2) = -\frac{V'(\phi,0)}{\phi}$ and $v = 246$ GeV.

In Fig. 3.3 we show the enhancements of the trilinear couplings for different values of the singlet mass m_{singlet} and the quartic coupling λ_h. The orange region in the Fig. 3.3 corresponds to the region consistent with a FOEPT, i.e. the boundaries correspond to $v_c^2 = 0$ and $T_c^2 = 0$.

From Eq. (3.32) and Eq. (3.28), it follows that for $T_c = 0$, or equivalently $v_c = v$ one

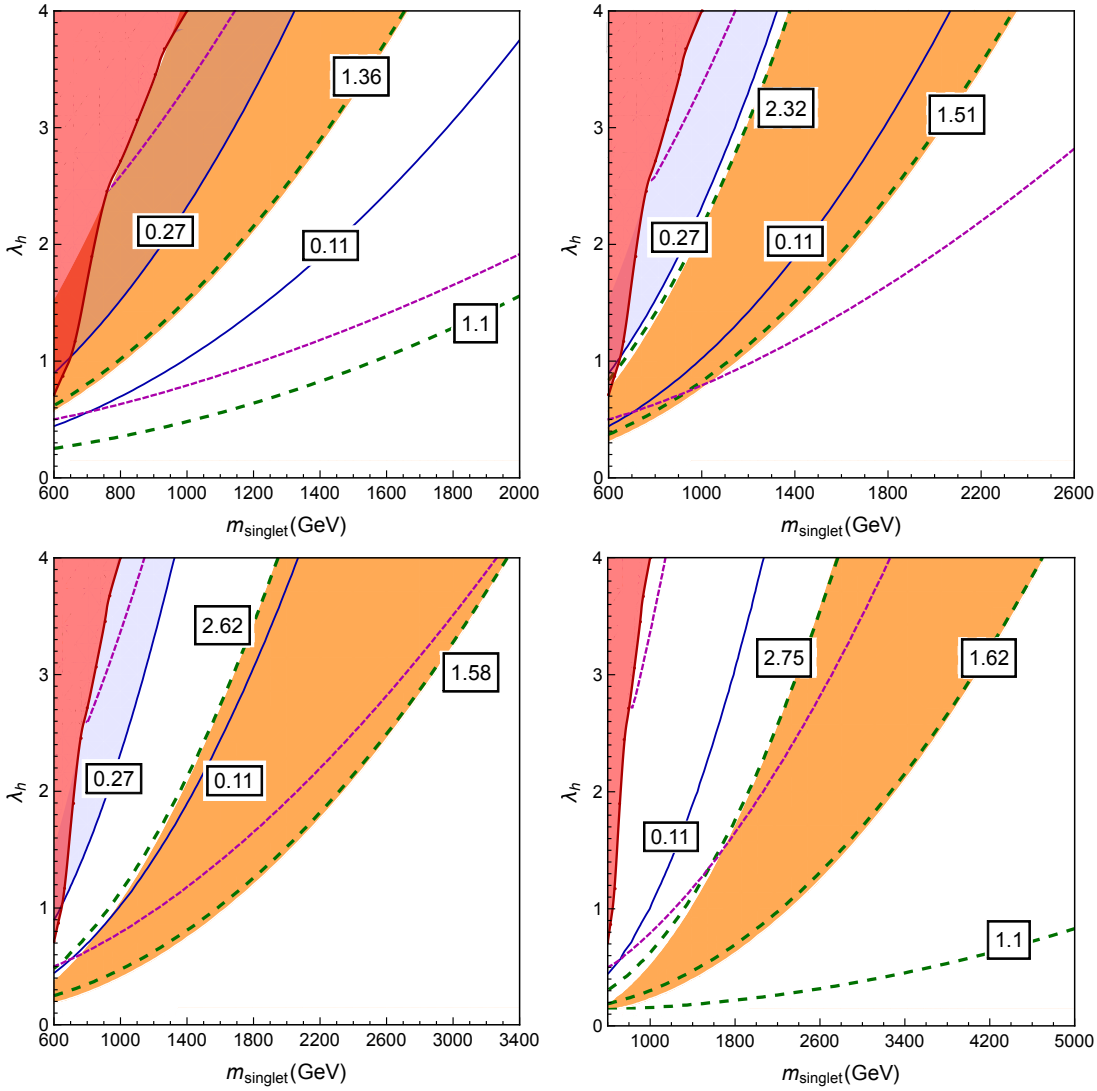

Figure 3.3: Contours of the mixing parameter $\sin^2\theta$ (solid blue line) and of the enhancement of the triple-Higgs coupling (dashed green line) given by Eq. (3.29) in the m_{singlet}–λ_h plane. Blue shaded region denotes 2σ exclusion due to gluon fusion channel. The orange shaded region represents the region consistent with a FOEPT. The region excluded up to 2σ confidence level by Higgs precision measurements is shaded in red. The constraints coming from m_W are shown by magenta (short-dashed) lines. In the top-left panel we present results for $\lambda_{hs} = 0.5$, while in the top-right, bottom-left and bottom-right panels we present results for $\lambda_{hs} = 1$, 2, 4 respectively.

obtains

$$\tan^2\theta(v_c = v) \simeq \frac{m_h^2}{\lambda_{hs} v^2} \tag{3.35}$$

Similarly, for $v_c = 0$, one obtains

$$\tan^2\theta(v_c = 0) \simeq \frac{m_h^2}{3\lambda_{hsv^2}} \tag{3.36}$$

Using these expressions for small mixing angles, Eq. (3.30), one can easily show that

$$\delta(v_c = v) \simeq 2 - \frac{3\ m_h^2}{2\lambda_{hs} v^2} \tag{3.37}$$

while in the case of $v_c = 0$ one obtains

$$\delta(v_c = 0) \simeq \frac{2}{3} - \frac{m_h^2}{2\lambda_{hs} v^2}. \tag{3.38}$$

The region compatible with a FOEPT is always between these boundaries of $v_c = 0$ and $v_c = v$. Thus, the enhancement to the triple Higgs coupling is always less than 3, a result similar to the one obtained in the $(\phi^\dagger\phi)^3$ extension of the Higgs potential discussed in section 3.3.1. Finally, let us mention that the SFOEPT constraint of $v_c > 0.6\,T_c$, is almost always satisfied in the showed orange region.

In Fig. 3.3, we also show experimental constraints coming from Higgs physics and electroweak precision measurements. The mixing parameter $\sin^2\theta$ is denoted by the blue contours. The precision measurements of the SM-like Higgs properties at the LHC already impose strong constraints on the possible mixing angle of the singlet with the doublet. For example, the measurement of the Higgs production signal rates imposes an upper bound on $\sin^2\theta$. If one takes the gluon fusion production process, the combined measurement of ATLAS and CMS gives a signal strength [35]

$$\mu_{\rm ggF} = 1.03^{+0.17}_{-0.15}. \tag{3.39}$$

When the other subleading processes, including the weak boson fusion, associated production and tth production are considered z, one obtains a combined signal strength

$$\mu = 1.09^{+0.11}_{-0.10}. \tag{3.40}$$

Since the mixing with a singlet leads to an overall decrease of all couplings to fermions and gauge bosons, the Higgs decay branching ratios will not be affected and the signal strength will be proportional to $\cos^2\theta$. Hence, from Eqs. (3.39) and (3.40) one obtains a 95% confidence level upper bound on $\sin^2\theta$, namely

$$\sin^2\theta < 0.11 \tag{3.41}$$

if the fit to all production processes is considered, and $\sin^2\theta < 0.27$ if only the more precisely measured gluon fusion processes are considered. In our work, we shall considered both bounds, as an indication of the constraints on the possible realization of this scenario.

In the case of small θ, as seen from the Eq. (3.30), the correction to λ_3 compared to the SM is proportional to $\sin^2\theta$. From this, it is evident that the upper bound on the mixing will be translated into an upper bound on the enhancement of λ_3,

$$\delta < \sin^2\theta_{\max}\left(\frac{2\lambda_{hs}v^2}{m_h^2} - \frac{3}{2}\right) \sim \sin^2\theta_{\max}\left(8\lambda_{hs} - \frac{3}{2}\right). \tag{3.42}$$

Hence, these constraints become more severe for smaller values of λ_{hs}.

From Eqs. (3.30) and (3.42), we also see that reducing λ_{hs} below $\frac{3m_h^2}{4v^2}$ leads to small negative values of δ. Therefore, a small suppression of the triple higgs coupling with respect to the SM is viable for these values of λ_{hs}. As shown in Fig. 3.3, for these values of λ_{hs} the FOEPT region shifts rapidly to the higher mixing values and becomes unviable. Thus, there is trade-off between FOEPT and supression of the triple Higgs coupling with respect to the SM as shown in the EFT case in the previous section.

Moreover, a light singlet that mixes with the SM Higgs will be produced at the LHC and may be searched for in various decay channels. This puts an additional constraint on the realization of this model, which is also shown in Fig. 3.3. The region to the left of the dark red solid line is excluded by the Higgs searches in the WW and ZZ channels [155].

The mixing between the doublet and the singlet is also constrained by precision W mass measurement [156, 157]. The world average for the mass of the W boson is [158]:

$$m_W \;=\; 80.385 \;\pm\; 0.015\; GeV \tag{3.43}$$

including data from LEP II [159], CDF [160] and D0 [161]. The prediction of the W mass is obtained by calculating the muon life time, which yields the relation,

$$m_W^2(1-\frac{m_W^2}{m_Z^2}) = \frac{\pi\alpha}{\sqrt{2}G_F}(1+\Delta r), \tag{3.44}$$

where Δr summarizes the radiative corrections. In the SM, $m_W^{SM} = 80.361 \pm 0.007$ GeV [162, 163], which corresponds to $\Delta r^{SM} = (37.979 \pm 0.406) \times 10^{-3}$, with the mass of the Higgs $m_h = 125$ GeV. From Eq (3.44), $\Delta r^{exp} = (36.32 \pm 0.96) \times 10^{-3}$, which is about 1.7σ from the SM value. Δr can be parametrized as

$$\Delta r = \Delta\alpha + \frac{c_w^2}{s_w^2}(\frac{\delta m_Z^2}{m_Z^2} - \frac{\delta m_W^2}{m_W^2}) + (\Delta r)_{rem}, \tag{3.45}$$

where $\Delta\alpha$ is the radiative correction to the fine structure constant α, and c_w and s_w are the cosine and sine of the weak mixing angle. The second term is the on-shell self-energy correction to the gauge boson masses, which is well approximated by its value at zero momenta, and relates to the ρ parameter as $-\frac{c_w^2}{s_w^2}\Delta\rho$. The last term, $(\Delta r)_{rem}$, includes vertex corrections and box diagrams at one loop level, which are subleading. In the case of having

a singlet mixed with the SM Higgs, Δr is given by

$$\Delta r = \Delta r^{SM} - \frac{c_w^2}{s_w^2}(\Delta\rho^{\text{singlet}} - \Delta\rho^{SM}), \tag{3.46}$$

where $\Delta\rho^{\text{singlet}}$ and $\Delta\rho^{SM}$ are the $\Delta\rho$ calculated in the the case with a mixed-in singlet and the SM [164].

$$\Delta\rho^{\text{singlet}} - \Delta\rho^{SM} = G_F \frac{m_Z^2}{2\sqrt{2}\pi^2} sin^2\theta \left(H_T(\frac{m_{Singlet}^2}{m_Z^2}) - H_T(\frac{m_h^2}{m_Z^2}) \right), \tag{3.47}$$

where

$$H_T(x) = \frac{3}{4}x \left(\frac{\log(x)}{1-x} - \frac{\log(x \times m_Z^2/m_W^2)}{1 - x \times m_Z^2/m_W^2} \right). \tag{3.48}$$

The constraints on $\sin^2\theta$ obtained from the W mass become quite severe since as mentioned above, the SM is already in tension with the W mass measurement, and the singlet contribution increases this tension. The 2 σ constraint coming from Δr calculated from Eq (3.46) is shown by the lowered dashed magenta line in Fig. 3.3. On the other hand, if one assumes that some other new physics, which does not modify the loop induced Higgs production processes in a relevant way is responsible for the difference between the SM and the current W mass measurement the bounds become significantly weaker as seen from the upper dashed magenta line in Fig. 3.3. It follows from Fig. 3.3 that even considering the tight constraints coming from Higgs measurements and precision electroweak parameters, a strongly first order phase transition is possible in these scenarios, provided $\lambda_{hs} \gtrsim 1$. Large values of the singlet mass, of the order of the TeV scale, are possible in this case, making $\sin^2\theta$ small. In our analysis, we ignore the one loop contributions to the effective potential since they are suppressed compared to the tree level mixing effects. When λ_{hs} is sizable, as we show in the lower panels in Fig. 3.3, those corrections may not be negligible and should be taken into account in a more refine analysis of the critical parameters.

Before concentrating on the EFT analysis let us stress that an important contribution to

the double Higgs production cross section that is always missed in this analysis is the resonant double Higgs production induced by the singlet. This can lead to a relevant contribution if the singlet is below the TeV scale and the mixing is sizable [165]. For instance, at the LHC with a center of mass energy of 14 TeV a 500 GeV singlet with a mixing of $\sin^2\theta = 0.2$, will lead to a resonant production cross section through gluon fusion for the singlet of about 1.13 pb [166]. Under these conditions the branching ratio $\mathrm{BR}(S \to hh) \sim 0.013$. Then the double Higgs production rate induced by the singlet is about 15 fb, which is about a factor of 4 smaller than the SM double Higgs production rate. Such a singlet would show up in the invariant mass distribution as a narrow resonance, as the singlet width is about 17 GeV. When the singlet gets heavier, say about 1 TeV, and for a mixing angle $\sin^2\theta = 0.1$, the double Higgs production induced by the singlet is reduced to about 2.6 fb, which is significantly suppressed compared to the double Higgs production from the box and triangle diagrams, and difficult to detect in the standard decay channels. Then, in the region of a heavy singlet and small mixing angle, the EFT gives a proper description of the physics involved in double Higgs production. In this case, the singlet presence may only be inferred indirectly and one can make contact with an effective theory description of the modification of the trilinear couplings and of the double Higgs production rate.

3.4.2 EFT formulation for the singlet extension

In the limit of large values of the singlet mass m_s, and small mixing between the SM-like Higgs and the heavy singlet, we can integrate out the heavy singlet, and the resulting EFT should describe the same physics as we have described in the previous subsection.

For momenta very small compared to the masses of the scalars, solving the equation of motion for the singlet gives

$$\phi_s = -\frac{t_s + a_{hs}h^2}{m_s^2 + \lambda_{hs}h^2}. \tag{3.49}$$

Substituting this into the original potential in Eq. (3.21) yields an effective potential for h, which is given by [94]

$$V(h,T) = \frac{m^2(T)}{2}\phi_h^2 + \frac{\lambda_h}{4}\phi_h^4 - \frac{\left(t_s + a_{hs}\phi_h^2\right)^2}{2\left(m_s^2 + \lambda_{hs}\phi_h^2\right)}. \tag{3.50}$$

where $m^2(T) = m_0^2 + a_0 T^2$. The integration out of the singlet also leads to a modification of the Higgs kinetic term, which means that the well normalized Higgs field H will no longer be given by h, but will be affected by the mixing with the singlet. In other words, substituting the EOM of S in its kinetic term leads to an h dependent normalization factor,

$$(\partial_\mu\phi_h)(\partial^\mu\phi_h) + (\partial_\mu\phi_s)(\partial^\mu\phi_s) \to \left(1 + \frac{4\,\phi_h^2(am_s^2 - t_s\lambda_{hs})^2}{(ms^2 + \lambda_{hs}\phi_h^2)^4}\right)(\partial_\mu\phi_h)(\partial^\mu\phi_h). \tag{3.51}$$

Demanding H to be well normalized and retaining up to first order in the small parameter

$$z = \frac{(am_s^2 - t\lambda_{hs})^2 v^2}{m_s^8} \tag{3.52}$$

we obtain

$$\phi_H = \phi_h + \frac{2z\phi_h^3}{3\,v^2} + \mathcal{O}(\phi_h^5). \tag{3.53}$$

The corresponding c_H is

$$\frac{c_H}{4\Lambda^2} = \frac{z}{v^2}. \tag{3.54}$$

The variable z defined above is related to the mixing angle between the singlet and the doublet. From Eq. (3.26), we can write

$$\tan^2 2\theta = \frac{16z}{(2\lambda_h y - 1 - \lambda_{hs}y)^2\,(1 + \lambda_{hs}y)^2} = 4\tan^2\theta + \mathcal{O}(\tan^3\theta). \tag{3.55}$$

Substituting Eq. (3.61) and retaining first order in z we get

$$\tan^2 2\theta = 16z + \mathcal{O}(z^2) = 4\tan^2\theta + \mathcal{O}(\tan^3\theta) \implies \tan^2\theta \sim 4z \tag{3.56}$$

Inverting the relation between ϕ_h and ϕ_H given in Eq. (3.53) one obtains

$$\phi_h = \phi_H - \frac{2z}{3\,v^2}\phi_H^3 + \mathcal{O}(\phi_H^5), \tag{3.57}$$

Substituting this in Eq. (3.50), we get an effective potential, which retaining up to order H^6 corrections is given by

$$V_{eff}(\phi_H, T) = \frac{m^2}{2}\phi_H^2 + \left(\frac{\lambda_h - 2z/y}{4} - \frac{2m^2 z}{3v^2}\right)\phi_H^4 + \left(\frac{-4z(\lambda_h - 2z/y) + 3z\lambda_{hs}}{6v^2}\right)\phi_H^6, \tag{3.58}$$

where $y = v^2/m_s^2$. This shows that the presence of a large negative correction to the quartic coupling, of order $2z/y$. This correction, which depends only on ratios of mass parameters, allows for the presence of a negative effective quartic coupling which according to our analysis of the EFT at this order in section 3.3.1, is essential for the obtention of a FOEPT.

Using this potential Eq. (3.50) we apply the Higgs mass condition to write

$$\left(V''_{eff} - \frac{V'_{eff}}{\phi_H}\right)\Big|_{\phi_H=\langle\phi_H\rangle} = m_H^2, \quad \text{where} \quad \langle\phi_H\rangle = v + \frac{2zv}{3}. \tag{3.59}$$

Solving this simultaneously with

$$\frac{V'_{eff}}{\phi_H}\Big|_{\phi_H=\langle\phi_H\rangle} = 0, \tag{3.60}$$

leads to a relation of the value of λ and the Higgs mass.

$$\lambda = \lambda_h - \frac{2z}{y} = \frac{m_H^2}{2v^2} + \left(\frac{2\, m_H^2}{v^2} - 6\lambda_{hs} \right) z. \tag{3.61}$$

Since $m_H^2/(2v^2) \simeq 1/8$, for small values of z the coefficient of the quartic coupling λ is small in magnitude and may be negative for λ_{hs} of order 1.

Moreover, a sizable correction to the sixth order term appears, which is there even in the absence of kinetic terms corrections. Observe that $\lambda_h - 2z/y$, which as shown above corresponds to λ in the EFT analysis, appears also in the first term in the ϕ_H^6 coefficient. Since λ is small as discussed above, the ϕ_H^6 coefficient is dominated by the second term in the bracket. The cut off scale can be then calculated from

$$\frac{c_6}{8\Lambda^2} \sim \frac{3\lambda_{hs} z}{6v^2} = \frac{\lambda_{hs}(am_s^2 - t\lambda_{hs})^2}{2m_s^8}. \tag{3.62}$$

The corresponding cutoff scale is, for $c_6 = 1$

$$\Lambda^2 = \frac{m_s^8}{4\lambda_{hs}(am_s^2 - t\lambda_{hs})^2}. \tag{3.63}$$

Thus, when $(am_s^2 - t\lambda_{hs})$ and λ_{hs} become sizable, Λ could be significantly lower than m_s. However, $am_s^2 - t\lambda_{hs}$ is related to $\sin^2\theta$, which is constrained by electroweak symmetry breaking, precision Higgs measurements, heavy SM-like Higgs searches, and W mass as discussed above, the cutoff scale can not be lowered arbitrarily. For example, since λ is small, from Eq. (3.61), we have

$$\lambda_h \sim \frac{2z}{y} = \frac{2(am_s^2 - t\lambda_{hs})^2}{m_s^6}. \tag{3.64}$$

Then the cutoff scale is about

$$\Lambda^2 \sim \frac{m_s^2}{2\lambda_h \lambda_{hs}.} \tag{3.65}$$

It is instructive to compare these results with those shown in Fig. 3.3. For instance, when $m_{\rm singlet}$ is about 1.4 TeV, $\lambda_{hs} = 2$, and $\lambda_h = 2$, that is close to the boundary of the orange region in the bottom-left panel of Fig. 3.3, the cutoff scale is about 494 GeV, which is about the lower bound of the cutoff scale in a $(\phi^\dagger\phi)^3$ theory and is consistent with the left boundary of the orange region in this figure. Similarly, for the same results of λ_h and λ_{hs}, and for $m_{\rm singlet} = 2.4$ TeV, that is closed to the other boundary in the bottom-left panel of Fig. 3.3, the effective cutoff scale that is obtained from Eq. (3.65) is about 848 GeV that is very close to the upper bound on Λ that is obtained for a FOEPT in the $(\phi^\dagger\phi)^3$ extension. One can check that similar values of the cutoff are obtained at the left and right boundaries of the orange regions in Fig. 3.3 for other values of λ_h, λ_{hs} and $m_{\rm singlet}$.

After substituting Eq. (3.61) and considering the field fluctuations of the field ϕ_H,

$$\phi_H = v_H + H, \tag{3.66}$$

we obtain,

$$\lambda_3 \equiv g_{HHH} = \frac{3m_H^2}{v}\left(1 + 4\,z\,\left(\frac{2\lambda_{hs}v^2}{m_H^2} - \frac{3}{2}\right)\right). \tag{3.67}$$

Using this in Eq. (3.67) we obtain

$$\lambda_3 = \frac{3m_H^2}{v}\left(1 + \left(\frac{2\lambda_{hs}v^2}{m_h^2} - \frac{3}{2}\right)\tan^2\theta\right) \tag{3.68}$$

This formula is the same as that obtained in Eq. (3.30) from the small mixing limit of the enhancement up to $\tan^2\theta$ order in the full renormalizable Lagrangian. Thus, as expected, the EFT approach is equivalent to the small mixing limit of the full theory. To make the analogy more transparent let's emphasize that from Eq. (3.57) the fluctuations of the field

$\phi_h = v + h$ and H are related by

$$h = \left(1 - \frac{\tan^2\theta}{2}\right)\ H \simeq\ \cos\theta\ H \tag{3.69}$$

That is the same relation we obtain between h_1 and h in the full theory, Eq. 3.24, when we consider negligible h_2 fluctuations associated with its decoupling from the low energy theory.

We note that the effective potential derived in Eq. (3.58) is of order ϕ_H^6. This is the same order as the $(\phi^\dagger\phi)^3$ potential described in section 3.3.1. In this case, however, the range of values of δ is not constrained from 2/3 to 2 as expected from the $(\phi^\dagger\phi)^3$ theory, but is shifted to lower values. This is due to the kinetic terms corrections we were not considered in the analysis in Section 3.2. For $\lambda_{hs} \gtrsim 1$, the kinetic term corrections remain significantly smaller than the ones associated with the effective potential modification, which are controlled by the λ_{hs} coupling. Expressing Eq. (3.67) in terms of c_6 and c_H, using Eq. (3.62) and Eq. (3.54), we obtain

$$\lambda_3 = \frac{3m_H^2}{v}\left(1 + c_6\frac{2v^4}{m_h^2\Lambda^2} - \frac{3}{2}c_H\frac{v^2}{\Lambda^2}\right), \tag{3.70}$$

This is consistent with Eq. (3.6) when $c_H = 0$. Also, this is consistent with Eq.(34) in Ref [148] and Eq. (124) of Ref. [167] when taking $\lambda = m_h^2/(2v^2)$. As mentioned before, our expression is more suitable for the study of the region of parameters consistent with a FOEPT in which λ is small and negative and the proper relation between λ and the Higgs mass can only be obtained after including the higher order corrections proportional to c_6, Eq. (3.9).

Higher powers of ϕ_H in the Eq. (3.58) can be obtained by retaining more terms in the expansions with respect to z and y variables. For instance, we have checked that at next order the well normalized field is given by

$$\phi_H = \phi_h + \frac{2z\phi_h^3}{3v^2} - \frac{2(z^2 + 4yz\lambda_{hs})\phi_h^5}{5v^4} \tag{3.71}$$

Expressing h in terms of H,

$$\phi_h = \phi_H - \frac{2z\phi_H^3}{3v^2} + \frac{2(13z^2 + 12yz\lambda_{hs})\phi_H^5}{15v^4} \tag{3.72}$$

one can obtain the value of δ, as we did below, that is given by

$$\delta = \left(-6 + \frac{8v^2\lambda_{hs}}{m_h^2}\right) z + \left(30 - \frac{48v^2\lambda_{hs}}{m_h^2}\right) z^2 + \left(40\lambda_{hs} - \frac{32v^2\lambda_{hs}^2}{m_h^2}\right) yz \tag{3.73}$$

That indeed reproduces the small θ expansion of the exact formula, Eq. (3.30).

Again, it is straightforward to see that H and h are related by

$$h = \left(1 - \frac{\tan^2\theta}{2} + \frac{3\tan^4\theta}{8}\right)\ H \simeq\ \cos\theta\ H \tag{3.74}$$

as expected from the relation between h_1 and h in the full theory, Eq. (3.24).

Before we concentrate on collider phenomenology, let us comment on the negative enhancement in a theory with a mixed-in singlet. Once a small singlet quartic coupling λ_s is turned on to stabilize the potential, λ_{hs} can go to negative values, as long as $|\lambda_{hs}| < \sqrt{\lambda_h\lambda_s}$. A small λ_s leads to a contribution to λ_3 suppressed by $\sin^3\theta$, $\sim 6\lambda_s v_s \sin^3\theta$. As seen in Eq. (3.68), a negative λ_{hs} provokes a negative enhancement while a small positive λ_s adds negligible contribution to λ_3. We note that, in the EFT context, the λ_s term generates a term of order $\frac{1}{4}\lambda_s\frac{a_{hs}^4}{ms^8}H^8$ in the effective potential, and allows for the terms of order of H^6 negative. Therefore, a theory with a negative λ_{hs} may results in a negative enhancement in λ_3 as we go beyond a $(\phi^\dagger\phi)^3$ theory described before, as shown for instance in the green region in Fig 3.1.

3.5 measurement of the triple Higgs coupling at the LHC

The triple Higgs coupling λ_3 can be probed by the double Higgs production at the LHC. At the leading order (LO), there are two diagrams contributing to the process. The triangle

diagram, which is sensitive to λ_3 and the box diagram. The two diagrams interfere with each other destructively. The LO matrix elements of the subprocess are known [168–170]. NLO QCD corrections are known [171] in an EFT approach, by applying the low energy theorem (LET) [172] within the infinite quark mass approximation. NNLO corrections in the large quark mass limit are calculated in [173–175]. Next-to-next-to-leading logarithmic (NNLL) corrections are calculated in [176]. For our analysis, we shall take a NNLO K-factor = 2.27 [173].

For our analysis, we assume the double Higgs production is modified because of the altered λ_3 coupling. The double Higgs production rate could also be modified by introducing new particles that couple to gluon, and the Higgs in the loop [177, 178]. Those new particles change the amplitudes corresponding to the triangle diagram and the box diagram at the same time and also contribute to the single Higgs production, which is well measured at the LHC. Therefore, those contributions are constrained and tend to be small for the double Higgs production [178].

For the Higgs decays, we consider $\gamma\gamma$, $\tau^+\tau^-$, W^+W^- and $b\bar{b}$ modes, which are measured in the single Higgs production at the LHC. The production rate of double Higgs is suppressed by three orders of magnitude compared to the single Higgs production at the LHC [166], so one of the two Higgs bosons needs to decay to $b\bar{b}$ for statistics, and $\gamma\gamma$, $\tau^+\tau^-$, and W^+W^- modes can be considered for the other Higgs boson. We do not study the $b\bar{b}W^+W^-$ decay mode due to the overwhelming $t\bar{t}$ background, that renders a low significance [115, 116]. The four b final states suffers from a large QCD background and therefore are very difficult for the LHC even in the boosted region of the Higgs, where the jet substructure techniques may be used [115]. In this work, we are therefore going to focus on the $b\bar{b}\gamma\gamma$ mode.

The irreducible background in the $hh \to b\bar{b}\gamma\gamma$ channel include $b\bar{b}\gamma\gamma$, $t\bar{t}h(\gamma\gamma)$ and $z(b\bar{b})h(\gamma\gamma)$ processes. Considering the possibility that a charm or light quarks fake a bottom quark, and a light jet fakes a photon, the processes $c\bar{c}\gamma\gamma$, $jj\gamma\gamma$, and $b\gamma jj$ also contribute to the background. The $t\bar{t}h$ background can be efficiently suppressed by vetoing extra jets, leptons or

missing energy. Requiring the invariant mass of the two b-jets, $m_{b\bar{b}}$ and the two photons, $m_{\gamma\gamma}$ within some window of the Higgs mass helps to reduce the Zh background and the QCD background. In the previous studies, a cut on the invariant mass of the two Higgs bosons, m_{hh} [116, 118, 120], or some equivalent cuts were required [121] was imposed to further reject the background. In those studies, it was shown that an $O(1)$ precision in the triple Higgs boson coupling λ_3 may be achieved at the 14 TeV run of the LHC, with a high integrated luminosity of order 3000 fb^{-1}.

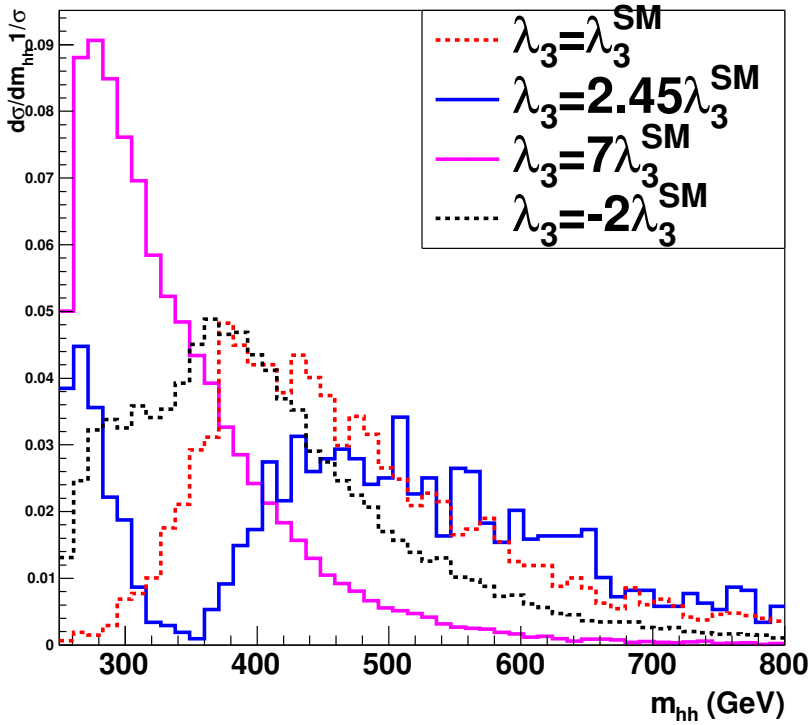

Figure 3.4: Normalized m_{hh} distributions for $\lambda_3 = \lambda_3^{SM}$, $\lambda_3 = 2.45\lambda_3^{SM}$ and $\lambda_3 = 7\lambda_3^{SM}$ and $\lambda_3 = -2\,\lambda_3^{SM}$. The cancellation between the box and triangle diagram is exact at $\lambda_3 = 2.45\lambda_3^{SM}$ at $2m_t$ threshold, that explains the dip. Note that the distribution shifts to smaller values as λ_3 increases

.

As pointed out in [118], and also noticed in [121], the acceptance for new physics with large λ_3 compared to the SM value is much lower for the same set of cuts. The reason for this behavior is that the m_{hh} distribution is very different for the SM and for new physics with

a large λ_3. When m_{hh} is below the $2m_t$ threshold, there are only real parts of the triangle and the box diagram, and these two diagrams interfere with each other destructively. The cancellation is exact at the 2 m_t threshold at $\lambda_3 = 2.45\lambda_3^{SM}$. When m_{hh} is above the 2 m_t threshold, imaginary parts start to develop, and the destructive interference is not as strong as it is below the $2m_t$ threshold. So as λ_3 increases, the cross section increases more significantly below the 2 m_t threshold than above the 2 m_t threshold. This means that, as λ_3 increases, the distribution of m_{hh} shifts to smaller values, as shown in Fig 3.4, where we plot the normalized m_{hh} distribution using MCFM [179] for various values of λ_3. Thus, using the same set of cuts for new physics with a large λ_3 lead to a low acceptance at the LHC. Therefore, a modified cut on m_{hh}, $m_{hh} < 2m_t$ should be used when search for new physics with a large λ_3.

The m_{hh} distribution also helps to distinguish positive and negative values of λ_3. For negative λ_3, the m_{hh} distribution shifts to larger values compared to the positive λ_3 that yields the same production for gluon fusion because of the constructive interference between the box and the triangle diagrams, as shown in Fig 3.4. Then, the negative and positive values of λ_3 that have the same total rate of gluon fusion can be distinguished by studying the m_{hh} distribution.

3.5.1 Double Higgs production in the $b\bar{b}\gamma\gamma$ channel

In order to understand the impact of the cuts in the m_{hh} invariant mass distribution on the reach for double Higgs production at the LHC and future colliders, we have performed a collider study of this process for different values of the triple Higgs coupling and in different Higgs decay channels. In spite of the low rate, one of the most sensitive channels is when the Higgs decays into photons, since it allows a good Higgs reconstruction with relatively low background. We therefore performed a collider study for the $hh \to b\bar{b}\gamma\gamma$ channel. The signal with various values of λ_3 is generated by MCFM [179] and passed to Pythia8 [180] for parton shower and hadronization, and then passed to Delphes [181] for detector simulation.

We apply a NNLO K-factor of about 2.27 for the signal [173], The background processes are generated with MadGraph [182] and then passed to Pythia and Delphes. We apply a NLO K-factor = 1.1 for $t\bar{t}h$ and a NNLO QCD, NLO EW K-factor = 1.33 for Zh [166]. There are no higher order corrections known for the QCD backgrounds, and therefore, all the QCD processes are normalized to LO. We take a b-tagging efficiency of 70% and a mistag rate of 24% for c-jets and 2% for light jets [183]. We adopt a photon tagging rate of 85% and a jet to photon fake rate $\epsilon_{j\to\gamma} = 1.2 \times 10^{-4}$ [184]. We require the following cuts

$$\begin{aligned} p_t(b) > 30 \text{ GeV}, |\eta(b)| < 2.5,\ p_t(\gamma) > 30 \text{ GeV}, |\eta(\gamma)| < 2.5 \\ 112.5 \text{ GeV} < m_{bb} < 137.5 \text{ GeV},\ 120 \text{ GeV} < m_{\gamma\gamma} < 130 \text{ GeV}. \end{aligned} \tag{3.75}$$

For the SM case, we further require

$$m_{hh} > 350 \text{ GeV}, \tag{3.76}$$

while for $\lambda_3 > 3\ \lambda_3^{SM}$, we require

$$250 \text{ GeV} < m_{hh} < 350 \text{ GeV}. \tag{3.77}$$

The results for LHC 14 TeV are displayed in Table 3.1. As shown in Table 3.2, the significance reaches 5σ level at $\lambda_3 \sim 6.5\lambda_3^{SM}$, and $\lambda_3 \sim -0.2\lambda_3^{SM}$ at 14 TeV and 3000 fb^{-1}. One caveat of this analysis is that we include a K-factor for the signal (and also for the ZH and tth background), but the QCD background is only considered at LO. If we assume a K-factor of about 2 for the QCD processes, the significance will drop by a factor of $\sqrt{2}$, which can be compensated by the fact that there are two detectors.

It is instructive to compare these results with those obtained by the LHC experimental collaborations. ATLAS and CMS have performed similar studies on the $hh \to bb\gamma\gamma$ channel. For HL-LHC, ATLAS expects a 1.3 σ significance for the SM case [121], and the CMS

	σ (fb)	Eq (3.75) + Eq (3.76) (fb)	Eq (3.75) + Eq (3.77) (fb)
hh($b\bar{b}\gamma\gamma$) ($\lambda_3 = \lambda_3^{SM}$)	0.15	1.0×10^{-2}	-
hh($b\bar{b}\gamma\gamma$) ($\lambda_3 = 5\lambda_3^{SM}$)	0.26	-	1.12×10^{-2}
hh($b\bar{b}\gamma\gamma$) ($\lambda_3 = 7\ \lambda_3^{SM}$)	0.71	-	3.3×10^{-2}
hh($b\bar{b}\gamma\gamma$) ($\lambda_3 = 9\ \lambda_3^{SM}$)	1.43	-	6.08×10^{-2}
hh($b\bar{b}\gamma\gamma$) ($\lambda_3 = 0$)	0.29	1.33×10^{-2}	-
hh($b\bar{b}\gamma\gamma$) ($\lambda_3 = -\lambda_3^{SM}$)	0.50	2.26×10^{-2}	-
hh($b\bar{b}\gamma\gamma$) ($\lambda_3 = -2\lambda_3^{SM}$)	0.77	2.94×10^{-2}	-
$b\bar{b}\gamma\gamma$	5.05×10^{3}	1.34×10^{-2}	4.0×10^{-2}
$c\bar{c}\gamma\gamma$	6.55×10^{3}	$4.19\ \times10^{-3}$	2.68×10^{-2}
$b\bar{b}\gamma j$	9.66×10^{6}	4.60×10^{-3}	1.38×10^{-2}
$jj\gamma\gamma$	7.82×10^{5}	2.38×10^{-3}	5.26×10^{-3}
$t\bar{t}h$	1.39	1.40×10^{-3}	2.33×10^{-3}
zh	0.33	6.86×10^{-4}	9.01×10^{-4}
$b\bar{b}jj$	7.51×10^{9}	5.34×10^{-4}	$6.47\ \times10^{-4}$

Table 3.1: Cross section in fb of the hh signal and various backgrounds expected at the LHC at $\sqrt{s} = 14$ TeV after applying the cuts discussed in Eq (3.75), (3.76) and (3.77).

λ_3	λ_3^{SM}	$5\lambda_3^{SM}$	$7\lambda_3^{SM}$	$9\lambda_3^{SM}$	0	-λ_3^{SM}	-$2\lambda_3^{SM}$
$S/\sqrt{B}$	3.3	2.1	6.0	11	4.4	7.5	9.8

Table 3.2: Significance expected for hh at the LHC at $\sqrt{s} = 14$ TeV for an integrated luminosity of 3000 fb^{-1} after applying cuts in Eq (3.75) + Eq (3.76) ($\lambda_3 < 3\lambda_3^{SM}$), or Eq (3.75)+Eq (3.77) ($\lambda_3 > 3\ \lambda_3^{SM}$).

expectation is about 1.6 σ [185]. These results are about a factor two weaker than the ones we obtain in our study. On the other hand, the results from current theoretical studies show a significance range from 2σ to 6σ [114, 116, 118, 120]. The difference with the experimental results may proceed from different sources. In our analysis, we use very simple cuts, and we do not attempt to optimize the cuts for the SM background, but we believe extra cuts do not help much in this case as it is a rare process. We also do not try to perform a realistic detector simulation.

The main issue we want to stress is the impact of the cuts in the invariant mass distribution when studying possible modifications of the triple Higgs coupling. We obtain a very significant sensitivity improvement in the case where λ_3 deviates significantly from the SM, when we implement the new cuts in Eq. (3.77) we propose for such cases. For instance, when $\lambda_3 = 5\lambda_3^{SM}$, if we use the cuts in Eq. (3.76), we only expect a 0.67σ significance, while we expect 2.1σ significance if we use the cuts in Eq. (3.77). Similar large improvements are obtained for other sizable values of $\lambda_3 > 3\lambda_3^{SM}$.

Due to the relatively low sensitivity of the LHC in looking for double Higgs production, it is interesting to consider similar signatures at future colliders, in particular a future high energy pp collider. The sensitivity will depend on many factors, including the center of mass energy and the detector performance. To be specific, we shall consider the case of 100 TeV pp collider, assuming that the detector performance stays the same as at the LHC, performing similar cuts as the ones in the LHC analysis. We show the results in Table 3.3 and Table 3.4. In our analysis, we considered only positive values of λ_3, since as shown above, the LHC is already sensitive to the negative values. It is then easy to extrapolate the same analysis for higher energies. The results presented in Table 3.3 show that a 100 TeV collider should be sensitive to triple Higgs boson couplings $\lambda_3 \sim 5\lambda_3^{SM}$, where the same cuts proposed in Eq (3.75) were used. The significance we obtain is similar the ones obtained in Refs. [186] and [101] for the same process. Again, we obtain a significant improvement of the sensitivity at large values of $\lambda_3 > 3\lambda_3^{SM}$ when the new cuts on m_{hh} given in Eq. (3.77) are used.

	σ (fb)	Eq (3.75) + Eq (3.76) (fb)	Eq (3.75) + Eq (3.77) (fb)
hh($\lambda_3 = \lambda_3^{SM}$)	3.4	0.11	-
hh($\lambda_3 = 3\lambda_3^{SM}$)	1.48	0.042	-
hh($\lambda_3 = 5\lambda_3^{SM}$)	4.45	-	0.10
$b\bar{b}\gamma\gamma$	1.7×10^{6}	0.129	0.52
$c\bar{c}\gamma\gamma$	1.0×10^{5}	6.45×10^{-2}	0.42
$b\bar{b}\gamma j$	1.19×10^{5}	1.68×10^{-2}	6.72×10^{-2}
$jj\gamma\gamma$	2.73×10^{6}	1.92×10^{-2}	7.3×10^{-2}
$t\bar{t}h$	86.41	2.72×10^{-2}	2.53×10^{-2}
zh	0.88	1.76×10^{-3}	1.4×10^{-3}
$b\bar{b}jj$	4.07×10^{10}	2×10^{-3}	4.7×10^{-3}

Table 3.3: Cross section of the hh signal and various backgrounds expected at a 100 TeV collider after applying the cuts discussed in Eq (3.75), (3.76) and (3.77).

λ_3	λ_3^{SM}	$3\lambda_3^{SM}$	$5\lambda_3^{SM}$
$S/\sqrt{B}$	11	4.5	5.3

Table 3.4: The significance of double Higgs production expected for hh at a 100 TeV collider for an integrated luminosity of 3000 fb^{-1} after applying cuts in Eq (3.75) + Eq (3.76) ($\lambda_3 < 3\lambda_3^{SM}$), or Eq (3.75) + Eq (3.77) ($\lambda_3 > 3\ \lambda_3^{SM}$)

.

3.5.2 Double Higgs production in the $b\bar{b}\tau^+\tau^-$ channel

Since the Higgs has many different significant decay channels, it is useful to think about double Higgs production in channels different from the $bb\gamma\gamma$ considered in this work. A particularly interesting one is the $bb\tau\tau$ channel. The $b\bar{b}\tau^+\tau^-$ channel enjoys a larger cross section but suffers from the difficulty in the event reconstruction due to the missing energy associated with τ decays. It also suffers from larger backgrounds that should be properly considered to obtain a realistic reach estimate.

The τ pair invariant mass $m_{\tau\tau}$ may be estimated by the missing mass calculator [187], and similar methods could be used to estimate m_{hh} in this channel. In order to estimate the reach in this channel, we shall assume that the $m_{\tau\tau}$ invariant mass can be reconstructed with a similar resolution as m_{bb} [187] invariant mass. Furthermore, we shall assume that the two Higgs invariant mass m_{hh} can be reconstructed as well as it is obtained at the parton level. The discovery reach is then estimated adopting the cuts and background calculations

presented in Ref. [116].

We go beyond the analysis of Ref. [116] by including the relevant background coming from the $bbjj$ process. Under the above conditions, and assuming a jet to τ fake rate $\epsilon_{j\to\tau} = 1/100$ [118], we obtain a significance $S/\sqrt{B} \sim 3.75$ for $\lambda_3 = \lambda_3^{SM}$, that is similar to the one obtained in the $\gamma\gamma$ channel. However, estimating m_{hh} in the $bb\tau\tau$ channel is very difficult. For that reason, CMS preforms a preliminary study using the Stransverse mass m_{T2} instead of m_{hh} to distinguish the signal from the background, and shows a 0.9σ significance for HL-LHC [185]. That is significantly smaller than the one found in [119] using a similar method. Therefore, the $bb\tau\tau$ channel may represent a good complementary channel to the $bb\gamma\gamma$ one, and should be studied further.

3.6 Conclusions

In this work, we have studied the modifications of the triple Higgs couplings in theories in which the Higgs potential is modified by the addition of higher order, non-renormalizable operators, induced by the presence of new physics at the weak scale. Contrary to previous statements in the literature, we have shown that, a simple addition of a dimension six operators may lead to a large modification of the triple Higgs coupling λ_3 with respect to its SM value in the regions of parameter space consistent with a FOEPT.

Furthermore, the addition of higher order operators may also lead to a reduction of the triple Higgs coupling, or even its change of sign, with relevant implications for collider physics. Interestingly, negative enhancements of the triple Higgs coupling tend to be associated with a second order phase transition, while a first order phase transition tends to be associated with a large positive enhancement of this coupling.

We also argue, building up on the previous results in the literature, that different values of the triple Higgs coupling will have a strong impact not only on the total cross section, but also on the invariant mass distribution of double Higgs production at the LHC. This motivates the use of different cuts for double Higgs production for values of the trilinear coupling about

or smaller than the SM value than for the large values of λ_3. The determination of the total cross section, together with the analysis of the invariant mass distribution may give hints not only about the magnitude of the departure of the Higgs coupling with respect to the SM value, but also of its sign. Considering these different cuts in the invariant mass distribution and including background processes that were previously ignored in the literature, we showed that at the 14 TeV run of the LHC at high luminosities of order of a 3.3σ is expected for $\lambda_3 = \lambda_3^{SM}$, and a 5 σ significance is expected for $\lambda_3 = 6.5\lambda_3^{SM}$ (-0.2 λ_3^{SM}) for the $b\bar{b}\gamma\gamma$ channel. The $b\bar{b}\tau^+\tau^-$ channel presents a promising complementary channel.

CHAPTER 4

WRONG-SIGN BOTTOM YUKAWA COUPLING IN LOW-ENERGY SUPERSYMMETRY

4.1 Introduction

The Higgs discovery [188],[189] has led to the confirmation of the Standard Model as the proper effective theory at the weak scale. No new particle has been seen at the LHC, implying that physics at the weak scale is weakly interacting or that strongly interacting particles, if present, should lead to signatures involving soft decay products or in channels with large irreducible backgrounds. Searches for new physics under these conditions should be complemented by precision measurements of the properties of the Standard Model particles as well as rare processes rates.

Although the gauge sector of the Standard Model has been tested with high precision, the Higgs sector properties are still greatly unknown. The signal strength of different production and decay channels are in overall agreement with the Standard Model, but the errors are still large, and the coupling of the Higgs with third generation quarks and leptons is subject to big uncertainties. Indeed, while the central value of the production rate of the Higgs in association with top quarks is currently a factor two larger than the SM value, the central value of the production rate of the Higgs decaying into bottom quarks and produced in association with heavy gauge bosons seems to be 40 percent lower than the SM prediction [190]. Although the differences between the theoretical predictions and the experimental values could be the result of statistical fluctuations, it is interesting to consider the possibiiity that the couplings of the Higgs to top and bottom quarks differ from the SM values due to new physics effects.

In this article, we shall consider the possibility that not only the magnitude but also the sign of the Higgs coupling to bottom quarks differ from the Standard Model predictions. This is an intriguing possibility that could be realized in the simplest two Higgs doublet

extension of the Standard Model [191]. Such region of parameters has been invoked recently also in models that lead to large rates of lepton flavor violating decays of the Higgs bosons $h \to \tau\mu$[198] and on theories of flavor at the weak scale [199]. In this article we study the possible realization of this scenario within the minimal supersymmetric extensions of the SM, namely the MSSM [192],[193],[194],[195] and the NMSSM[196].

Low energy supersymmetry [197] leads to the stability of the weak scale under the large radiative effects induced by possible heavy particles, like the ones associated with an hypothetical Grand Unified Theory (GUT). It also leads to the radiative breaking of the electroweak symmetry, induced by corrections associated with the superpartners of the third generation quarks. The low energy theory contains at least two Higgs doublets and therefore the coupling of the Higgs to bottom quarks may be affected by mixing between the different CP-even Higgs bosons in the theory. Such region of parameters has been invoked recently also in models that lead to large rates of lepton flavor violating decays of the Higgs bosons $h \to \tau\mu$ [198] and on theories of flavor at the weak scale [199].

Large negative variation of the bottom quark coupling to the SM Higgs may be obtained in the MSSM at large values of $\tan\beta$, the standard ratio of the Higgs vacuum expectation values, and values of the heaviest CP-even Higgs boson masses not far above the weak scale [191]. This region of parameter space, however, is strongly restricted by searches for Higgs bosons decaying into τ-lepton pairs [200],[201], what makes the realization of this scenario difficult. As we shall show in this article, the scenario is more easily realized in the NMSSM, although the necessary values of the coupling λ of the singlet superfield to the doublet Higgs superfields are larger than the ones leading to perturbative consistency of the theory up to the GUT scale.

This article is organized as follows. In section 2 we analyze the possibility of a wrong Yukawa coupling within two Higgs doublet models. In section 3 we study the possible realization of this idea within the MSSM and the NMSSM. After pointing out the difficulties of its realization in the MSSM, in section 4 we present a numerical analysis of this question

within the NMSSM. In section 5 we study the question of perturbativity of the theory while studying the evolution of couplings up to high scales. In section 6 and 7 we study the experimental probes of this scenario. We reserve section 8 for our conclusions.

4.2 Wrong sign Yukawa in Type II Two Higgs Doublet Models

The tree-level couplings of 2HDM Higgs to Gauge bosons and fermions, are listed as below,

$$g_{hVV} = s_{\beta-\alpha}\,, \tag{4.1}$$

$$g_{ht\bar{t}} = \frac{m_t}{v}\,\frac{c_\alpha}{s_\beta} \equiv \frac{m_t}{v}\left(s_{\beta-\alpha} + c_{\beta-\alpha}t_\beta^{-1}\right), \tag{4.2}$$

$$g_{hb\bar{b}} = -\frac{m_b}{v}\,\frac{s_\alpha}{c_\beta} \equiv \frac{m_b}{v}\left(s_{\beta-\alpha} - c_{\beta-\alpha}t_\beta\right), \tag{4.3}$$

where s_α (s_β) $= \sin\alpha$ ($\sin\beta$), c_α (c_β) $= \cos\alpha$ ($\cos\beta$) and $s_{\beta-\alpha}$ ($c_{\beta-\alpha}$) $= \sin(\beta-\alpha)$ ($\cos(\beta-\alpha)$). As we can see from Eq. (4.2), for the gauge boson couplings to be SM-like, we need $s_{\beta-\alpha} \approx 1$. In this case, for moderate values of $\tan\beta$, the Higgs coupling to top-quarks or other up type fermions becomes SM-like due the $\tan\beta$ suppression of the second term on the right hand side of Eq. (4.2). However, for the Higgs to b-quark coupling, Eq. (4.3), a wrong sign could arise without changing the Higgs decay width and branching ratio when $g_{hb\bar{b}}/g_{hb\bar{b}}^{SM} \simeq -1$. This could be achieved with minor changes of the Higgs couplings to top-quarks and weak gauge bosons for sizable values of $\tan\beta$ and

$$t_\beta\; c_{\beta-\alpha} \approx 2. \tag{4.4}$$

This is in contrast with the condition $t_\beta c_{\beta-\alpha} \simeq 0$ that ensures a SM-like coupling of the bottom-quark to the Higgs boson.

The scalar potential of the most general two-Higgs-doublet extension of the SM may be

written as :

$$\begin{aligned} V &= m_{11}^2\Phi_1^\dagger\Phi_1 + m_{22}^2\Phi_2^\dagger\Phi_2 - m_{12}^2(\Phi_1^\dagger\Phi_2 + \text{h.c.}) + \tfrac{1}{2}\lambda_1(\Phi_1^\dagger\Phi_1)^2 + \tfrac{1}{2}\lambda_2(\Phi_2^\dagger\Phi_2)^2 \\ &\quad +\lambda_3(\Phi_1^\dagger\Phi_1)(\Phi_2^\dagger\Phi_2) + \lambda_4(\Phi_1^\dagger\Phi_2)(\Phi_2^\dagger\Phi_1) \\ &\quad + \left\{\tfrac{1}{2}\lambda_5(\Phi_1^\dagger\Phi_2)^2 + [\lambda_6(\Phi_1^\dagger\Phi_1) + \lambda_7(\Phi_2^\dagger\Phi_2)]\Phi_1^\dagger\Phi_2 + \text{h.c.}\right\} \ , \end{aligned} \tag{4.5}$$

After converting to the Higgs basis [202],[203], the Higgs potential above could be rewritten as:

$$\mathcal{V} \supset \ldots + \tfrac{1}{2}Z_1(H_1^\dagger H_1)^2 + \ldots + \left[Z_5(H_1^\dagger H_2)^2 + Z_6(H_1^\dagger H_1)H_1^\dagger H_2 + \text{h.c.}\right] + \ldots \ , \tag{4.6}$$

where we have only retained those terms relevant for the following discussion and the new couplings $Z_i's$ are associated with previous $\lambda_i's$ by the following relations [58],[204],[54]

$$Z_1 \equiv \lambda_1 c_\beta^4 + \lambda_2 s_\beta^4 + \tfrac{1}{2}(\lambda_3+\lambda_4+\lambda_5)s_{2\beta}^2 + 2s_{2\beta}\left[c_\beta^2\lambda_6 + s_\beta^2\lambda_7\right] , \tag{4.7}$$

$$Z_5 \equiv \tfrac{1}{4}s_{2\beta}^2\left[\lambda_1+\lambda_2-2(\lambda_3+\lambda_4+\lambda_5)\right] + \lambda_5 - s_{2\beta}c_{2\beta}(\lambda_6-\lambda_7) , \tag{4.8}$$

$$Z_6 \equiv -\tfrac{1}{2}s_{2\beta}\left[\lambda_1 c_\beta^2 - \lambda_2 s_\beta^2 - (\lambda_3+\lambda_4+\lambda_5)c_{2\beta}\right] + c_\beta c_{3\beta}\lambda_6 + s_\beta s_{3\beta}\lambda_7 , \tag{4.9}$$

The CP-even Higgs mixing angle in this basis is identified with $\beta-\alpha$. Consequently, we have [58],[54]

$$c_{\beta-\alpha} = \frac{-Z_6 v^2}{\sqrt{(m_H^2-m_h^2)(m_H^2-Z_1v^2)}} . \tag{4.10}$$

This term should be small and can be realized in both the decoupling limit, i.e. $m_H \gg v$ and the alignment limit, i.e. $Z_6 \approx 0$.

4.3 Wrong sign Yukawa couplings in the MSSM and the NMSSM

The Higgs sector of the MSSM is a type-II 2HDM and it consists of two Higgs doublets with tree-level quartic couplings which are related to the squares of the weak gauge couplings. Since Supersymmetry imposes concrete values for the quartic couplings λ_i it is interesting to check whether the wrong sign Yukawa coupling could arise in the frame of MSSM without conflicting with other Higgs phenomenology. For this, one has to take into account the relevant radiative corrections arising from the interaction of the Higgs field with the third generation fermions and their scalar superpartners. In the MSSM, it's well known that a SM-like neutral Higgs boson could only be obtained in two distinct scenarios, i.e. the decoupling limit [58]-[216] and the alignment limit [58],[204],[216],[59]. The decoupling limit happens when $m_h \ll m_H$, while the alignment limit arises when one of the CP-even Higgs bosons, when expressed as a linear combination of the real parts of the two neutral Higgs fields, lies in the same direction in the two Higgs doublet field space as neutral Higgs vacuum expectation values. This alignment does not in general depend on the masses of the non-standard Higgs bosons.

It's not difficult to work out the expression of Z_6 at the one-loop level. The largest one-loop contributions are proportional to the fourth power of the top-quark Yukawa coupling h_t, namely:

$$Z_6 v^2 = -s_{2\beta}\left\{m_Z^2 c_{2\beta} - \frac{3v^2 s_\beta^2 h_t^4}{16\pi^2}\left[\ln\left(\frac{M_S^2}{m_t^2}\right) + \frac{X_t(X_t+Y_t)}{2M_S^2} - \frac{X_t^3 Y_t}{12M_S^4}\right]\right\}, \tag{4.11}$$

where m_Z is the neutral gauge boson mass, m_t is the top quark mass, M_S is the stop mass scale, $X_t = A_t - \mu/t_\beta$, $Y_t = \mu\ t_\beta + A_t$, A_t is the trilinear stop-Higgs coupling and μ is the Higgsino mass parameter. Combined with Eq. (4.10), we get:

$$t_\beta\ c_{\beta-\alpha} \simeq \frac{-1}{m_H^2 - m_h^2}\left[m_h^2 + m_Z^2 + \frac{3m_t^4 X_t(Y_t - X_t)}{4\pi^2 v^2 M_S^2}\left(1 - \frac{X_t^2}{6M_S^2}\right)\right]. \tag{4.12}$$

In Equation (4.12), if we substitute in $Y_t - X_t = \mu(t_\beta + \frac{1}{t_\beta})$, in the large $\tan\beta$ limit where $X_t = A_t - \mu/t_\beta \approx A_t$, we get the following estimate [54]:

$$t_\beta \; c_{\beta-\alpha} \simeq \frac{-1}{m_H^2 - m_h^2}\left[m_h^2 + m_Z^2 + \frac{3m_t^4}{4\pi^2 v^2}\frac{\mu}{M_S}\left(\frac{A_t}{M_S} - \frac{A_t^3}{6M_S^3}\right)\left(t_\beta + \frac{1}{t_\beta}\right)\right] . \qquad (4.13)$$

If we want $t_\beta \; c_{\beta-\alpha}$ to be as large as 2, it's clear that we need to let the third term in the square bracket to be as negative as possible. Unfortunately this will lead to an unacceptably large value of $\tan\beta$, which makes the Yukawa coupling to down type fermions non-perturbative. In order to see that, let's recall the fact that stability of the Higgs potential demands that $|A_t|$ and $|\mu|$ should both be smaller than 3 [205]. Under this constraint, the minimum of the expression $\frac{\mu}{M_S}\left(\frac{A_t}{M_S} - \frac{A_t^3}{6M_S^3}\right)$ is -4.5, which is achieved for $A_t/M_S = 3$ and $\mu/M_S = 3$. A rough estimate of the coefficient $\frac{3m_t^4}{4\pi^2 v^2}$ is $m_h^2/16$ which is very small compared to the first two positive terms in the square bracket. Thus, for $t_\beta \; c_{\beta-\alpha}$ to reach the target value 2, $\tan\beta$ needs to be large. More specifically, for $m_H \approx 250\ GeV$, the necessary values of $\tan\beta \approx 30$, while for $m_H \approx 500\ GeV$ these values become very large, $\tan\beta \approx 120$. These values of m_H and $\tan\beta$ are excluded by heavy Higgs searches at the LHC [200],[201]. One could avoid these constraints for larger values of the heavy Higgs mass, larger than 1 TeV. However, for $m_H \approx 1\ TeV$ the necessary values of $\tan\beta \approx 500$, and it is difficult to keep the perturbative consistency of the theory at such large values of $\tan\beta$. Thus we reach the conclusion that the current LHC bounds make it very difficult to invert the sign of the Higgs coupling to bottom quarks within the MSSM.

Next let's turn to the Next-to-Minimal supersymmetric extension of the SM (NMSSM) [196], with only an extra singlet superfield added on top of the MSSM. The CP-even singlet will mix with the two neutral CP-even Higgs bosons. We considered the simpler case when the superpotential is scale invariant and and thus the complete Lagrangian would have

an accidental Z_3 symmetry,

$$W = \lambda \widehat{S} \widehat{H}_u \cdot \widehat{H}_d + \frac{\kappa}{3} \widehat{S}^3 + h_u \widehat{Q} \cdot \widehat{H}_u \, \widehat{U}^c_R + h_d \widehat{H}_d \cdot \widehat{Q} \, \widehat{D}^c_R + h_\ell \widehat{H}_d \cdot \widehat{L} \, \widehat{E}^c_R \,, \tag{4.14}$$

where $\widehat{S}, \widehat{H_u}, \widehat{H_d}$ denote the singlet and doublet Higgs superfields, and $\widehat{Q}, \widehat{D}_R, \widehat{U}_R$ are the quark superfields, while $\widehat{L}, \widehat{E}_R$ are the lepton superfields, h_i are the Yukawa couplings and λ and κ are both dimensionless couplings. The most significant change in the NMSSM would be that at tree level, there is an extra correction proportional to $\frac{1}{2}\lambda^2 v^2$ in the M^2_{11} term of the Higgs basis. This term is well known since it can lift up the upper limit of the lightest Higgs mass at tree level [206], thus make it possible to reach 125 GeV without the large quantum corrections needed in the MSSM [207],[208],[209]–[213]. What's more important in this case, is that it can modify the Z_6 and Z_1 terms introduced earlier in the MSSM case and release the strong tension between $\tan\beta$ and M_A present in the MSSM to make $c_{\beta-\alpha} t_\beta = 2$ feasible. In the NMSSM, it's straightforward to get the expression for Z_6 at moderate or large values of t_β, including only the stop loop corrections, namely [218]:

$$Z_6 v^2 \approx \frac{1}{\tan\beta} \left[m_h^2 + m_Z^2 - \lambda^2 v^2 \right] + \frac{3 v^2 h_t^4 \mu X_t}{16\pi^2 M_S^2} \left(1 - \frac{X_t^2}{6 M_S^2} \right) \tag{4.15}$$

which leads to

$$t_\beta \; c_{\beta-\alpha} \approx \frac{-1}{m_H^2 - m_h^2} \left[\left(m_h^2 + m_Z^2 - \lambda^2 v^2 \right) + \frac{3 m_t^4 A_t \mu t_\beta}{4\pi^2 v^2 M_S^2} \left(1 - \frac{A_t^2}{6 M_S^2} \right) \right] \tag{4.16}$$

Compared with Equation (4.12), we got an extra $-\lambda^2 v^2$ term in the parenthesis, which tends to push $t_\beta \; c_{\beta-\alpha}$ towards positive values and makes it promising to get $t_\beta \; c_{\beta-\alpha} = 2$ with smaller values of $\tan\beta$. However, for that purpose we need λ to be of order 1. We found that when λ or κ are large, say $\lambda \approx \kappa \approx 1$, the chargino, neutralino and Higgs loop contributions are also sizable and can not be neglected when evaluating Higgs mass and couplings, more specifically $t_\beta \; c_{\beta-\alpha}$ in this case. After taking these into consideration, the phenomenological

analysis becomes more complicated and a numerical analysis with full quantum corrections up to two-loop level are necessary to select the proper region of parameter space leading to the inversion of the bottom coupling. On the other hand, large λ could lead to a Landau pole problem at energies lower than the Grand Unification scale. In the following two sections we will discuss these two issues and assess the possibility of negative Yukawa couplings in the NMSSM.

As we will show in later sections, beyond the problems associated with perturbativity, this simple framework leads to problems in the CP-even Higgs sector, since the square of the lightest CP-even Higgs boson mass is generically pushed to negative values due to large mixing effects. A possible solution to this problem is to add a non-zero singlet tadpole term χ_S to the potential

$$\Delta V = \xi_S \, S + h.c. \tag{4.17}$$

This term breaks the accidental Z_3 symmetry and could be a result of the supersymmetry breaking mechanism at high scales [214]. A large $|\xi_S|$ could keep the singlet decoupled from the two neutral Higgs bosons [196], reducing the problem to an approximate 2x2 Higgs mixing one, with low energy quartic couplings that are modified by terms proportional to powers of the couplings λ and κ.

4.4 NMSSM Results: Full Analysis

As mentioned in the last section, besides the large one-loop quantum corrections to $\mathcal{M}^2_{11}$, there are relevant two-loop corrections in the NMSSM from various sources, which also give non-trivial contributions to the Higgs mass matrix at large values of λ, κ and that modify the bottom Yukawa coupling in a significant way, by adjusting the mixing between the two light CP-even Higgs bosons. From the full expression of the squared mass matrix elements at two-loop level [196], it's straightforward to see that the most important κ or λ dependent contributions come from Higgs and chargino/neutralino loops. After a short numerical check,

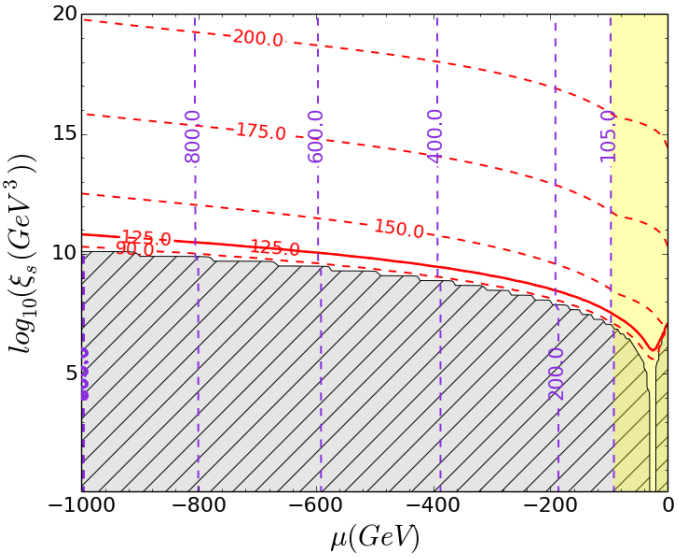

Figure 4.1: In this plot, $\lambda = 1.3$ and $\kappa = 0.1$ are fixed, and μ and χ_s are varied. The gray area is excluded for negative Higgs mass. And Red contour lines are the lightest Higgs mass, you can see we show the 125GeV with solid style. And the lightest chargino mass contours are displayed in purple.

we found that for values of κ and λ of order one, these Higgs and electroweakino-loop corrections could be as large as a few tens of percent of the unperturbed squared mass matrix elements. This observation points to the fact that in order to find the accurate Higgs mixing and Yukawa couplings at large valudes of κ and λ, one has to take these loop corrections into account.

In the rest of this section, we conducted a numerical search for a wrong-sign Yukawa coupling within NMSSM model using the NMSSMTools code [219], which includes the most relevant two-loop radiative corrections. Some typical parameters can be found in Table 4.1. In this calculation, we took a large value of the tadpole term and scanned parameters including $\tan\beta, m_A, \mu, \lambda$ and κ. More specifically, we fixed A_t, A_τ and A_b at 1500 GeV and used squark and slepton masses $M_S = 1$ TeV. The weak gauginos were assumed to be heavy $M_{1,2} \simeq 1$ TeV, while the gluino mass was fixed at $M_3 = 2$ TeV.

Since we would like to modify the bottom-quark coupling without strongly affecting the coupling to gauge bosons, $\sin(\beta - \alpha) \simeq 1$. This implies that $\cos(\beta - \alpha)\tan\beta \simeq 2$ may

only be obtained for moderate or large values of $\tan\beta$. Taking into account the strong existing constraints on this region of parameters for the low values of the MSSM-like CP-odd Higgs mass [200],[201] necessary to induce a large correction to the bottom coupling, we concentrated on moderate values of $\tan\beta$. In particular in our analysis, $\tan\beta$ was chosen to be in the range 6–8, while μ was scanned over the whole range consistent with a stable Higgs potential, i.e. from $-3M_S$ to $3M_S$. At last we vary m_A within the interval between 250 GeV and 350 GeV.

As we stressed above, in order to reduce the problem to an effective 2x2 mass matrix, similar to the MSSM case, we added a singlet tadpole term. In addition, we verified that for zero tadpole values it is difficult to obtain parameter sets that satisfy the lightest Higgs mass constraint (e.g. 122 GeV - 128 GeV), proper chargino and neutralino masses and Higgs decay rates at the same time. A typical example of this tension is shown in Figure 4.1. In this plot we fixed the λ, κ, m_A, A_f etc. at values that favor a large values of $\tan\beta\cos(\beta-\alpha)$ (at least for larger ξ_S) and then we scanned over the values of μ and χ_S to search for changes in the sign of the bottom coupling. As we can see, when ξ_S is close to 0, the proper Higgs mass and chargino masses above the current bound may not be obtained for any of the values in our scan of parameters. To let the proper Higgs mass coexist with proper chargino properties, χ_S should be at least of order 10^8 to 10^9 GeV^3. The same qualitative result is obtained for all sizable values of λ and κ necessary to obtain a change of sign of he bottom coupling. Therefore, in the following analysis, we set the tadpole term χ_S to a fixed value, which was arbitrary chosen to be 6×10^{10}. Parameters are randomly drawn from uniform distributions and we discard all points which give the wrong lightest Higgs mass or fail other collider experimental constraints. The results of this analysis are shown in Figure 4.2.

From Figure 4.2, it's clear that the demand of wrong-sign bottom Yukawa fixes λ to be of order 1, and all λ's leading to a solution have values above 0.8; the constraint on κ is not quite tight, possible values of κ span the whole region from 0 to 1, with a gentle dependency on λ. All points have κ_b close to -1 as demanded, and satisfy the constraints in the Higgs

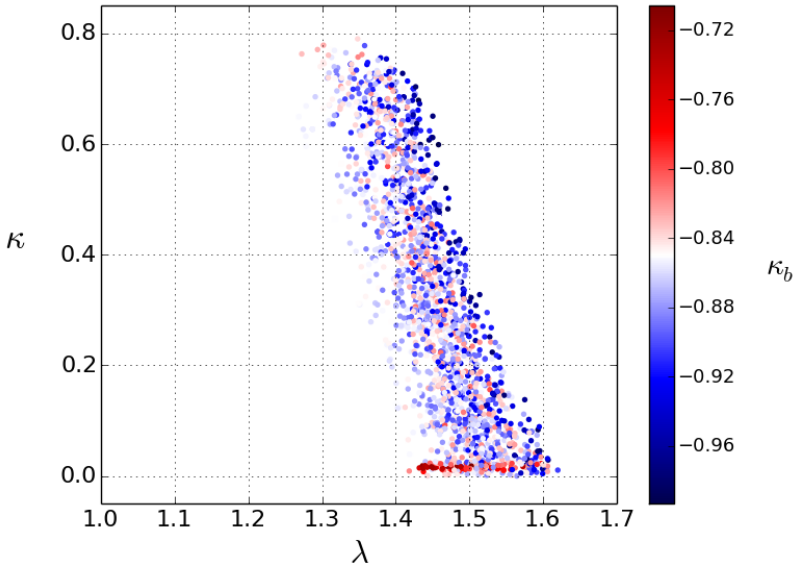

Figure 4.2: Scatter plot of all points that survive the 125 GeV mass constraint and predict a wrong-sign bottom Yukawa coupling. The colorbar shows the value of κ_b which is the ratio between Higgs to $b\bar{b}$ coupling and its SM value, i.e. $g^{NMSSM}_{hb\bar{b}}/g^{SM}_{hb\bar{b}}$. All points have κ_b close to -1 as demanded.

Table 4.1: Typical parameters found by NMSSMTools that gave negative Higgs to $b\bar{b}$ couplings

No.	$\tan\beta$	m_A	μ	λ	κ	$M_{i,(i=1,2)}$	A_{f3}	m_{h_1}	κ_b	$BR(h_1 \to b\bar{b})$	m_{h_2}	m_{H^+}
1	8.0	335	-1121	1.51	0.076	1000	1500	124.2	-0.86	60.6%	293	158
2	7.0	338	-1089	1.50	0.280	1000	1500	128.0	-0.83	54.0%	292	160
3	8.0	347	-1096	1.42	0.423	1000	1500	124.0	-0.86	61.0%	278	157
4	8.0	339	-1020	1.36	0.730	1000	1500	126.1	-0.87	56.3%	270	157

sector.

In figure 4.3, we plotted the κ_g v.s. κ_b and κ_γ v.s. κ_b, with κ_i being the ratio of the Higgs coupling to the particle i to its value in the SM. All points are consistent with the current experimental constraints. We see that apart from a change in sign of the bottom Yukawa, all solutions show values of the couplings that are within 20% of the SM values, that coincide with the naive requirement for general 2HDM provided by the authors of Ref. [191]. In particular, Fig. 4.3, shows that κ_γ is below 0.96 and κ_g is between 1.12 and 1.13.

Another characteristic of those surviving points in Table 4.1 is that they all have low charged Higgs mass. Even though they are heavy enough to avoid the search for $t \to$

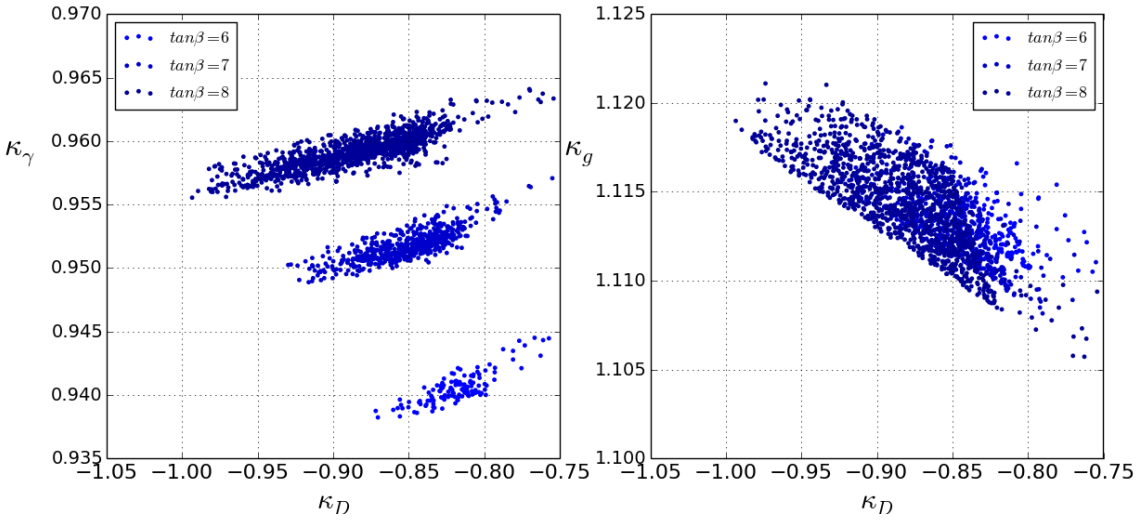

Figure 4.3: Display the couplings of the SM-like Higgs to γ, down-type quark and gluon and κ is the ratio between the calculated value and the SM value. The points here are the same points shown in Fig 4.2 that survived relevant experiments and gave wrong-sign Yukawa couplings to down-type quarks. Left panel: κ_γ v.s. κ_D; right panel: κ_g v.s. κ_D. In the left panel, the three stripes correspond to the three values of $\tan\beta$ we used in our search, namely $\tan\beta = 6$, 7, and 8.

H^+b decay, but the $H \to H^\pm W^\mp$ channel opens up and becomes the dominant decay mode of the heavier neutral Higgs H and the CP-odd Higgs A. This observation has many phenomenological consequences. On one hand, the branching ratio of $H \to \tau^+\tau^-$ would be squeezed even when $\tan\beta$ is large, so that we could push $\tan\beta$ higher than the current bound provided by CMS for the m_h^{max} senario. This speculation is confirmed by the Fig. 4.4, in which we see that all the $Br_{H\to\tau^+\tau^-}$ values are lower than 3%. On the other hand, this large $Br_{H\to H^\pm W^\mp}$ also means that measurement through this exotic decay channel at LHC is possible.

4.5 Renormalization Group Evolution

The discussions in previous sections demonstrated that to reverse the sign of Higgs to bottom coupling the values of the λ or κ couplings, or both need to take sizable values. However this region of parameter leads to the so-called Landau-pole problem, i.e. coupling constants will

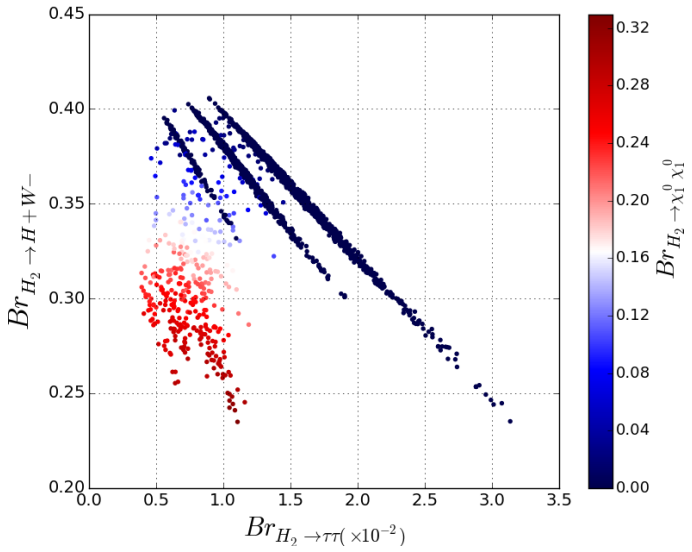

Figure 4.4: Correlations between the branching ratios of the main decay channels of H_2 when bottom Yukawa coupling is negative.

reach infinity at some energies much lower than the GUT scale during the renormalization group evolution [221]. This problem can be solved by extending the gauge groups, for example, to $SU(3)_c \times SU(2)_1 \times SU(2)_2 \times U(1)_Y$, more specifically $SU(2)_1$ is the weak group coupling with the third generation and Higgs sector while $SU(2)_2$ couples with the first two generations [220]. The symmetry breaking from $SU(2)_1 \times SU(2)_2$ to the regular $SU(2)$ is achieved by a bi-doublet chiral field Σ happening at energies $< \Sigma >= u$ of the oder of a few TeV. Considering only the particles in the NMSSM, we get the following one-loop RGE

equations for α's and Yukawa couplings.

$$\frac{d\tilde{\alpha}_1}{dt} = -\frac{33}{5}\tilde{\alpha}_1^2, \tag{4.18}$$

$$\frac{d\tilde{\alpha}_2}{dt} = -\tilde{\alpha}_2^2, \tag{4.19}$$

$$\frac{d\tilde{\alpha}_3}{dt} = 3\tilde{\alpha}_3^2, \tag{4.20}$$

$$\frac{dY_t}{dt} = -Y_t\left(Y_\lambda + 6Y_t - \frac{16}{3}\tilde{\alpha}_3 - 3\tilde{\alpha}_2 - \frac{13}{15}\tilde{\alpha}_1\right), \tag{4.21}$$

$$\frac{dY_\lambda}{dt} = -Y_\lambda\left(4Y_\lambda + 2Y_\kappa + 3Y_t - 3\tilde{\alpha}_2 - \frac{3}{5}\tilde{\alpha}_1\right), \tag{4.22}$$

$$\frac{dY_\kappa}{dt} = -6Y_\kappa\left(Y_\lambda + Y_\kappa\right) \tag{4.23}$$

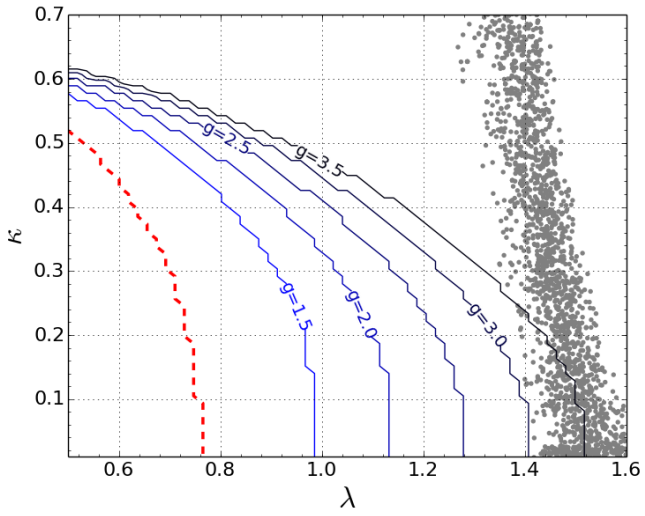

Figure 4.5: Below the red dashed line is the allowed region of λ and κ in the NMSSM model; the blue contours shows the allowed boundaries of λ and κ for different values of the new $SU(2)$ coupling g_1 at $u = 3$ TeV. Below each line all couplings are perturbative during 1-loop RG evolution up to the energies of $10^{16}GeV$. The contour lines correspond to $g_1 = 3.5, 3.0, 2.5, 2.0$ and 1.5 from right to left. Values of g_1 greater than 3.5 would violate the perturbative condition and are ignored. The grey points show the values of κ and λ associated with negative values of the bottom Yukawa, shown in Fig. 4.2.

Taking the new symmetry breaking sector into consideration, above the symmetry breaking scale, due to the presence of new particles the previous RGE equations would be replaced

by the ones shown below:

$$\frac{d\tilde{\alpha'}_2}{dt} = 2\tilde{\alpha'}_2^2, \tag{4.24}$$

$$\frac{d\tilde{\alpha''}_2}{dt} = -4\tilde{\alpha''}_2^2, \tag{4.25}$$

$$\frac{d\tilde{\alpha}_3}{dt} = 2\tilde{\alpha}_3^2, \tag{4.26}$$

$$\frac{dY_t}{dt} = -Y_t\left(Y_\lambda + 6Y_t - \frac{16}{3}\tilde{\alpha}_3 - 3\tilde{\alpha'}_2\right), \tag{4.27}$$

$$\frac{dY_\lambda}{dt} = -Y_\lambda\left(4Y_\lambda + 2Y_\kappa + 3Y_t - 3\tilde{\alpha'}_2\right), \tag{4.28}$$

$$\frac{dY_\kappa}{dt} = -6Y_\kappa\left(Y_\lambda + Y_\kappa\right), \tag{4.29}$$

where

$$\tilde{\alpha}_i(t) = g_i^2(t)/(4\pi)^2, Y_\lambda(t) = \lambda^2(t)/(4\pi)^2, Y_\kappa(t) = \kappa^2(t)/(4\pi)^2 \tag{4.30}$$

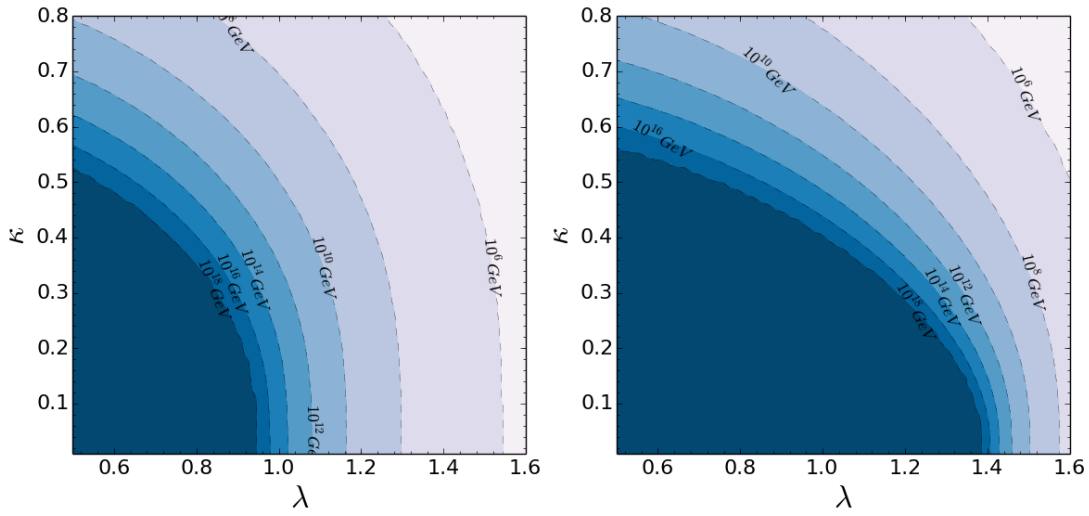

Figure 4.6: Energy at which some coupling becomes non-perturbative for each λ and κ combination for a fixed values of g_1 at $u = 3$ TeV. The left panel corresponds to $g_1 = 1.5$ while the right panel corresponds to $g_1 = 3.0$. The lines labeled with $10^{16}GeV$ in the two panels are consistent with the two contour lines in Figure 4.5 with the corresponding g_1 values.

The modification to the renormalization group equations gives us more flexibility in the

choice of λ and κ. In Fig. 4.5, we displayed the RGE result with and without new gauge couplings. We can see that the constraint from the requirement of avoiding the Landau-pole problem is quite stringent since the maximum viable values for λ is of order 0.7 and becomes smaller for larger values of κ. Therefore, all solutions with negative bottom Yukawa couplings, which are associated with values of $\lambda > 0.8$, lead to the loss of perturbativity below the GUT scale. In Fig. 4.5, we also show the improvement after including the extended gauge sector. The running of the parameters are dictated by the modified RGE's as shown below. It is clear that large values of α_2' lead to a smaller β function for λ and hence to a slower increase of λ at large energies. From Figure 4.5, we can see that the strong constraint on the λ and κ plane is pushed outwards towards larger values of both parameters. For instance, when g_1 is 3.5, a combination of $\lambda = 1.4$ and $\kappa = 0.2$ would be allowed, which has been guaranteed to give a negative value of the Higgs to $b\bar{b}$ coupling. In order to show this, in Fig. 4.5 we also show the values of λ and κ associated with the NMSSM solutions found in Fig. 4.2 (grey points).

4.6 Radiative Higgs Decay to Quarkonia

The change of sign of the bottom Yukawa coupling may have relevant phenomenological consequences. One Higgs process affected by the bottom Yukawa coupling is the radiative decay of the Higgs to Quarkonium, in particular to the Υ meson, which is composed of $b\bar{b}$. Within the Standard Model, the direct and indirect Feynman diagrams have an approximate accidental cancelation, which effectively excludes this decay process at all but very high luminosities. Figures 4.7 and 4.8 show the direct and indirect Feynman diagrams, taken from Ref. [222].

The resulting decay widths of $H \to \Upsilon(nS)+\gamma$ in terms of κ_b, the bottom Yukawa coupling

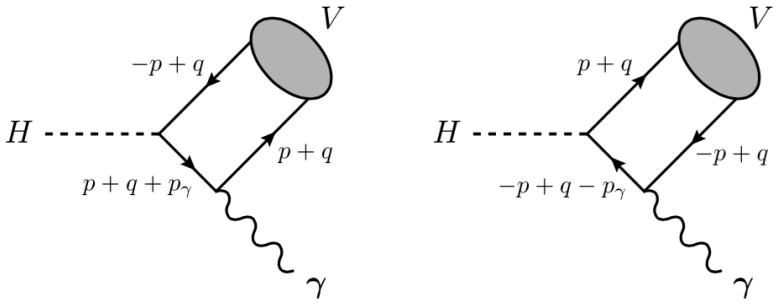

Figure 4.7: Feynman diagrams for the direct amplitude of $H \to V + \gamma$, where V represents the quarkonium bound state [222].

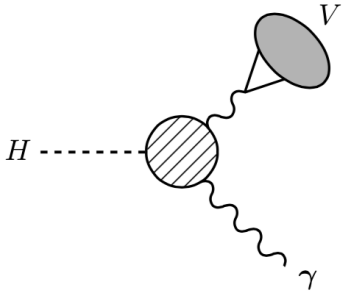

Figure 4.8: Feynman diagram for the indirect amplitude of $H \to V + \gamma$ [222].

relative to the SM value, are given by [222]

$$\begin{aligned}
\Gamma[H \to \Upsilon(1S) + \gamma] &= |(3.33 \pm 0.03) - (3.49 \pm 0.15)\kappa_b|^2 \times 10^{-10} \text{ GeV} \\
\Gamma[H \to \Upsilon(2S) + \gamma] &= |(2.18 \pm 0.03) - (2.48 \pm 0.11)\kappa_b|^2 \times 10^{-10} \text{ GeV} \\
\Gamma[H \to \Upsilon(3S) + \gamma] &= |(1.83 \pm 0.02) - (2.15 \pm 0.10)\kappa_b|^2 \times 10^{-10} \text{ GeV},
\end{aligned} \tag{4.31}$$

where the first term derives from the indirect diagram and the second term, which is modified by κ_b, derives from the direct diagram. Note that the change in sign from $\kappa_b = 1$ to $\kappa_b = -1$ gives a factor increase of between 10^2 and 10^4 in the decay widths. Using $\Gamma(H) = 4.195^{+0.164}_{-0.159} \times 10^{-3}$ GeV [223], the Higgs branching ratio to $\Upsilon(1S, 2S, 3S) + \gamma$ final states for the SM are (0.610, 2.15, 2.44)$\times 10^{-9}$. For $\kappa_b = -1$, the branching ratios are (1.11, 0.518, 0.378)$\times 10^{-6}$, which are still small but significantly larger than the SM values.

The predicted number of $H \to \Upsilon(nS) + \gamma$ events at the LHC is calculated as

$$N = \frac{\Gamma(H \to \Upsilon(nS) + \gamma)}{\Gamma(H)} \times \sigma(p + p \to H) \times \mathcal{L}_{int}. \tag{4.32}$$

We calculate the expected number of $H \to \Upsilon(nS) + \gamma$ events for both $\kappa_b = 1$ and $\kappa_b = -1$ using an integrated luminosity of $\mathcal{L}_{int} = 30$ fb^{-1}, the to-date LHC integrated luminosity for 2016 [224]. The Higgs total cross section is taken to be $\sigma(p + p \to H) = 5.57 \times 10^4$ fb [223]. The results are shown in Table 4.2.

κ_b	$\Upsilon(1S)$	$\Upsilon(2S)$	$\Upsilon(3S)$
1	0.001 ± 0.01209	0.0036 ± 0.0094	0.0041 ± 0.008
-1	1.85 ± 0.01	0.865 ± 0.009	0.631 ± 0.008

Table 4.2: Number of expected events for $H \to \Upsilon(nS) + \gamma$ decays for $\kappa_b = 1$ and $\kappa_b = -1$ with an integrated luminosity of 30 fb^{-1}.

We also examine the number of expected events by the end of LHC Run 2 and Run 3. The approximate target integrated luminosity gathered by the end of Run 2 is 130 fb^{-1}, while the expected total integrated luminosity by the end of Run 3 is 300 fb^{-1} [225]. The predicted number of events for each case are shown in Table 4.3.

κ_b	$\Upsilon(1S)$	$\Upsilon(2S)$	$\Upsilon(3S)$
	Run 2 (130 fb^{-1})		
1	0.00442 ± 0.06214	0.0155 ± 0.0483	0.0178 ± 0.0414
-1	8.02 ± 0.32	3.75 ± 0.15	2.73 ± 0.11
	Run 3 (300 fb^{-1})		
1	0.0102 ± 0.1434	0.358 ± 0.1115	0.0408 ± 0.0956
-1	18.5 ± 0.7	8.65 ± 0.36	6.31 ± 0.26

Table 4.3: Number of expected events for $H \to \Upsilon(nS) + \gamma$ decays at the end of Run 2 and Run 3.

Of particular interest within the phenomenology of the wrong-sign bottom Yukawa are the affected processes which can be examined at the LHC. We focus specifically on the Higgs decays $h \to \Upsilon(nS) + \gamma$, $h \to gg$, and $h \to \gamma\gamma$. While the gluon coupling may be constrained mostly by the rate of gluon fusion production processes, the photon coupling is constrained by Higgs decays, namely

$$\kappa_\gamma^2 = \frac{\Gamma^{NMSSM}(h \to \gamma\gamma)}{\Gamma(h_{SM} \to \gamma\gamma)}. \tag{4.33}$$

Searches for $h \to \Upsilon(nS) + \gamma$ have been performed previously for the 8 TeV runs with approximately 20.3 fb^{-1} of luminosity [228]. The current limits on the branching ratios at 95% CL are given for $\Upsilon(1S, 2S, 3S) + \gamma$ final states as (1.3, 1.9, 1.3)$\times 10^{-3}$ ([227], [228]). An increase in sensitivity for these decays on the order of 10^3 is therefore required in order to probe the affects of a wrong-sign bottom Yukawa, which we have found to give branching ratios of approximately (1.11, 0.518, 0.378)$\times 10^{-6}$. This process is therefore not an effective method of searching for a wrong-sign bottom Yukawa with current luminosity, and will require a significant improvement in the search method.

4.7 Higgs coupling to gluons and photons

The $h \to gg$ decay is a loop-mediated process with contributions from the top and bottom quark loops, which in an appropriate normalization contribute 4.1289 and $-0.2513 + 0.3601i$ to the amplitude, respectively, with SM values [191].

Changing the sign of κ_b therefore results in a shift in κ_g of approximately +13% . As can

be seen in Figure 4.3, the actual values of κ_g for our set of points range between 1.11 and 1.14. This is a large effect, but observing this effect at the LHC is complicated by systematic errors in the primary gg fusion production cross section. Ref. [229] provides expected error estimates for κ_g of 6-8% for an integrated luminosity of 300 fb^{-1} and 3-5% for an integrated luminosity of 3000 fb^{-1}. Any effects from the bottom Yukawa coupling are therefore unlikely to be resolvable from systematic errors at the current gathered luminosity of 30 fb^{-1}, but hints may become observable by the end of Run 2 and the effects should be resolvable by the end of Run 3.

Similarly, the $h \to \gamma\gamma$ decay amplitude includes top and bottom quark loop contributions, among others. We note from Figure 4.3 that the value of κ_γ within our set of points ranges from between approximately 0.90 to 0.96. Estimates for LHC uncertainties in the measurement of κ_γ are given as 5-7% for 300 fb^{-1} integrated luminosity and 2-5% for 3000 fb^{-1} integrated luminosity [229]. The measurement of κ_γ may therefore allow an examination of the viability of the wrong-sign bottom Yukawa within the NMSSM by the end of LHC Run 3.

4.8 Conclusions

The current uncertainties in the determination of the Higgs coupling to bottom quarks leave room for a change of magnitude and sign of this coupling. In this article we have studied the possible implementation of this idea within the MSSM and the NMSSM. We have shown hat in the MSSM this could only be achieved for values of m_A and $\tan\beta$ that are ruled out by current searches for heavy Higgs bosons decaying into tau pairs. On the other hand, in the NMSSM, consistent solutions may be found, that avoid current experimental limits, but for values of the couplings λ and κ that lead to a Landau pole at scales below the GUT scale. This perturbativity problem may be solved by the introduction of an extended gauge sector that slows down the evolution of λ at high energies.

In general, the required low values of m_A and large values of λ lead to charged Higgs

bosons mass that are lower than the top quark mass, and hence, strongly constrained by searches for charged Higgs bosons proceeding from the decay of top quarks. Models that avoid these constraints have masses of the charged Higgs within 10 to 15 GeV of the top quark mass.

We studied the possible experimental implications of such a change of sign, in particular in the radiative decay of the Higgs to quarkonia and on the modification of the gluon and Higgs couplings.

APPENDIX A

SUPPLEMENTARY MATERIAL

A.1 Triple Higgs Coupling

We add tree-level non renormalizable operators to the Higgs potential to get the most general effective potential at the tree-level

$$V(\phi) = \sum_{n=1}^{\infty} \frac{k_{2n}}{2n} \phi^{2n}, \tag{A.1}$$

where $k_2 = m^2$, $k_4 = \lambda$ and, for $n \geq 3$,

$$\frac{k_{2n}}{2n} = \frac{c_{2n}}{2^n \Lambda^{2(n-2)}} \tag{A.2}$$

For the potential to have minimum at the VEV it must satisfy

$$\left.\frac{\partial V}{\partial \phi}\right|_{\phi=v} = \sum_{n=1}^{\infty} k_{2n} v^{2n-1} = 0. \tag{A.3}$$

The second derivative at the VEV must be the square of the Higgs boson mass as discovered by the CMS and ATLAS experiments at the LHC [107, 188]

$$\begin{aligned} \frac{\partial^2 V}{\partial \phi^2} &= \sum_{n=1}^{\infty} (2n-1) k_{2n} \phi^{2n-2}, \\ \left.\frac{\partial^2 V}{\partial \phi^2}\right|_{\phi=v} &= \sum_{n=1}^{\infty} (2n-1) k_{2n} v^{2n-2} = m_h^2. \end{aligned} \tag{A.4}$$

Dividing A.3 by v and then subtracting it from A.4, we get

$$\sum_{n=2}^{\infty}(2n-2)k_{2n}v^{2n-2} = m_h^2,$$
$$\sum_{n=2}^{\infty}(n-1)k_{2n}v^{2n-4} = \frac{m_h^2}{2v^2}. \tag{A.5}$$

The third derivative will give the triple Higgs coupling as we are already in the canonical normalization, where we can substitute $\phi = h + v$ and $v = 246$ GeV.

$$\left.\frac{\partial^3 V}{\partial\phi^3}\right|_{\phi=v} = \sum_{n=2}^{\infty}(2n-1)(2n-2)k_{2n}v^{2n-3}. \tag{A.6}$$

Multiplying A.5 by $6v$ and subtracting it from A.6 we get

$$\lambda_3 = \left.\frac{\partial^3 V}{\partial\phi^3}\right|_{\phi=v} = \frac{3m_h^2}{v}\left(1 + \sum_{n=3}^{\infty}\frac{4(n-1)(n-2)k_{2n}v^{2(n-1)}}{3m_h^2}\right). \tag{A.7}$$

Substituting for k in terms of the cut-off of the effective theory (Λ) and the corresponding dimensionless coefficients (c_{2n}) from Eq. (A.2), we obtain

$$\lambda_3 = \frac{3m_h^2}{v}\left(1 + \frac{8v^2}{3m_h^2}\sum_{n=3}^{\infty}\frac{n(n-1)(n-2)c_{2n}v^{2(n-2)}}{2^n\Lambda^{2(n-2)}}\right), \tag{A.8}$$

where $|c_{2n}| < 1$. This can be written as

$$\lambda_3 = \frac{3m_h^2}{v}\left(1 + \frac{8\Lambda^2}{3m_h^2v^2}\sum_{n=3}^{\infty}n(n-1)(n-2)c_{2n}\left(\frac{v^2}{2\Lambda^2}\right)^n\right). \tag{A.9}$$

From this we clearly see that the the series converges, even if all c_{2n} are 1, for

$$\Lambda > \frac{v}{\sqrt{2}} \sim 174\,\text{GeV}. \tag{A.10}$$

A.2 Maximal Negative Enhancements of λ_3 for $(\phi^\dagger\phi)^4$ and $(\phi^\dagger\phi)^5$

The value of the triple Higgs coupling λ_3 is associated with the third derivative of the potential at the minimum, which corresponds to the change in the potential curvature. At the minimum of the Higgs potential at the VEV, the curvature value is a measured positive constant. Therefore, a negative λ_3 implies even lower curvatures for the higher values of ϕ. In the extreme case, where the curvature turns negative, this will generate a maximum. Hence there has to be one more minimum for even higher values of ϕ sot that the potential is stable in the limit of $\phi \to \infty$. Let the position of such a minimum be $\phi = p$.

This potential can be written as

$$v(\phi) = \frac{k_8}{8}\left(\phi^2 - v^2\right)^2\left(\phi^2 - p^2\right)^2 - \frac{k_8}{8}v^4p^4 \tag{A.11}$$

Comparing this expression with the generic form of the Higgs potential, Eq. (3.16), we get

$$\frac{k_6}{6} = -\frac{3k_8}{4}(p^2 + v^2), \quad \frac{\lambda}{4} = -\frac{k_8}{8}(p^4 + v^4 + 4p^2v^2) \tag{A.12}$$

Substituting this in Eq. (A.5) we obtain a relation between k_8 and the Higgs mass, namely

$$k_8 = \frac{m_h^2}{v^2(p^2 - v^2)^2} \tag{A.13}$$

Substituting in Eq. (A.12) gives

$$k_6 = -\frac{3m_h^2}{2v^2}\frac{(p^2 + v^2)}{(p^2 - v^2)^2} \tag{A.14}$$

k_8 has to be positive for the stability of the potential. Therefore k_6 is the only term that contributes to the enhancement with opposite sign. The maximal negative value it can take

is, for $c_6 < 1$,

$$k_6 = -\frac{3}{4\Lambda^2}, \tag{A.15}$$

Equating the right hand sides of the Eqs. (A.14) and Eq. (A.15) yields

$$2m_h^2(p^2+v^2)\Lambda^2 = (p^2-v^2)^2v^2 \tag{A.16}$$

Solving for p^2 gives

$$p^2 - v^2 = \frac{m_h^2\Lambda^2 \pm \sqrt{m_h^4\Lambda^4 + 4m_h^2\Lambda^2v^4}}{v^2} \tag{A.17}$$

The right hand side must be greater than 0 as $p > v$. This implies

$$p^2 - v^2 = \frac{m_h\Lambda}{v^2}\left(m_h\Lambda + \sqrt{m_h^2\Lambda^2 + 4v^4}\right) \tag{A.18}$$

From Eq. (A.7), we know

$$\frac{\lambda_3}{\lambda_3^{SM}} - 1 = \frac{8v^4}{3m_h^2}(k_6 + 3k_8v^2) \tag{A.19}$$

Substituting Eq. (A.14) in Eq. (A.19) gives

$$\frac{\lambda_3}{\lambda_3^{SM}} - 1 = -\frac{4v^2}{p^2 - v^2} \tag{A.20}$$

Using Eq. (A.18), we get the maximum negative enhancement, namely

$$\delta = \frac{\lambda_3}{\lambda_3^{SM}} - 1 = -\frac{x}{1+\sqrt{1+x}}, \quad \text{where} \quad x = \frac{4v^4}{m_h^2\Lambda^2}. \tag{A.21}$$

A.3 The Order of Phase Transition and The Sign of Enhancement in $(\phi^\dagger\phi)^4$

In the main text, we mentioned the correlation between the sign of the Higgs self-coupling enhancement δ and the order of the EW phase transition. More specifically, we found that all the models with negative enhancement correspond to second-order phase transition. Now let's give it a rigorous mathematical proof. Let's assume the form of our effective Higgs potential is as follows:

$$V(\phi) = \frac{m^2 + \alpha T^2}{2}\phi^2 + \frac{\beta}{4}\phi^4 + \frac{\gamma}{6}\phi^6 + \frac{\kappa}{8}\phi^8 \tag{A.22}$$

At zero temperature, the minimum is at $\phi = v$ and at higher temperature when the ϕ^2 term dominates, the potential looks like a parabola with the minimum at $\phi = 0$. First let's think of what dynamic behavior the potential should have for a second-order PT. In order to have a second-order PT, the global minimum should have a smooth and continuous transition from $\phi = 0$ to $\phi = v$ when the universe cools down. To make things easier, we can think of the moment right after the global minimum moves away from zero, say, moves a tiny distance $\phi = \epsilon$ away, now the minimum potential is negative. If we take this time point as a critical point, around this point, the second-order derivative of the potential at $\phi = 0$ is exactly zero. Above that temperature or say before that time point, the global minimum should have been at $\phi = 0$ all the time and the minimum potential is also zero. This critical point corresponds to the time when $m^2 + \alpha T^2 = 0$, and by claiming that $\phi = 0$ be the global minimum, we get the necessary and sufficient condition for the second-order PT to be:

$$V(\phi) = \frac{\beta}{4}\phi^4 + \frac{\gamma}{6}\phi^6 + \frac{\kappa}{8}\phi^8 > 0, for\ \forall\phi \in (0, v) \tag{A.23}$$

And next we only need to prove that Eq. (A.23) always holds as long as the enhancement δ

is negative. First, let's write down the second-order derivative of Eq. (A.22),

$$\frac{\partial^2 V(\phi)}{\partial \phi^2}_{\phi=v} = m^2 + 3\beta v^2 + 5\gamma v^4 + 7\kappa v^6 = m_h^2 \tag{A.24}$$

And the following first-order derivative condition,

$$\frac{\partial V(\phi)}{\partial \phi}_{\phi=v} = m^2 v + \beta v^3 + \gamma v^5 + \kappa v^7 = 0 \tag{A.25}$$

Combining Eq. (A.24) and Eq. (A.25), we can get rid of m,

$$\beta + 2\gamma v^2 + 3\kappa v^4 = \frac{m_h^2}{2v^2} > 0 \tag{A.26}$$

In the meantime, we have the enhancement of the Higgs self-coupling to be,

$$\delta \propto \gamma + 3\kappa v^2 \tag{A.27}$$

$$\gamma + 3\kappa v^2 < 0 \tag{A.28}$$

The last step of this proof would be to prove the condition A.23 holds given the two constraints Eq. (A.26) and Eq. (A.28). To simplify it, we'll define some new variables to substitute the existing ones. We are going to use $x = \beta/v^4$ and $y = \gamma/v^2$ and $t = \phi^2/v^2$ instead of the old β, γ and ϕ. Now in the 2D plane spanned by axis x and y, we see the two constraints above corresponds to a triangular area shown below in Fig. (A.1) Now it's clear that all the shadowed area lies on the right of all of those red dashed lines, which means no matter what ϕ is in Eq. (A.23), it's always satisfied as long as the enhancement is negative. Thus till now, our proof is done. One more word, in the same way we could prove that the same conclusion doesn't hold after including the higher-order term $(\phi^\dagger\phi)^5$. In that case, there is no tight correlation between the sign of the enhancement and the order of the phase transition, as the example shows in the main text.

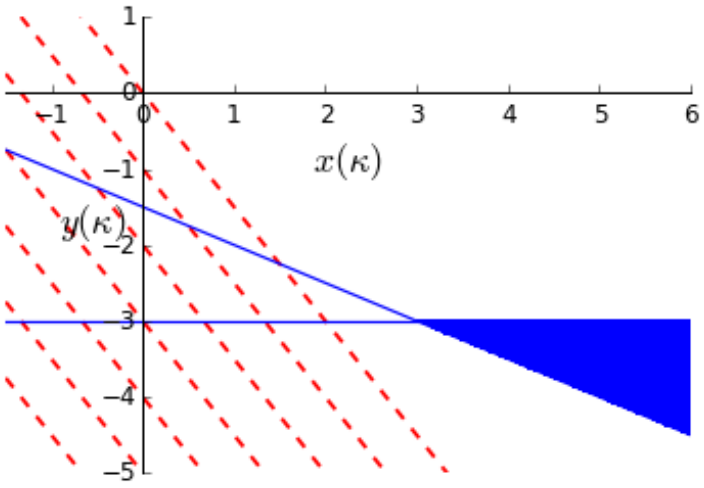

Figure A.1: Allowed region is colored by blue.

REFERENCES

[1] H. P. Nilles, Phys. Rept. **110** (1984) 1;
H. E. Haber and G. L. Kane, Phys. Rept. **117**(1985) 75;
S. P. Martin, arXiv:hep-ph/9709356.

[2] H. Goldberg, Phys. Rev. Lett. **50**, 1419 (1983) [Erratum-ibid. **103**, 099905 (2009)].

[3] J. R. Ellis, J. S. Hagelin, D. V. Nanopoulos, K. A. Olive and M. Srednicki, Nucl. Phys. B **238**, 453 (1984).

[4] H. E. Haber and R. Hempfling, Phys. Rev. Lett. **66**, 1815 (1991); Y. Okada, M. Yamaguchi and T. Yanagida, Prog. Theor. Phys. **85**, 1 (1991); J. R. Ellis, G. Ridolfi and F. Zwirner, Phys. Lett. B **262**, 477 (1991).

[5] H. E. Haber and R. Hempfling, Phys. Rev. D **48**, 4280 (1993) [hep-ph/9307201].

[6] J. A. Casas, J. R. Espinosa, M. Quiros and A. Riotto, Nucl. Phys. B **436**, 3 (1995) [Erratum-ibid. B **439**, 466 (1995)] [hep-ph/9407389].

[7] M. S. Carena, J. R. Espinosa, M. Quiros and C. E. M. Wagner, Phys. Lett. B **355**, 209 (1995) [hep-ph/9504316].

[8] M. S. Carena, M. Quiros and C. E. M. Wagner, Nucl. Phys. B **461**, 407 (1996) [hep-ph/9508343].

[9] H. E. Haber, R. Hempfling and A. H. Hoang, Z. Phys. C **75**, 539 (1997) [hep-ph/9609331].

[10] S. Heinemeyer, W. Hollik and G. Weiglein, Phys. Rev. D **58**, 091701 (1998) [hep-ph/9803277]; S. Heinemeyer, W. Hollik and G. Weiglein, Eur. Phys. J. C **9**, 343 (1999) [hep-ph/9812472]; S. Heinemeyer, W. Hollik and G. Weiglein, Phys. Lett. B **440**, 296 (1998) [hep-ph/9807423].

[11] J. R. Espinosa and R. -J. Zhang, JHEP **0003**, 026 (2000) [hep-ph/9912236].

[12] J. R. Espinosa and R. -J. Zhang, Nucl. Phys. B **586**, 3 (2000) [hep-ph/0003246].

[13] M. S. Carena, H. E. Haber, S. Heinemeyer, W. Hollik, C. E. M. Wagner and G. Weiglein, Nucl. Phys. B **580**, 29 (2000) [hep-ph/0001002].

[14] S. P. Martin, Phys. Rev. D **65**, 116003 (2002) [hep-ph/0111209].

[15] S. P. Martin, Phys. Rev. D **66**, 096001 (2002) [hep-ph/0206136].

[16] S. P. Martin, Phys. Rev. D **71**, 016012 (2005) [hep-ph/0405022].

[17] S. P. Martin, Phys. Rev. D **75**, 055005 (2007) [hep-ph/0701051].

[18] R. V. Harlander, P. Kant, L. Mihaila and M. Steinhauser, Phys. Rev. Lett. **100**, 191602 (2008) [Phys. Rev. Lett. **101**, 039901 (2008)] [arXiv:0803.0672 [hep-ph]].

[19] P. Kant, R. V. Harlander, L. Mihaila and M. Steinhauser, JHEP **1008**, 104 (2010) [arXiv:1005.5709 [hep-ph]].

[20] A. Brignole, G. Degrassi, P. Slavich and F. Zwirner, Nucl. Phys. B **631**, 195 (2002) [hep-ph/0112177].

[21] G. Degrassi, S. Heinemeyer, W. Hollik, P. Slavich and G. Weiglein, Eur. Phys. J. C **28**, 133 (2003) [hep-ph/0212020].

[22] B. C. Allanach, A. Djouadi, J. L. Kneur, W. Porod and P. Slavich, JHEP **0409**, 044 (2004) [hep-ph/0406166].

[23] M. Frank, T. Hahn, S. Heinemeyer, W. Hollik, H. Rzehak and G. Weiglein, "The Higgs Boson Masses and Mixings of the Complex MSSM in the Feynman-Diagrammatic Approach," JHEP **0702** (2007) 047 [hep-ph/0611326]; . Hahn, S. Heinemeyer, W. Hollik, H. Rzehak and G. Weiglein, "FeynHiggs: A program for the calculation of MSSM Higgs-boson observables - Version 2.6.5," Comput. Phys. Commun. **180** (2009) 1426.

[24] S. Heinemeyer, O. Stal and G. Weiglein, Phys. Lett. B **710**, 201 (2012) [arXiv:1112.3026 [hep-ph]], L. J. Hall, D. Pinner and J. T. Ruderman, JHEP **1204**, 131 (2012) [arXiv:1112.2703 [hep-ph]], U. Ellwanger, JHEP **1203**, 044 (2012) [arXiv:1112.3548 [hep-ph]], P. Draper, P. Meade, M. Reece and D. Shih, Phys. Rev. D **85**, 095007 (2012) [arXiv:1112.3068 [hep-ph]], A. Arbey, M. Battaglia, A. Djouadi, F. Mahmoudi and J. Quevillon, Phys. Lett. B **708**, 162 (2012) [arXiv:1112.3028 [hep-ph]], M. Carena, S. Gori, N. R. Shah and C. E. M. Wagner, JHEP **1203**, 014 (2012) [arXiv:1112.3336 [hep-ph]].

[25] A. Pilaftsis, Phys. Lett. B **435**, 88 (1998) [hep-ph/9805373].

[26] D. A. Demir, Phys. Rev. D **60**, 055006 (1999) [hep-ph/9901389].

[27] A. Pilaftsis and C. E. M. Wagner, "Higgs bosons in the minimal supersymmetric standard model with explicit CP violation," Nucl. Phys. B **553** (1999) 3 [hep-ph/9902371].

[28] S. Y. Choi, M. Drees and J. S. Lee, "Loop corrections to the neutral Higgs boson sector of the MSSM with explicit CP violation," Phys. Lett. B **481** (2000) 57 [hep-ph/0002287].

[29] J. S. Lee, A. Pilaftsis, M. S. Carena, S. Y. Choi, M. Drees, J. R. Ellis and C. E. M. Wagner, Comput. Phys. Commun. **156**, 283 (2004) [hep-ph/0307377].

[30] M. S. Carena, J. R. Ellis, A. Pilaftsis and C. E. M. Wagner, Nucl. Phys. B **586**, 92 (2000) [hep-ph/0003180].

[31] S. Heinemeyer, W. Hollik, H. Rzehak and G. Weiglein, "The Higgs sector of the complex MSSM at two-loop order: QCD contributions," Phys. Lett. B **652** (2007) 300 [arXiv:0705.0746 [hep-ph]];

[32] J. S. Lee, M. Carena, J. Ellis, A. Pilaftsis and C. E. M. Wagner, Comput. Phys. Commun. **180**, 312 (2009) [arXiv:0712.2360 [hep-ph]].

[33] J. S. Lee, M. Carena, J. Ellis, A. Pilaftsis and C. E. M. Wagner, Comput. Phys. Commun. **184**, 1220 (2013) [arXiv:1208.2212 [hep-ph]].

[34] A. D. Sakharov, Pisma Zh. Eksp. Teor. Fiz. **5**, 32 (1967) [JETP Lett. **5**, 24 (1967)] [Sov. Phys. Usp. **34**, 392 (1991)] [Usp. Fiz. Nauk **161**, 61 (1991)]; A. G. Cohen, D. B. Kaplan and A. E. Nelson, Ann. Rev. Nucl. Part. Sci. **43**, 27 (1993) [arXiv:hep-ph/9302210]; M. Quiros, Helv. Phys. Acta **67**, 451 (1994); M. Quiros, hep-ph/9901312; V. A. Rubakov and M. E. Shaposhnikov, Usp. Fiz. Nauk **166**, 493 (1996) [Phys. Usp. **39**, 461 (1996)] [arXiv:hep-ph/9603208]; D. E. Morrissey and M. J. Ramsey-Musolf, New J. Phys. **14**, 125003 (2012) [arXiv:1206.2942 [hep-ph]]; J. Shu and Y. Zhang, Phys. Rev. Lett. **111**, no. 9, 091801 (2013) [arXiv:1304.0773 [hep-ph]].

[35] G. Aad *et al.* [ATLAS Collaboration], "Observation of a new particle in the search for the Standard Model Higgs boson with the ATLAS detector at the LHC," Phys. Lett. B **716** (2012) 1 [arXiv:1207.7214 [hep-ex]]; S. Chatrchyan *et al.* [CMS Collaboration], "Observation of a new boson at a mass of 125 GeV with the CMS experiment at the LHC," Phys. Lett. B **716** (2012) 30 [arXiv:1207.7235 [hep-ex]].

[36] C. A. Baker, D. D. Doyle, P. Geltenbort, K. Green, M. G. D. van der Grinten, P. G. Harris, P. Iaydjiev and S. N. Ivanov *et al.*, Phys. Rev. Lett. **97**, 131801 (2006) [hep-ex/0602020].

[37] W. C. Griffith, M. D. Swallows, T. H. Loftus, M. V. Romalis, B. R. Heckel and E. N. Fortson, Phys. Rev. Lett. **102**, 101601 (2009).

[38] J. Baron *et al.* [ACME Collaboration], Science **343**, no. 6168, 269 (2014) [arXiv:1310.7534 [physics.atom-ph]].

[39] C. Wang, X. -H. Guo, Y. Liu and R. -C. Li, arXiv:1408.0086 [hep-ph].

[40] M. Brhlik, G. J. Good and G. L. Kane, Phys. Rev. D **59**, 115004 (1999) [hep-ph/9810457].

[41] D. Chang, W. Y. Keung and A. Pilaftsis, Phys. Rev. Lett. **82**, 900 (1999) [Erratum-ibid. **83**, 3972 (1999)] [hep-ph/9811202].

[42] J. R. Ellis, J. S. Lee and A. Pilaftsis, "Electric Dipole Moments in the MSSM Reloaded," JHEP **0810** (2008) 049 [arXiv:0808.1819 [hep-ph]].

[43] S. M. Barr and A. Zee, Phys. Rev. Lett. **65**, 21 (1990) [Erratum-ibid. **65**, 2920 (1990)].

[44] D. Stockinger, J. Phys. G **34**, R45 (2007) [hep-ph/0609168].

[45] N. Yamanaka, Phys. Rev. D **87**, no. 1, 011701 (2013) [arXiv:1211.1808 [hep-ph]].

[46] S. Abel, S. Khalil and O. Lebedev, Nucl. Phys. B **606**, 151 (2001) [hep-ph/0103320].

[47] T. Ibrahim and P. Nath, Rev. Mod. Phys. **80**, 577 (2008) [arXiv:0705.2008 [hep-ph]].

[48] A. Chakraborty, B. Das, J. L. Diaz-Cruz, D. K. Ghosh, S. Moretti and P. Poulose, Phys. Rev. D **90**, no. 5, 055005 (2014) [arXiv:1301.2745 [hep-ph]].

[49] A. Arbey, J. Ellis, R. M. Godbole and F. Mahmoudi, arXiv:1410.4824 [hep-ph].

[50] CMS Collaboration, "Search for Neutral Higgs Bosons Decaying to Tau Pairs in pp Collisions at sqrts=7 TeV," CMS-PAS-HIG-11-029

[51] V. Khachatryan *et al.* [CMS Collaboration], JHEP **1410**, 160 (2014) [arXiv:1408.3316 [hep-ex]].

[52] G. Aad *et al.* [ATLAS Collaboration], JHEP **1411**, 056 (2014) [arXiv:1409.6064 [hep-ex]].

[53] See e.g., J. M. Frere, D. R. T. Jones and S. Raby, Nucl. Phys. B **222**, 11 (1983); J. F. Gunion, H. E. Haber and M. Sher, Nucl. Phys. B **306**, 1 (1988); J. A. Casas, A. Lleyda and C. Munoz, Nucl. Phys. B **471**, 3 (1996) [hep-ph/9507294]; A. Kusenko, P. Langacker and G. Segre, Phys. Rev. D **54**, 5824 (1996) [hep-ph/9602414]; W. Altmannshofer, M. Carena, N. R. Shah and F. Yu, JHEP **1301**, 160 (2013) [arXiv:1211.1976 [hep-ph]]; M. Carena, S. Gori, I. Low, N. R. Shah and C. E. M. Wagner, JHEP **1302**, 114 (2013) [arXiv:1211.6136 [hep-ph]]; J. E. Camargo-Molina, B. O'Leary, W. Porod and F. Staub, JHEP **1312**, 103 (2013) [arXiv:1309.7212 [hep-ph]]; N. Blinov and D. E. Morrissey, JHEP **1403**, 106 (2014) [arXiv:1310.4174 [hep-ph]]; D. Chowdhury, R. M. Godbole, K. A. Mohan and S. K. Vempati, JHEP **1402**, 110 (2014) [arXiv:1310.1932 [hep-ph]]; J. E. Camargo-Molina, B. Garbrecht, B. O'Leary, W. Porod and F. Staub, Phys. Lett. B **737**, 156 (2014) [arXiv:1405.7376 [hep-ph]]; M. Bobrowski, G. Chalons, W. G. Hollik and U. Nierste, Phys. Rev. D **90**, 035025 (2014) [arXiv:1407.2814 [hep-ph]]; U. Chattopadhyay and A. Dey, arXiv:1409.0611 [hep-ph].

[54] M. Carena, H. E. Haber, I. Low, N. R. Shah and C. E. M. Wagner, arXiv:1410.4969 [hep-ph].

[55] V. Khachatryan *et al.* [CMS Collaboration], arXiv:1412.8662 [hep-ex].

[56] G. Aad *et al.* [ATLAS Collaboration], Phys. Rev. D **90**, no. 11, 112015 (2014) [arXiv:1408.7084 [hep-ex]].

[57] G. Aad *et al.* [ATLAS Collaboration], Phys. Rev. D **91**, 012006 (2015) [arXiv:1408.5191 [hep-ex]].

[58] J. F. Gunion and H. E. Haber, Phys. Rev. D **67**, 075019 (2003) [hep-ph/0207010].

[59] M. Carena, I. Low, N. R. Shah and C. E. M. Wagner, JHEP **1404**, 015 (2014) [arXiv:1310.2248 [hep-ph]].

[60] J. Brod, U. Haisch and J. Zupan, JHEP **1311**, 180 (2013) [arXiv:1310.1385 [hep-ph], arXiv:1310.1385].

[61] L. Bian, T. Liu and J. Shu, "Post-ACME2013 CP-violation in Higgs Physics and Electroweak Baryogenesis," arXiv:1411.6695 [hep-ph].

[62] R. Barbieri and G. F. Giudice, Phys. Lett. B **309**, 86 (1993) [hep-ph/9303270].

[63] M. Ciuchini, G. Degrassi, P. Gambino and G. F. Giudice, Nucl. Phys. B **534**, 3 (1998) [hep-ph/9806308].

[64] M. S. Carena, D. Garcia, U. Nierste and C. E. M. Wagner, Phys. Lett. B **499**, 141 (2001) [hep-ph/0010003].

[65] K. S. Babu and C. F. Kolda, Phys. Rev. Lett. **84** (2000) 228 [hep-ph/9909476].

[66] A. Dedes and A. Pilaftsis, Phys. Rev. D **67**, 015012 (2003) [hep-ph/0209306].

[67] J. R. Ellis, J. S. Lee and A. Pilaftsis, Phys. Rev. D **76**, 115011 (2007) [arXiv:0708.2079 [hep-ph]].

[68] M. Carena, A. Menon and C. E. M. Wagner, Phys. Rev. D **79**, 075025 (2009) [arXiv:0812.3594 [hep-ph]].

[69] E. Barberio *et al.* [Heavy Flavor Averaging Group (HFAG) Collaboration], hep-ex/0603003.

[70] CMS and LHCb Collaborations [CMS and LHCb Collaboration], CMS-PAS-BPH-13-007, LHCb-CONF-2013-012, CERN-LHCb-CONF-2013-012.

[71] M. Misiak, H. M. Asatrian, K. Bieri, M. Czakon, A. Czarnecki, T. Ewerth, A. Ferroglia and P. Gambino *et al.*, Phys. Rev. Lett. **98**, 022002 (2007) [hep-ph/0609232].

[72] M. Misiak and M. Steinhauser, Nucl. Phys. B **764**, 62 (2007) [hep-ph/0609241].

[73] T. Becher and M. Neubert, Phys. Rev. Lett. **98**, 022003 (2007) [hep-ph/0610067].

[74] C. Bobeth, M. Gorbahn, T. Hermann, M. Misiak, E. Stamou and M. Steinhauser, Phys. Rev. Lett. **112**, 101801 (2014) [arXiv:1311.0903 [hep-ph]].

[75] G. Klamke and D. Zeppenfeld, JHEP **0704**, 052 (2007) [hep-ph/0703202 [HEP-PH]].

[76] A. Y. Korchin and V. A. Kovalchuk, Phys. Rev. D **88**, no. 3, 036009 (2013) [arXiv:1303.0365 [hep-ph]].

[77] J. F. Gunion and X. G. He, Phys. Rev. Lett. **76**, 4468 (1996) [hep-ph/9602226].

[78] F. Boudjema, R. M. Godbole, D. Guadagnoli and K. A. Mohan, arXiv:1501.03157 [hep-ph].

[79] M. B. Voloshin, Phys. Rev. D **86**, 093016 (2012) [arXiv:1208.4303 [hep-ph]].

[80] F. Bishara, Y. Grossman, R. Harnik, D. J. Robinson, J. Shu and J. Zupan, JHEP **1404**, 084 (2014) [arXiv:1312.2955 [hep-ph]].

[81] R. Harnik, A. Martin, T. Okui, R. Primulando and F. Yu, Phys. Rev. D **88**, no. 7, 076009 (2013) [arXiv:1308.1094 [hep-ph]].

[82] S. Berge, W. Bernreuther and S. Kirchner, Eur. Phys. J. C **74**, no. 11, 3164 (2014) [arXiv:1408.0798 [hep-ph]].

[83] M. J. Dolan, P. Harris, M. Jankowiak and M. Spannowsky, Phys. Rev. D **90**, no. 7, 073008 (2014) [arXiv:1406.3322 [hep-ph]].

[84] S. Moretti, S. Munir and P. Poulose, Phys. Rev. D **89**, no. 1, 015022 (2014) [arXiv:1305.0166 [hep-ph]].

[85] P. S. Bhupal Dev, A. Djouadi, R. M. Godbole, M. M. Muhlleitner and S. D. Rindani, Phys. Rev. Lett. **100**, 051801 (2008) [arXiv:0707.2878 [hep-ph]].

[86] R. M. Godbole, C. Hangst, M. Muhlleitner, S. D. Rindani and P. Sharma, Eur. Phys. J. C **71**, 1681 (2011) [arXiv:1103.5404 [hep-ph]].

[87] B. Ananthanarayan, S. K. Garg, J. Lahiri and P. Poulose, Phys. Rev. D **87**, no. 11, 114002 (2013) [arXiv:1304.4414 [hep-ph]].

[88] B. Ananthanarayan, S. K. Garg, C. S. Kim, J. Lahiri and P. Poulose, Phys. Rev. D **90**, no. 1, 014016 (2014) [arXiv:1405.6465 [hep-ph]].

[89] G. Aad *et al.* [ATLAS Collaboration], Phys. Lett. B **716**, 1 (2012), doi:10.1016/j.physletb.2012.08.020 [arXiv:1207.7214 [hep-ex]].

[90] S. Chatrchyan *et al.* [CMS Collaboration], Phys. Lett. B **716**, 30 (2012), doi:10.1016/j.physletb.2012.08.021 [arXiv:1207.7235 [hep-ex]].

[91] G. Aad *et al.* [ATLAS and CMS Collaborations], Phys. Rev. Lett. **114**, 191803 (2015), doi:10.1103/PhysRevLett.114.191803 [arXiv:1503.07589 [hep-ex]].

[92] The ATLAS collaboration [ATLAS Collaboration], ATLAS-CONF-2015-007.

[93] V. Khachatryan *et al.* [CMS Collaboration], Eur. Phys. J. C **75**, no. 5, 212 (2015) doi:10.1140/epjc/s10052-015-3351-7 [arXiv:1412.8662 [hep-ex]].

[94] A. Menon, D. E. Morrissey and C. E. M. Wagner, Phys. Rev. D **70**, 035005 (2004) doi:10.1103/PhysRevD.70.035005 [hep-ph/0404184].

[95] C. Grojean, G. Servant and J. D. Wells, Phys. Rev. D **71**, 036001 (2005) doi:10.1103/PhysRevD.71.036001 [hep-ph/0407019].

[96] A. Noble and M. Perelstein, Phys. Rev. D **78**, 063518 (2008) doi:10.1103/PhysRevD.78.063518 [arXiv:0711.3018 [hep-ph]].

[97] V. Barger, D. J. H. Chung, A. J. Long and L. T. Wang, Phys. Lett. B **710**, 1 (2012) doi:10.1016/j.physletb.2012.02.040 [arXiv:1112.5460 [hep-ph]].

[98] D. J. H. Chung, A. J. Long and L. T. Wang, Phys. Rev. D **87**, no. 2, 023509 (2013) doi:10.1103/PhysRevD.87.023509 [arXiv:1209.1819 [hep-ph]].

[99] A. Katz and M. Perelstein, JHEP **1407**, 108 (2014) doi:10.1007/JHEP07(2014)108 [arXiv:1401.1827 [hep-ph]].

[100] D. Curtin, P. Meade and C. T. Yu, JHEP **1411**, 127 (2014) doi:10.1007/JHEP11(2014)127 [arXiv:1409.0005 [hep-ph]].

[101] H. J. He, J. Ren and W. Yao, Phys. Rev. D **93**, no. 1, 015003 (2016) doi:10.1103/PhysRevD.93.015003 [arXiv:1506.03302 [hep-ph]].

[102] A. D. Sakharov, [Usp. Fiz. Nauk161,61(1991)].

[103] F. R. Klinkhamer and N. S. Manton, Phys. Rev. D30 (1984) 2212.

[104] M. E. Shaposhnikov, Nucl. Phys. **B287** (1987) 757–775.

[105] M. Dine, R. G. Leigh, P. Huet, A. D. Linde, and D. A. Linde, Phys. Lett. **B283** (1992) 319–325, `arXiv:hep-ph/9203201 [hep-ph]`.

[106] K. Kajantie, M. Laine, K. Rummukainen, and M. E. Shaposhnikov, Nucl. Phys. **B466** (1996) 189–258, `arXiv:hep-lat/9510020 [hep-lat]`.

[107] **CMS** Collaboration, S. Chatrchyan. arXiv:1207.7235 [hep-ex].

[108] R. Apreda, M. Maggiore, A. Nicolis, and A. Riotto, arXiv:gr-qc/0107033 [gr-qc].

[109] C. Grojean and G. Servant, arXiv:hep-ph/0607107 [hep-ph].

[110] L. Leitao, A. Megevand, and A. D. Sanchez, arXiv:1205.3070 [astro-ph.CO].

[111] Y. Kikuta, K. Kohri, and E. So, arXiv:1405.4166 [hep-ph].

[112] M. Kakizaki, S. Kanemura, and T. Matsui, arXiv:1509.08394 [hep-ph].

[113] R. Frederix, S. Frixione, V. Hirschi, F. Maltoni, O. Mattelaer, P. Torrielli, E. Vryonidou, and M. Zaro, arXiv:1401.7340 [hep-ph].

[114] U. Baur, T. Plehn, and D. L. Rainwater, arXiv:hep-ph/0310056 [hep-ph].

[115] M. J. Dolan, C. Englert, and M. Spannowsky, arXiv:1206.5001 [hep-ph].

[116] J. Baglio, A. Djouadi, J. Quevillon, and M. Spira, arXiv:1212.5581 [hep-ph].

[117] M. J. Dolan, C. Englert, and M. Spannowsky, arXiv:1210.8166 [hep-ph].

[118] V. Barger, L. L. Everett, C. Jackson, and G. Shaughnessy, arXiv:1311.2931 [hep-ph].

[119] A. J. Barr, M. J. Dolan, C. Englert, and M. Spannowsky, arXiv:1309.6318 [hep-ph].

[120] W. Yao, arXiv:1308.6302 [hep-ph].

[121] Tech. Rep. ATL-PHYS-PUB-2014-019, CERN, Geneva, Oct, 2014.

[122] C.-T. Lu, J. Chang, K. Cheung, and J. S. Lee, arXiv:1505.00957 [hep-ph].

[123] A. G. Cohen, D. B. Kaplan, and A. E. Nelson, arXiv:hep-ph/9302210 [hep-ph].

[124] A. Riotto and M. Trodden, "Recent progress in baryogenesis," arXiv:hep-ph/9901362 [hep-ph].

[125] D. E. Morrissey and M. J. Ramsey-Musolf, "Electroweak baryogenesis," arXiv:1206.2942 [hep-ph].

[126] J. M. Cline, K. Kainulainen, and A. P. Vischer, arXiv:hep-ph/9506284 [hep-ph].

[127] M. Carena, M. Quiros, and C. E. M. Wagner, arXiv:hep-ph/9603420 [hep-ph].

[128] B. de Carlos and J. R. Espinosa, arXiv:hep-ph/9703212 [hep-ph].

[129] M. Carena, M. Quiros, and C. E. M. Wagner, arXiv:hep-ph/9710401 [hep-ph].

[130] M. Laine and K. Rummukainen, arXiv:hep-lat/9804019 [hep-lat].

[131] M. Carena, G. Nardini, M. Quiros, and C. E. M. Wagner, arXiv:0809.3760 [hep-ph].

[132] T. Cohen and A. Pierce, arXiv:1110.0482 [hep-ph].

[133] M. Laine, G. Nardini, and K. Rummukainen, arXiv:1211.7344 [hep-ph].

[134] D. Curtin, P. Jaiswal, and P. Meade, arXiv:1203.2932 [hep-ph].

[135] M. Carena, G. Nardini, M. Quiros, and C. E. M. Wagner, arXiv:1207.6330 [hep-ph].

[136] M. Carena, A. Megevand, M. Quiros, and C. E. M. Wagner, arXiv:hep-ph/0410352 [hep-ph].

[137] W. Huang, J. Shu, and Y. Zhang, arXiv:1210.0906 [hep-ph].

[138] R. Fok and G. D. Kribs, arXiv:0803.4207 [hep-ph].

[139] H. Davoudiasl, I. Lewis, and E. Ponton, arXiv:1211.3449 [hep-ph].

[140] M. Pietroni, arXiv:hep-ph/9207227 [hep-ph].

[141] A. T. Davies, C. D. Froggatt, and R. G. Moorhouse, arXiv:hep-ph/9603388 [hep-ph].

[142] S. J. Huber, T. Konstandin, T. Prokopec, and M. G. Schmidt, arXiv:hep-ph/0606298 [hep-ph].

[143] M. Carena, N. R. Shah, and C. E. M. Wagner, arXiv:1110.4378 [hep-ph].

[144] W. Huang, Z. Kang, J. Shu, P. Wu, and J. M. Yang, arXiv:1405.1152 [hep-ph].

[145] T. Corbett, O. J. P. Eboli, J. Gonzalez-Fraile, and M. C. Gonzalez-Garcia, arXiv:1211.4580 [hep-ph].

[146] F. Goertz, A. Papaefstathiou, L. L. Yang, and J. Zurita, "Higgs boson pair production in the D=6 extension of the SM," arXiv:1410.3471 [hep-ph].

[147] A. Azatov, R. Contino, G. Panico, and M. Son, arXiv:1502.00539 [hep-ph].

[148] R. S. Gupta, H. Rzehak, and J. D. Wells, arXiv:1305.6397 [hep-ph].

[149] S. Profumo, M. J. Ramsey-Musolf, and G. Shaughnessy, arXiv:0705.2425 [hep-ph].

[150] V. Barger, P. Langacker, M. McCaskey, M. J. Ramsey-Musolf, and G. Shaughnessy, arXiv:0706.4311 [hep-ph].

[151] C. L. Wainwright, S. Profumo, and M. J. Ramsey-Musolf, arXiv:1204.5464 [hep-ph].

[152] H. H. Patel and M. J. Ramsey-Musolf, arXiv:1212.5652 [hep-ph].

[153] J. M. No and M. Ramsey-Musolf, arXiv:1310.6035 [hep-ph].

[154] S. Profumo, M. J. Ramsey-Musolf, C. L. Wainwright, and P. Winslow, arXiv:1407.5342 [hep-ph].

[155] CMS Collaboration, V. Khachatryan, arXiv:1504.00936 [hep-ex].

[156] T. Robens and T. Stefaniak, arXiv:1501.02234 [hep-ph].

[157] D. Lopez-Val and T. Robens, arXiv:1406.1043 [hep-ph].

[158] CDF, D0 Collaboration, T. E. W. Group, arXiv:1204.0042 [hep-ex].

[159] DELPHI, OPAL, ALEPH, LEP Electroweak Working Group, L3 Collaboration, J. Alcaraz, arXiv:hep-ex/0612034 [hep-ex].

[160] CDF Collaboration, T. Aaltonen et al., , arXiv:1203.0275 [hep-ex].

[161] D0 Collaboration, V. M. Abazov et al., arXiv:1203.0293 [hep-ex].

[162] W. J. Marciano and A. Sirlin, PhysRevD.22.2695.

[163] M. Awramik, M. Czakon, A. Freitas, and G. Weiglein, arXiv:hep-ph/0311148 [hep-ph].

[164] K. Hagiwara, S. Matsumoto, D. Haidt, and C. S. Kim, arXiv:hep-ph/9409380 [hep-ph]. [Erratum: Z. Phys.C68,352(1995)].

[165] C.-Y. Chen, S. Dawson, and I. M. Lewis, arXiv:1410.5488 [hep-ph].

[166] LHC Higgs Cross Section Working Group Collaboration, S. Dittmaier et al..

[167] G. F. Giudice, C. Grojean, A. Pomarol, and R. Rattazzi

[168] E. N. Glover and J. van der Bij

[169] D. A. Dicus, C. Kao, and S. S. Willenbrock.

[170] T. Plehn, M. Spira, and P. Zerwas

[171] S. Dawson, S. Dittmaier, and M. Spira

[172] B. A. Kniehl and M. Spira,

[173] D. de Florian and J. Mazzitelli.

[174] D. de Florian and J. Mazzitelli.

[175] J. Grigo, K. Melnikov, and M. Steinhauser.

[176] D. de Florian and J. Mazzitelli.

[177] S. Dawson, A. Ismail, and I. Low.

[178] B. Batell, M. McCullough, D. Stolarski, and C. B. Verhaaren.

[179] J. M. Campbell and R. Ellis.

[180] T. Sjostrand, S. Mrenna, and P. Z. Skands.

[181] DELPHES 3 Collaboration, J. de Favereau. ARXIV:1307.6346.

[182] J. Alwall, R. Frederix, S. Frixione, V. Hirschi, F. Maltoni. ARXIV:1405.0301.

[183] CMS Collaboration. ARXIV:1307.7135.

[184] ATLAS Collaboration, G. Aad. ARXIV:0901.0512.

[185] CMS Collaboration, C. Collaboration, "Higgs pair production at the High Luminosity LHC,".

[186] A. J. Barr, M. J. Dolan, C. Englert, D. E. Ferreira de Lima, and M. Spannowsky.

[187] A. Elagin, P. Murat, A. Pranko, and A. Safonov.

[188] G. Aad *et al.* [ATLAS Collaboration], Phys. Lett. B **716**, 1 (2012) [arXiv:1207.7214 [hep-ex]]; G. Aad *et al.* [ATLAS Collaboration], Phys. Lett. B **726**, 88 (2013) [arXiv:1307.1427 [hep-ex]].

[189] S. Chatrchyan *et al.* [CMS Collaboration], Phys. Lett. B **716**, 30 (2012) [arXiv:1207.7235 [hep-ex]]; S. Chatrchyan *et al.* [CMS Collaboration], JHEP **1306**, 081 (2013) [arXiv:1303.4571 [hep-ex]].

[190] G. Aad *et al.* [ATLAS and CMS Collaborations], JHEP **1608**, 045 (2016) doi:10.1007/JHEP08(2016)045 [arXiv:1606.02266 [hep-ex]].

[191] P. M. Ferreira, J. F. Gunion, H. E. Haber and R. Santos, Phys. Rev. D **89**, 115003 (2014) [arXiv:1403.4736 [hep-ph]].

[192] K. Inoue, A. Kakuto, H. Komatsu and S. Takeshita, Prog. Theor. Phys. **67**, 1889 (1982); R. A. Flores and M. Sher, Annals Phys. **148**, 95 (1983).

[193] J. F. Gunion and H. E. Haber, Nucl. Phys. B **272**, 1 (1986) [Erratum-ibid. B **402**, 567 (1993)].

[194] M. S. Carena and H. E. Haber, Prog. Part. Nucl. Phys. **50**, 63 (2003) [hep-ph/0208209].

[195] A. Djouadi, Phys. Rept. **459**, 1 (2008) [hep-ph/0503173].

[196] U. Ellwanger, C. Hugonie and A. M. Teixeira, Phys. Rept. **496**, 1 (2010) doi:10.1016/j.physrep.2010.07.001 [arXiv:0910.1785 [hep-ph]].

[197] S. P. Martin, Adv. Ser. Direct. High Energy Phys. **21**, 1 (2010) [Adv. Ser. Direct. High Energy Phys. **18**, 1 (1998)] [hep-ph/9709356].

[198] D. Aloni, Y. Nir and E. Stamou, JHEP **1604**, 162 (2016) doi:10.1007/JHEP04(2016)162 [arXiv:1511.00979 [hep-ph]].

[199] M. Bauer, M. Carena and K. Gemmler, JHEP **1511**, 016 (2015) doi:10.1007/JHEP11(2015)016 [arXiv:1506.01719 [hep-ph]].

[200] M. Aaboud *et al.* [ATLAS Collaboration], Eur. Phys. J. C **76**, no. 11, 585 (2016) doi:10.1140/epjc/s10052-016-4400-6 [arXiv:1608.00890 [hep-ex]].

[201] CMS Collaboration [CMS Collaboration], CMS-PAS-HIG-16-037.

[202] H. Georgi and D. V. Nanopoulos, Phys. Lett. B **82**, 95 (1979); J. F. Donoghue and L. F. Li, Phys. Rev. D **19**, 945 (1979); L. Lavoura and J. P. Silva, Phys. Rev. D **50**, 4619 (1994) [hep-ph/9404276]; L. Lavoura, Phys. Rev. D **50**, 7089 (1994) [hep-ph/9405307]; F. J. Botella and J. P. Silva, Phys. Rev. D **51**, 3870 (1995) [hep-ph/9411288].

[203] G. C. Branco, L. Lavoura and J. P. Silva, *CP Violation* (Oxford University Press, Oxford, UK, 1999).

[204] N. Craig, J. Galloway and S. Thomas, arXiv:1305.2424 [hep-ph].

[205] N. Blinov and D. E. Morrissey, JHEP **1403**, 106 (2014) doi:10.1007/JHEP03(2014)106 [arXiv:1310.4174 [hep-ph]].

[206] J. R. Espinosa and M. Quiros, Phys. Lett. B **279**, 92 (1992). doi:10.1016/0370-2693(92)91846-2

[207] H. E. Haber and R. Hempfling, Phys. Rev. Lett. **66**, 1815 (1991); Y. Okada, M. Yamaguchi and T. Yanagida, Prog. Theor. Phys. **85**, 1 (1991); J. R. Ellis, G. Ridolfi and F. Zwirner, Phys. Lett. B **257**, 83 (1991).

[208] See e.g., M. S. Carena, H. E. Haber, S. Heinemeyer, W. Hollik, C. E. M. Wagner and G. Weiglein, Nucl. Phys. B **580**, 29 (2000) [hep-ph/0001002]; G. Degrassi, S. Heinemeyer, W. Hollik, P. Slavich and G. Weiglein, Eur. Phys. J. C **28**, 133 (2003) [hep-ph/0212020].

[209] T. Hahn, S. Heinemeyer, W. Hollik, H. Rzehak and G. Weiglein, Phys. Rev. Lett. **112**, no. 14, 141801 (2014) doi:10.1103/PhysRevLett.112.141801 [arXiv:1312.4937 [hep-ph]].

[210] G. Lee and C. E. M. Wagner, Phys. Rev. D **92**, no. 7, 075032 (2015) doi:10.1103/PhysRevD.92.075032 [arXiv:1508.00576 [hep-ph]].

[211] J. Pardo Vega and G. Villadoro, JHEP **1507**, 159 (2015) doi:10.1007/JHEP07(2015)159 [arXiv:1504.05200 [hep-ph]].

[212] P. Draper, G. Lee and C. E. M. Wagner, Phys. Rev. D **89**, no. 5, 055023 (2014) doi:10.1103/PhysRevD.89.055023 [arXiv:1312.5743 [hep-ph]].

[213] H. Bahl and W. Hollik, Eur. Phys. J. C **76**, no. 9, 499 (2016) doi:10.1140/epjc/s10052-016-4354-8 [arXiv:1608.01880 [hep-ph]].

[214] C. Panagiotakopoulos and A. Pilaftsis, Phys. Rev. D **63**, 055003 (2001) doi:10.1103/PhysRevD.63.055003 [hep-ph/0008268].

[215] See Chapter 1.3 of D. M. Asner, T. Barklow, C. Calancha, K. Fujii, N. Graf, H. E. Haber, A. Ishikawa and S. Kanemura *et al.*, arXiv:1310.0763 [hep-ph].

[216] H. E. Haber, arXiv:1401.0152 [hep-ph].

[217] M. S. Carena, H. E. Haber, H. E. Logan and S. Mrenna, Phys. Rev. D **65**, 055005 (2002) [Erratum-ibid. D **65**, 099902 (2002)] [hep-ph/0106116].

[218] M. Carena, H. E. Haber, I. Low, N. R. Shah and C. E. M. Wagner, Phys. Rev. D **93**, no. 3, 035013 (2016) doi:10.1103/PhysRevD.93.035013 [arXiv:1510.09137 [hep-ph]].

[219] U. Ellwanger, J. F. Gunion and C. Hugonie, JHEP **0502**, 066 (2005) doi:10.1088/1126-6708/2005/02/066 [hep-ph/0406215].

[220] P. Batra, A. Delgado, D. E. Kaplan and T. M. P. Tait, JHEP **0406**, 032 (2004) doi:10.1088/1126-6708/2004/06/032 [hep-ph/0404251].

[221] R. B. Nevzorov and M. A. Trusov, Phys. Atom. Nucl. **64**, 1513 (2001) [Yad. Fiz. **64**, 1589 (2001)] doi:10.1134/1.1398945 [hep-ph/0112301].

[222] G. T. Bodwin, H. S. Chung, J. H. Ee, J. Lee and F. Petriello, Phys. Rev. D **90**, no. 11, 113010 (2014) doi:10.1103/PhysRevD.90.113010 [arXiv:1407.6695 [hep-ph]].

[223] https://twiki.cern.ch/twiki/bin/view/LHCPhysics/LHCHXSWG

[224] https://twiki.cern.ch/twiki/bin/view/CMSPublic/LumiPublicResults

[225] F. Bordry, Presentation at Higgs Hunting 2016

[226] A. Apollonio, M. Jonker, R. Schmidt, B. Todd, D. Wollmann and M. Zerlauth, IPAC 2014 Proceedings

[227] R. Contino *et al.*, arXiv:1606.09408 [hep-ph].

[228] G. Aad *et al.* [ATLAS Collaboration], Phys. Rev. Lett. **114**, no. 12, 121801 (2015) doi:10.1103/PhysRevLett.114.121801 [arXiv:1501.03276 [hep-ex]].

[229] S. Dawson *et al.*, arXiv:1310.8361 [hep-ex].